



PONTIFICIA
**UNIVERSIDAD
CATÓLICA**
DEL PERÚ


TECHNISCHE UNIVERSITÄT
ILMENAU

Pontificia Universidad Católica del Perú

Escuela de Posgrado

Tesis de Maestría

Prediction of Motion Trajectories based on Motor Imagery by a
Brain Computer Interface

Para obtener el grado de:

Master of Science (M. Sc.)

en Ingeniería Mecatrónica

Presentado por: Matthias Petersamer

Fecha y Lugar de Nacimiento: 29/07/1986 Viechtach, Alemania

Tutor Responsable (TU Ilmenau): Prof. Dr.-Ing. habil. J. Haueisen

Professor Responsable (TU Ilmenau): Prof. Dr.-Ing. habil. J. Haueisen

Professor Responsable (PUCP): M.Sc. D. R. Achanccaray Diaz

Lugar y Fecha: Lima, Noviembre 2017

Abstract

The aim of this Master's Thesis was to develop a naturally controllable BCI that can predict motion trajectories from the imagination of motor execution. The approach to reach this aim was to find a correlation between movement and brain data, which can subsequently be used for the prediction of movement trajectories only by brain signals. To find this correlation, an experiment was carried out, in which a participant had to do triggered movements with its right arm to four different targets. During the execution of the movements, the kinematic and EEG data of the participant were recorded. After a preprocessing stage, the velocity of the kinematic data in x and y directions, and the band power of the EEG data in different frequency ranges were calculated and used as features for the calculation of the correlation by a multiple linear regression. When applying the resulting regression parameter to predict trajectories from EEG signals, the best accuracies were shown in the mu and low beta frequency range, as expected. However, the accuracies were not as high as necessary for control of an application.

Abstracto

El objetivo de esta Tesis de Maestría fue desarrollar un interfaz cerebro computador controlable naturalmente que pueda predecir trayectorias de movimiento imaginadas. El enfoque para alcanzar este objetivo fue encontrar una correlación entre el movimiento y los datos cerebrales que puedan ser utilizados posteriormente para la predicción de las trayectorias de movimiento sólo por medio de señales cerebrales. Para encontrar esta correlación, se realizó un experimento, en cual un participante tuvo que realizar movimientos desencadenados con su brazo derecho a cuatro puntos diferentes. Durante el examen de los movimientos, se registraron los datos cinemáticos y de EEG del participante. Después de una etapa de pre-procesamiento, se calcularon las velocidades en las direcciones x y y, de los datos cinemáticos, y la potencia de la banda, de los datos EEG en diferentes rangos de frecuencia, y se utilizaron como características para el cálculo de la correlación mediante con una regresión lineal múltiple. Al aplicar el parámetro de regresión resultante para predecir trayectorias a partir de señales de EEG, las mejores precisiones estuvieron en el rango de frecuencia mu e inferior en beta, como se esperaba. Sin embargo, los resultados no fueron suficientemente precisos como para usarlas para el control de una aplicación.

Contents

List of Figures	V
List of Tables	VIII
Acronyms	IX
1 Introduction	1
2 State of the art	3
2.1 Functionality of a standard BCI	3
2.2 Brain Signals	4
2.2.1 Brain Waves	4
2.2.2 Control Signal Types	5
2.3 Neuro Imaging	8
2.3.1 Overview of the Imaging Procedures	8
2.3.2 Electroencephalography	9
2.3.3 Problems and artifacts in the data acquisition	10
2.4 Signal Processing	11
2.4.1 Signal Preprocessing	11
2.4.2 Feature Extraction	13
2.4.3 Translation Algorithm	13
2.4.4 Disadvantages of conventional Motor Imaginary-based BCIs	14
2.5 Motion Trajectory Prediction by a Brain Computer Interface	15
2.5.1 Differences to conventional Motor Imagery-based BCIs	15
2.5.2 Experiments	15
2.5.3 Specific Data Acquisition	16
2.5.4 Specific Signal Processing	16
2.5.5 Development of a Trajectory Decoder	19
2.5.6 Expectable accuracies	21
2.5.7 Applications and future prospects	22
3 Methodology	23
3.1 Introduction Methodology	23
3.2 Description of the experiment	23

3.3	Participants of the experiment	25
3.4	Experimental Task	25
3.5	Data Acquisition	27
3.5.1	EEG Data Acquisition	27
3.5.2	Kinematic Data Acquisition	28
3.6	Implementation of the experiment	28
3.7	Signal Processing of the experiment	32
3.7.1	Overview of the Signal Processing	32
3.7.2	Kinematic Data Preprocessing	33
3.7.3	Kinematic Data Feature Extraction	35
3.7.4	EEG data Preprocessing	37
3.7.5	EEG Data Feature Extraction	46
3.7.6	Data verification, data synchronization and creation of a Data Structure	47
3.8	Development of a Trajectory Decoder	51
3.8.1	Prediction of trajectories	51
3.8.2	Improvement of the Trajectory Decoder	54
4	Results	66
4.1	Achieved results	66
4.2	Discussion of the results and problems	68
5	Summary and Future Prospects	75
5.1	Summary	75
5.2	Future Prospects	76
5.2.1	Improvements to the current system	76
5.2.2	Concept for the practical use of the Trajectory Decoder	78
5.2.3	Finding of suitable participants	79
	Appendix	81
A.1	Commissioning of the EEG system	81
A.2	Commissioning of the Kinect system	82
A.3	Preliminary tests for the experiment	83
A.3.1	Memory requirements	83
A.3.2	Best suited skeletal point	86
A.3.3	Optimization of the experimental setup	87
A.3.4	EEG findings	92
A.4	Experimental Procedure	93
A.5	Request and approval of the local ethics committee	94
A.5.1	Declaration of commitment to the ethical principles of research	94
A.5.2	Explanation of the project	96
A.5.3	Informed consent protocol for the participants	106
A.5.4	Approved opinion	107



List of Figures

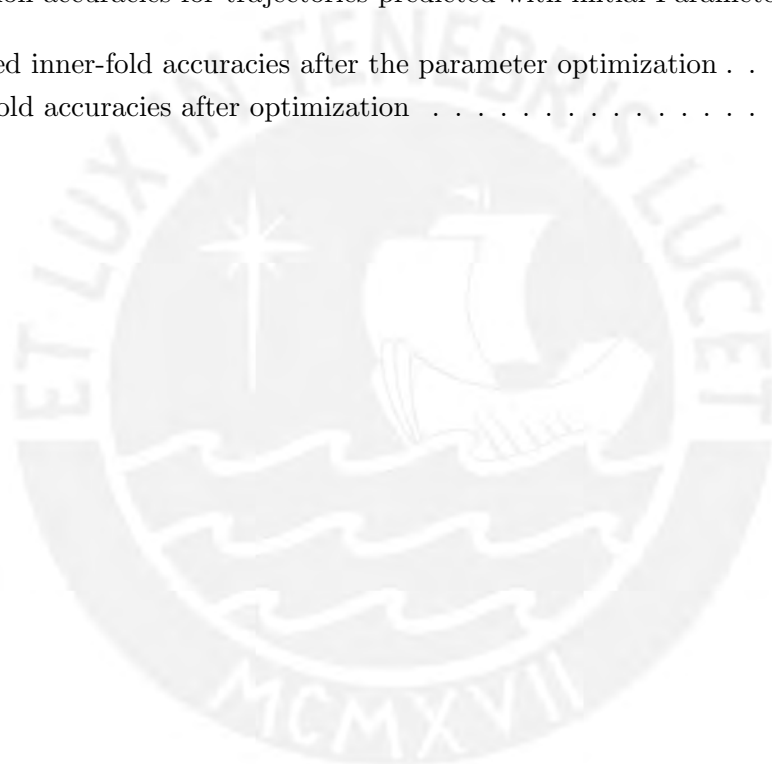
2.1	Functionality of a standard BCI	3
2.2	Illustration of Brain Waves	5
2.3	Band power time courses for two different frequency bands at a finger movement	7
2.4	Placement of EEG electrodes according to the 10-20 system	10
2.5	IIR Filters	12
2.6	Classification	14
2.7	Basic experiments for the development of a MTP BCI	16
2.8	Two steps of the trajectory prediction	20
2.9	Predicted trajectories from ECoG data	21
3.1	Principal structure of the experimental setup	24
3.2	Plate with targets	24
3.3	Movement Cycle	25
3.4	Movement Block	26
3.5	Time course of the experiment	26
3.6	Used EEG System	27
3.7	Kinect for Windows v2	28
3.8	Simulink model for the EEG data acquisition	29
3.9	Programming scheme for the experiment	30
3.10	Theoretical structure of the experimental setup	31
3.11	Implementation of the experimental setup	31
3.12	Signal Processing scheme for the experiment	32
3.13	Calibration of the kinematic data	33
3.14	Calibrated kinematic data	33
3.15	Fourier-Transformation of the kinematic data	34
3.16	Original trajectory of a Movement Cycle	34
3.17	Comparison of Moving Average smoothed movement trajectories	35
3.18	Final Moving Average smoothed movement trajectory	35
3.19	Time-course of the velocity data	36
3.20	Time-course of the smoothed velocity data	36
3.21	Comparison of the trajectories of a Movement Cycle	37
3.22	Comparison of a fir bandpass and a Butterworth bandpass filter	37

3.23 Results after filtering EEG raw data with a FIR bandpass and a Butterworth bandpass	38
3.24 Comparison of a bandpass filter with a high- and low-pass filter in series	38
3.25 Properties of a FIR filter with 1000 filter coefficients	39
3.26 Comparison of a linear-phase and a zero-phase FIR filtered signal	39
3.27 Properties of a Butterworth high-pass filter of 8th-order	40
3.28 Comparison of the results of a zero-phase and a non-linear-phase FIR filtered signal	40
3.29 Re-referencing with a CAR	41
3.30 EEG artifact findings	42
3.31 Calculated ICs by an ICA	43
3.32 Channel activations of different ICs	43
3.33 Power spectral density of the ICs	44
3.34 Blinking artifact reduced EEG signal	44
3.35 Six non-overlapping EEG frequency spectra	46
3.36 Band Power Time Windows	46
3.37 Standardized BP values	47
3.38 Corresponding kinematic data	47
3.39 Verification of the kinematic data	48
3.40 Transients at the beginning of the Movement Blocks	49
3.41 Data Input Structure	50
3.42 Overview of the prediction of trajectories and the calculation of the prediction accuracies	51
3.43 Creation of an outer-fold training and test set	51
3.44 Predicted initial outer-fold trajectories	53
3.45 Processing scheme for the optimization of the Trajectory Decoder	55
3.46 Creation of an inner-fold data structure	56
3.47 Inner-fold training and test set combinations	56
3.48 Inner-fold velocity profiles	57
3.49 Timelag-accuracy-courses using all 30 EEG channels (sep. in x and y dim.)	59
3.50 Timelag-accuracy-courses using all 30 EEG channels (av. in x and y dim.)	59
3.51 Reduction of the EEG channels to six over the motor cortex placed electrodes	60
3.52 Timelag-accuracy-courses using six central EEG channels (sep. in x and y dim.)	60
3.53 Timelag-accuracy-courses using six central EEG channels (av. in x and y dim.)	61
3.54 Optimization of the timelags	62
3.55 Optimization of the EEG channel montage	63
3.56 Re-optimization of the timelags	64
4.1 Optimized EEG channel montage	67
4.2 Topographic map of the predicted accuracies for each channel	67
4.3 Correlation between the EEG BP and associated velocity data	69
4.4 Examples of correlations between contemporaneous datasets	70

4.5	Examples of correlations between time-shifted datasets	70
4.6	Investigated EEG channel	71
4.7	Timelag-accuracy-courses for EEG channel <i>CP2</i> in the low beta band	71
4.8	Feature vectors of training and test sets with a timelag distance difference of 33 ms	72
4.9	Predicted trajectories from two timelags with a difference of 33 ms	73
5.1	Comparison of the timelag courses of the regression parameter and the predicted accuracies	77
5.2	Simplified model of the online-capable BCI system	78
5.3	Example for an application for the BCI system	79
5.4	Finger to thumb opposition	80
A1	Measuring of the EEG electrodes impedance	81
A2	EEG settings and EEG scope	82
A3	Trackable skeletal points	83
A4	Demonstration of the Matlab memory leaks	84
A5	Comparison of the measuring points of different skeletal points	86
A6	Spot on the target plate	87
A7	Measurement errors caused by a purified acrylic plate	88
A8	Measurement errors caused by reflections	89
A9	Measurement errors after optimizations	90
A10	Specification of the origin of a recurring error	90
A11	Results after optimization	91
A12	Transient phase at the beginning of the EEG data registration	92

List of Tables

2.1	Comparison of procedures for the brain data acquisition	8
3.1	Prediction accuracies for trajectories predicted with initial Parameters	58
4.1	Averaged inner-fold accuracies after the parameter optimization	66
4.2	Outer-fold accuracies after optimization	68



Acronyms

ALS	Amyotrophic Lateral Sclerosis
ANN	Artificial Neural Network
BCI	Brain Computer Interface
BMI	Brain Machine Interface
BP	Band Power
BTS	Band Power time-series
CAR	Common Average Reference
CC	Correlation Coefficient
CSP	Common Spatial Pattern
CV	Cross-Validation
ECG	Electrocardiography
ECoG	Electrocorticography
EEG	Electroencephalography
EMG	Electromyography
EOG	Electrooculography
ERD	event-related desynchronization
ERS	event-related synchronization
FFT	Fast Fourier Transformation
FIR	finite impulse response
fMRI	functional Magnetic Resonance Imaging
fps	frames per second
IC	Independent Component

ICA	Independent Component Analysis
IIR	infinite impulse response
INR	Intracortical Neuron Recording
k-NN	k-Nearest Neighbor
LDA	Linear Discriminant Analysis
MA	Moving Average
MB	Movement Block
MC	Multi-Class
MEG	Magnetoencephalography
MF	Matched Filtering
MI	Motor Imagery
mLR	multiple linear regression
MTP	Motion Trajectory Prediction
NIRS	Near Infrared Spectroscopy
PCA	Principal Component Analysis
PSD	Power Spectral Density
RAM	random access memory
SCP	Slow Cortical Potential
SMR	Sensorimotor rhythms
SNR	signal-to-noise ratio
SSVEP	steady-state Visual Evoked Potential
SVM	Support Vector Machine
VEP	Visual Evoked Potential

1 Introduction

For many years the interaction between human and computer took place nearly exclusively with a keyboard and a mouse. However, the possibilities for an interaction have expanded considerably in recent years [1]. Today, it is also very common to control a computer in non-haptic ways by touching a screen or using voices to command operations. Nowadays, a further possibility to control a computer is by a Brain Computer Interface (BCI), also known as Brain Machine Interface (BMI).

BCIs are systems that allow humans to interact with their environment by using control signals generated from brain activity without the intervention of peripheral nerves and muscles [2]. Originally, BCI systems were designed to provide a communication ability to people with severe motor impairments, such as Amyotrophic Lateral Sclerosis (ALS), paralysis by spinal cord injury (SCI) or strokes. With the aid of BCIs, not only external computers, but also speech synthesizer, assistive appliances, and neural prostheses can be controlled. Due to their enormous diversity of possible applications, BCIs are becoming also increasingly popular in the rehabilitation and entertainment industry.

BCIs are artificial intelligence based systems that can recognize particular sets of patterns in brain signals and convert these patterns into control signals. The functional principle of BCIs are the following steps: Signal Acquisition, Signal Preprocessing, Feature Extraction, Classification of the extracted features and creation of a Control Interface [3]. The necessary patterns in the brain can be generated by external stimuli but also by self-regulation of brain rhythms, like the imagination of a motor execution (Motor Imagery). In the case of Motor Imagery (MI), people can train to imply a change of the amplitudes especially in the mu and beta rhythms in the sensorimotor areas of the brain [4]. Features of these so called Sensorimotor rhythms (SMR) can be extracted and the feature vectors can be classified by comparing them with a reference [2]. The resulting classes can be used as control commands which enable the control of BCI devices and applications.

Common SMR-based BCIs often require an artificial association between the MI and the movement functionality since the scientists are forced to use the best classifiable MIs and not the to the movement most similar MIs [5]. Often used MIs are imagined repeated movements of the hands, feet and tongue [6]. For this reason the users have to learn new mental strategies to control devices like neuroprostheses or robot arms, what requires an extended training period

of weeks or months [5]. Furthermore, although there are some SMR BCIs, which use a classification into multiple classes, the most successful paradigms are based in only two mental states [6]. This means that common SMR-based BCIs need to deal with a very limited number of control signals. Another disadvantage is that these kind of BCIs are suitable for the decoding of a particular number of end target positions; however, decoding of trajectories is not possible with this technique.

For some years, there is a new approach for MI-based BCIs, which enable, in contrast to common Multi-Class (MC) SMR BCIs, the reconstruction of imagined movement trajectories, including the velocity vectors during an executed or an imagined movement. This technique does not use a classification, but a regression. The principle is that there is usually a correlation between brain and kinematic data calculated by a regression. The regression parameter can subsequently be used for the prediction of trajectories only from brain data. This technique can be utilized for the decoding of single limbs but also for complex movements like the movements of the fingers. Besides the advantage of the prediction of motion trajectories another advantage seems to be, that the time of training could probably be reduced significantly [7]. However, this technique has a significant disadvantage; today the accuracy of the predicted trajectories are not as high enough as necessary for applications, which require a very accurate control. For this reason, probably, no practical applications are known that use this technique.

Nowadays, the technique of Motion Trajectory Prediction is not feasible for the control of a neuroprostheses, wheel chairs or rehabilitation applications because the risk of hurting themselves or another person, as well as the risk of destroying material values seems to be high as a result of the low prediction accuracies. The technique today also seems not to be feasible for the control of a mouse cursor because reaching an object seems to be faster with the common technique of MC SMR BCIs.

The main objective of this Master's Thesis is to develop a BCI system that can predict motion trajectories in a natural way, as described before. A secondary goal is to show if the system could be used for a two-dimensional application on a PC, in which the users cannot hurt themselves or destroy material values because of the low system accuracy.

In chapter 2, there is an overview given about the state of the art for BCIs in general and for BCIs that can predict motion trajectories in particular. In chapter 3, in the methodology part, there is a very detailed explanation about how a BCI system that can predict trajectories was developed. In chapter 4, the results and problems of the developed system are discussed. Finally, in chapter 5 the thesis ends with a summary of the thesis and future prospects.

2 State of the art

2.1 Functionality of a standard BCI

To control an application via a BCI, the users need to create specific patterns in their brain signals (see section 2.2); to create these pattern, the users often have to learn first. The acquisition of the brain signals can be done in an invasive or non-invasive way (see subsection 2.3.1). Since the signal strength of the raw signals is weak, especially when the acquisition was done in a non-invasive way, the signals must be preprocessed to get it in an adequate quality for the further processing (see subsection 2.4.1). After the preprocessing part, features of the signals need to be extracted (see subsection 2.4.2). Depending on the resulting feature vectors, the signals can be translated to control commands with modern machine learning methods (see). The control commands are provided via an application interface. Typically, the applications provide an optical, acoustic or mechanical feedback, which supports the users by controlling the application and making the BCIs a closed loop system.

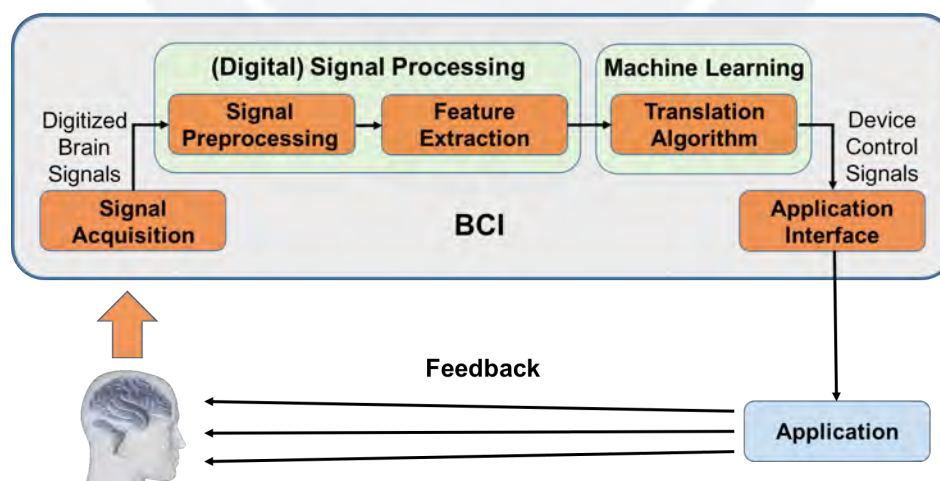


Figure 2.1: Functionality of a standard BCI. The head on the lower left symbolizes a BCI user, who creates brain signals. The brain signals are recorded and digitized by a signal acquisition system. Subsequently, the digitized signals are preprocessed, then features from the signals are extracted and finally translated into device control signals. Via an application interface these control signals are provided to an application. Typically, the application provides feedback to the user and makes the system a closed loop system.

2.2 Brain Signals

2.2.1 Brain Waves

The brain generates an amount of neural activity. These signals can be divided into two classes [8]:

- spikes, which reflect the action potentials of individual neurons and
- field potentials, which result of combined synaptic, neuronal, and axonal activity of neuron groups.

While the spikes can only be acquired by implanted microelectrodes, the field potentials can also be measured in a non-invasive way.

Each type of field potential (brain wave) control a variety of states of consciousness ranging from sleep to active thinking [9].

Delta Waves The frequency of delta waves ranges from approx. 0.5 to 3.5 Hz [10]. Delta waves are the slowest waves but tend to the highest amplitudes. These signals are normally seen in adults in slow wave sleep as well as in babies.

Theta Waves The frequency of theta waves ranges from approx. 3.5 to 7.5 Hz [10]. Theta is associated with inefficiency and daydreams. The deepest waves of Theta mark the boundary between waking and sleeping.

Alpha (Mu) Waves The frequency of alpha waves ranges from approx. 7.5 to 12 Hz [10]. The signal is seen in the posterior regions of the head on both sides. However, the amplitude is higher on the dominant side. It is appearing by closing the eyes and by relaxation. Furthermore, several studies have found a rise in alpha power after smoking marijuana. The frequency of the mu rhythms is similar to the frequency of the alpha rhythms but the mu wave is found over the motor cortex while the alpha waves occur over the resting visual cortex [11].

Beta Waves The frequency of beta waves ranges from approx. 12 Hz to 30 Hz [10]. It is usually seen on both sides in a symmetrical distribution and it is most evident frontally. The beta waves can be seen in active processing like thinking, concentration or cognition.

Gamma Waves The frequency of gamma waves ranges of approx. 30 Hz and up [10]. It reflects higher mental activity, including perception, problem solving, and consciousness. While all brain waves work simultaneously, one brainwave can be more predominant and active than the others. The dominant brainwave will determine your current state of mind [9].

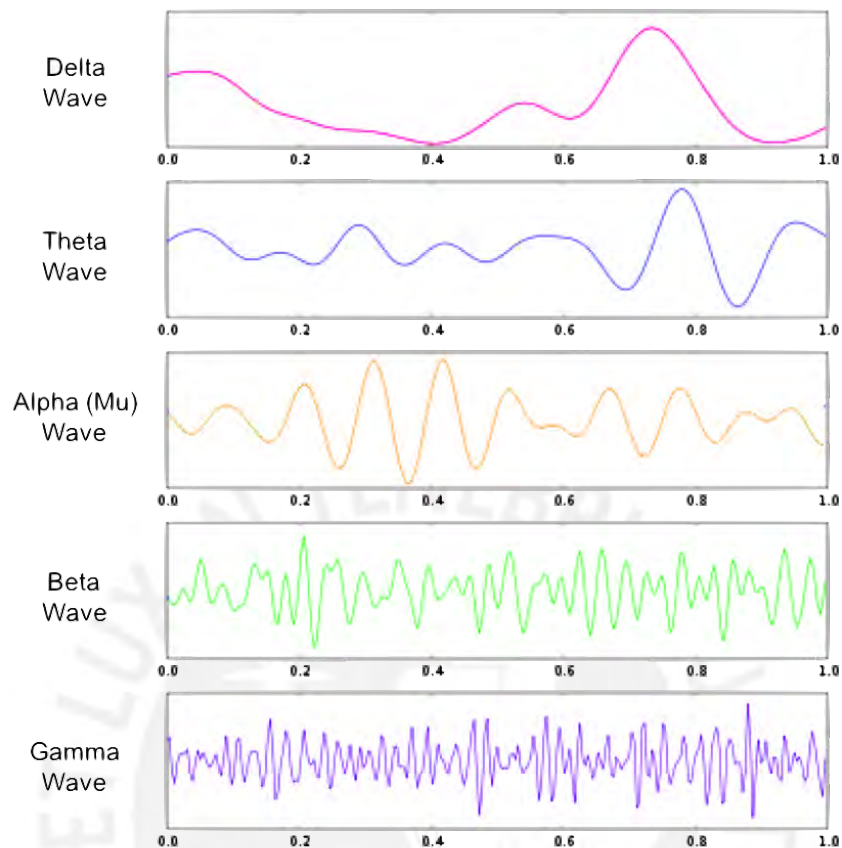


Figure 2.2: Illustration of Brain Waves (adapted from [9]). The image shows typical shapes of delta, theta, alpha (mu), beta and gamma waves in a time window of 1.0 s

2.2.2 Control Signal Types

Many specific characteristics in the brain waves are related to cognitive tasks. The physiological phenomena of some brain signals have been decoded in such a way that it enables the BCI systems to interpret the users intentions. These signals are suitable as possible control signals in BCIs.

The control signals that are used in BCIs can be divided in two groups: exogenous and endogenous signals [2]. While exogenous control signals use the neuronal activity produced by an external stimulus in the brain, endogenous control signals are based on self-regulation of brain rhythms and potentials without an external stimulus. The resulting advantage of a BCI system, which uses endogenous control signals, is that the users can operate at free will, while a BCI system, which uses exogenous control signals constrain the users to the presented choices. However, the users of endogenous BCI systems need to train with neurofeedback to learn to generate specific brain patterns.

Exogenous Control Signals

Exogenous BCIs use the paradigms of Visual Evoked Potentials (VEPs) [2]. VEPs are modulations of brain activity that occur in the visual cortex after receiving a visual stimulus. Since the amplitude of VEPs increase enormously at certain times after the stimulation the detection of these modulations is relatively easy. Typical modulations used for the control of a BCI application are steady-state Visual Evoked Potentials (SSVEPs) and P300 Evoked Potentials.

Steady-State Visual Evoked Potentials (SSVEPs) occur as reaction to longer stimuli with higher frequencies than 6 Hz [2]. Typical SSVEP BCI applications display flashing stimuli, like numbers or letters on a screen and induce so SSVEPs with the same frequency as the stimuli in the users visual cortex has, while the user stares at one of the symbols. By the analysis of the induced SSVEPs can be deduced which figure the user had stared at. Following, an advantage of the use of this type of control signal for a BCI is that there is just a little training required.

P300 Evoked Potentials are positive peaks due to infrequent visual but also to auditory or somatosensory stimuli [2]. The responses of P300 are elicited about 300 ms after attending to a stimulus. A typical application of a BCI based on visual P300 evoked potentials is a P300 speller. In the P300 spellers a matrix of letters, numbers or other symbols is contained on a screen. Columns and rows of this matrix are flashed in random order. To select a symbol on the screen the user need gaze at the desired symbol. When the desired symbol flashes a P300 evoked potential is elicited. After a few induced P300 evoked potentials the software can calculate what symbol the user wants to elect.

Endogenous Control Signals

Endogenous Signals used as control signals for BCIs are Slow Cortical Potentials and Sensorimotor Rhythms [10].

Slow Cortical Potentials (SCPs) are slow voltage shifts caused by shifts in the depolarization levels of certain dendrites [2]. Negative SCPs indicate an increased neuronal activity, whereas positive SCPs indicates a decreased activity in individual cells. The shifts of these brain signals last from one to several seconds while the signals are below 1 Hz. An advantage of the use of SCPs for a BCI is that these signals can be self-regulated by healthy users as well as by paralyzed patients after a training. A disadvantage is that the success of the self-regulation is very strongly dependent on psychological and physical factors like sleep or mood. Furthermore, the rates of information provided by SCPs are relatively low. A possible application using SCP shifts is, e.g., moving a cursor to select presented targets on screen.

Sensorimotor Rhythms (SMR) comprise the oscillating mu and central beta rhythms over the central and parietal cortex [12]. The task-related modulation in SMR is usually manifested as [13]:

- an increase of the power in the specific frequency bands because of a synchronization of the neurons (event-related synchronization) and
- a decrease of the power in the specific frequency bands because of a desynchronization of the neurons (event-related desynchronization).

The event-related synchronization (ERS) as well as the event-related desynchronization (ERD) can be generated by sensory stimulation, motor behaviour and MI. Hence, the execution of a movement is not required to modulate the amplitudes [2]. However, the users must learn modulating the amplitudes by MI first.

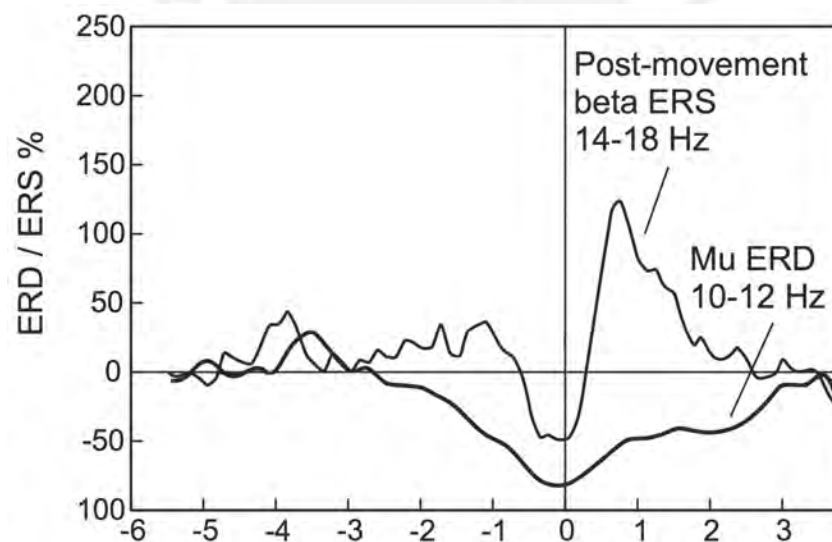


Figure 2.3: Band power time courses for two different frequency bands at a finger movement (adapted from [4]). The figure shows band power time courses computed for frequency ranges of 10-12 Hz (mu) and 14-18 Hz (low beta) from EEG trials recorded from electrode position *C3* during right index finger lifting. As you can see the mu band ERD starts about 2.5 s before movement on-set (vertical line), reaches the maximal ERD at the movement-onset, and recovers its original level within a few seconds. In contrast, the beta rhythm shows a short ERD during the initiation of movement, followed by ERS that reaches the maximum after movement execution. This ERS occurs while the mu rhythm is still attenuated.

2.3 Neuro Imaging

2.3.1 Overview of the Imaging Procedures

Two different types of brain activity may be monitored: the electrophysiological activity and the hemodynamic response [2].

Electrophysiological activity is generated by electro-chemical transmitters exchanging information between the neurons [2]. The neurons generate ionic currents which are passed as action potentials over the nerve cells. This electrophysiological activity can be measured directly, e.g. with the following methods:

- Electroencephalography (EEG),
- Electrocochography (ECoG)
- Magnetoencephalography (MEG)
- Intracortical Neuron Recording (INR)

The hemodynamic response is an effect, in which the ratio of oxyhemoglobin to deoxyhemoglobin changes locally due to increased metabolism turnover with increased neuronal activity [2]. Since the hemodynamic response is in contrast to the electrophysiological activity not directly related to neuronal activity, the measuring methods are referred as indirect. The hemodynamic changes can be measured e.g. by the following methods:

- functional Magnetic Resonance Imaging (fMRI)
- Near Infrared Spectroscopy (NIRS)

In principle, electrophysiological procedures have a very good time resolution but a poor spatial resolution, whereas hemodynamic methods have a very good spatial resolution but a poor time resolution [14].

Table 2.1 compares the procedures with each other. Risk = " - " means that this is an invasive procedure, for which an operation is necessary, which is associated with risks.

Procedure	Principle	Risk	Portability	Temp. res.	Spat. res.
EEG	electrophysiological (direct)	+	+	~ 0.05 s	~ 10 mm
ECoG		-	+	~ 0.003 s	~ 1 mm
MEG		+	-	~ 0.05 s	~ 5 mm
INR		-	+	~ 0.003 s	< 0.5 mm
fMRI	hemodynamic (indirect)	+	-	~ 1 s	~ 1 mm
NIRS		+	+	~ 1 s	~ 5 mm

Table 2.1: Comparison of procedures for the brain data acquisition (adapt. from [2])

The optimal imaging procedure for a BCI has a high portability and is not associated with any risk. Hence, EEG and NIRS are especially suitable for BCIs. Because of the low costs, relatively simple use and excellent time resolution, nowadays mainly EEG is used for the data acquisition of BCIs [15].

Since EEG is by far the most widely used neuroimaging modality for BCIs [2] and it is also used in this work, only this technique is described in more detail below.

2.3.2 Electroencephalography

Electroencephalography is the oldest of the neurophysiological investigations and enables the recording of brain activity as the potential difference over time between two electrodes [16]. In principle, the following two types of derivations are distinguished:

- The bipolar derivation, in which a measurement of potential differences is done between two adjacent voltage-active electrodes.
- The reference derivation, in which either a derivation of the potential differences between an active and a common reference electrode, which is attached to the patient or a technically manufactured reference, is done.

Usually, in the case of reference derivations, an ear electrode, which, however, may have a residual electrical activity, is selected [16]. The minimum configuration for the EEG measurement consists of an active, a reference and a ground electrode. Multi-channel configurations may include up to 256 active electrodes [17]. Since the voltage differences increase with the size of the distances between the electrodes, the distance between the individual active electrodes should be the same for better comparison [16]. To ensure the same distance, an internationally standardized procedure for the placement of EEG electrodes was introduced, the 10-20 system. In the 10-20 system, the skull is measured from the Nasion to the Inion along the cranium. The value of this route is assumed to be 100 %. Hence you divide the distance by going 10 % from the Nasion in the direction of the Inion, then follow four other steps of 20 % each and at the end again a step of 10 %. The same is done on the line between the two points located in front of the ears. A third line is obtained by measuring the circumference of the head and dividing half the distance in both directions according to the 10 and 20 % increments. Finally, the electrodes are placed on all the resulting points.

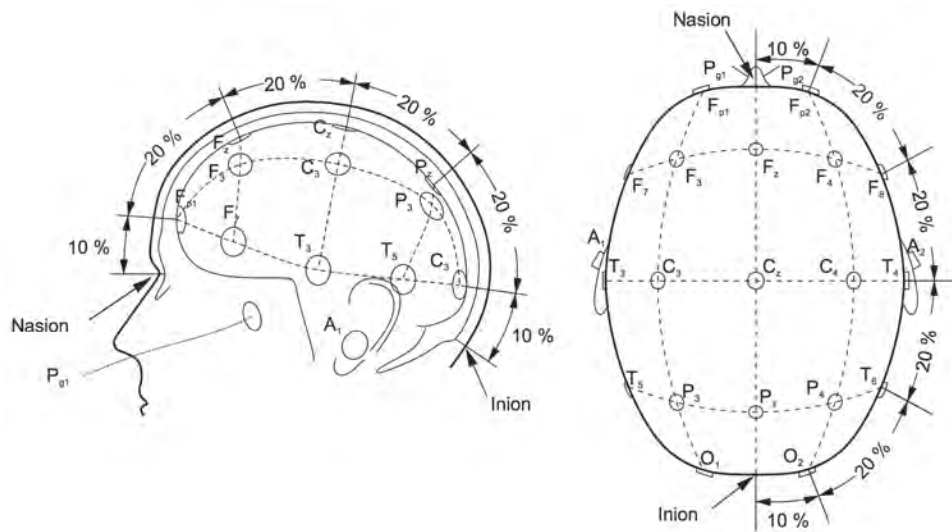


Figure 2.4: Placement of EEG electrodes according to the 10-20 system [2]. In this figure you can see the reference points (Nasion and Inion) of the 10-20 system. Between these points the distances are divided in 10 and 20% steps and the electrodes are placed on the resulting points.

The electrode positions are named according to the corresponding brain regions [16]:

- F - frontal • C - central • T - temporal • P - parietal • O - occipital
- The electrodes in the region of the right half of the head are named with even-numbers and the electrodes on the left half are named with odd-numbers.

Besides of the electrodes, the EEG recording system consists of amplifiers, A/D converters, and a recording device [17].

2.3.3 Problems and artifacts in the data acquisition

EEG is prone to several technical and biological disorders [18]. The most frequent technical interruption is caused by the power supply because the differential voltage of the electromagnetic fields superimposes the bio signals directly at the amplifier input. Even battery powered portable meters are affected by these interferences. Also, more and more high-frequency fields, especially from WLAN, Bluetooth, etc., interfere. The disturbances can be periodic or transient.

Further technical artifacts are [17]:

- impedance fluctuation
- low battery
- cable movements

- broken wire contacts
- too much electrode paste or dried pieces

While periodic disturbances can generally be reduced relatively easily, this is only hardly possible with transient disturbances, due to their unpredictable occurrence and their non-reproducible course [18]. Biological disorders are generally more difficult to reduce because the biological signal spectrum is approximately the same for all bio signals, the bio signals are not linearly coupled to each other and the bio signals are not deterministic and reproducible. Another biological problem is that the EEG electrodes are far from the individual neurons. Since there are around 86 billion neurons in the brain [19] whose signals are superimposed, the received EEG data contain a lot of noise. Also, the skull bone acts as a kind of low-pass filter [18].

Biological artifacts include e.g. [17]:

- Movement artifacts
- Electrooculography (EOG) artifacts: eye movements and eye blinking
- Electromyography (EMG) artifacts: muscular activity
- Electrocardiography (ECG) artifacts: heart activity
- Sweating artifacts

2.4 Signal Processing

2.4.1 Signal Preprocessing

The aim of the data acquisition is to avoid all sources of interference during the measurement. However, as the previous subsection has shown, it is practically impossible to prevent the bulk of biological artifacts. To be able to provide the signals in sufficient quality for the feature extraction and further processing step, a signal preprocessing is necessary.

Bandpass and band-stop filtering

To remove all the signals out of the spectrum of bio signals the signals are usually filtered by a bandpass from 0.1 to 100 Hz. In addition, a band-stop, also known as notch filter at around 50 or 60 Hz (depends on the utility frequency of the country) is used to remove the artifact caused by the power supply. However, a bandpass filter can also be used for limiting the frequency range to get the signals of specific frequency bands, like the mu or beta band.

Since common BCIs demand a real-time processing the bandpass and band-stop filters must have an infinite impulse response (IIR), which don't require a high computational effort. Chebyshev and Causer (Elliptical) filters have a much higher slope in the transition area than Butterworth filters at the same filter order but due to their ripples in the pass- and stop-band, these filters distort the EEG signals [20] and are therefore not suitable for the use in BCIs.

Usually used filters for BCIs are Butterworth filters with an order between 4 and 8.

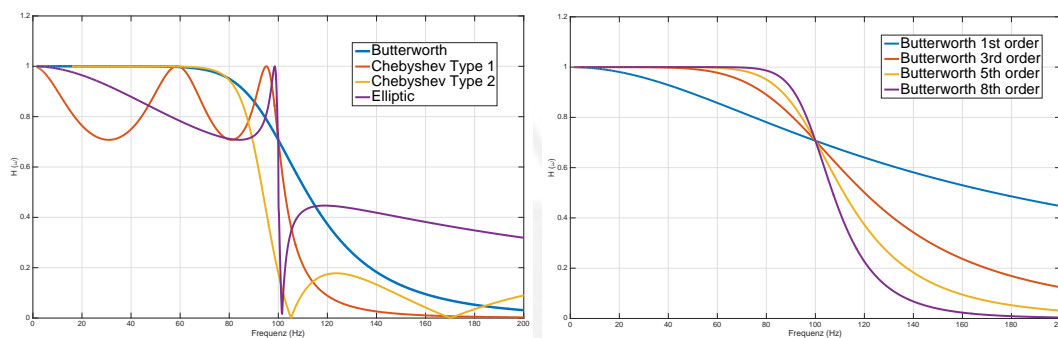


Figure 2.5: IIR Filters. Both pictures compare different types of IIR low-pass filters with a cutoff frequencies of 100 Hz, each. In the left picture are a Butterworth, Chebyshev Type 1 and 2 and an Elliptic filter, all with a filter order of 5, compared. It can be seen that the slope between the pass and stop band for the both Chebyshev as well as for the Elliptic filter is much higher, however, also the the ripples, which distort the signals can be seen. In the right picture are Butterworth filters with different filter orders compared to each other. As higher the filter order as higher the slope between the pass- and stop-band.

Re-referencing

EEG channels are referenced to a reference electrode, e.g. at the ear (see subsection 2.3.2). The use of a re-referencing method such as Common Average Reference (CAR), Laplacian or bipolar methods acts as spatial high-pass filter and enhance the focal activity from the local sources (e.g. the mu and beta rhythms) and reduce the widely distributed activity, including that resulting from distant sources (e.g. EMG, eye movements and blinks, visual alpha rhythm) [21].

A CAR is obtained to the mean values of all electrodes, a small Laplacian reference to the mean values of its four nearest, a large Laplacian reference to the mean values of its four next-nearest neighboring electrodes and a bipolar reference to the mean values of the electrodes in anterior and posterior direction [22]. For all the re-referencing methods, the references are subtracted for all time points from all electrodes.

2.4.2 Feature Extraction

BCIs have to extract features from brain signals, which are similar to certain classes (see subsection 2.4.3). The features are measured or derived from the characteristics of the signals containing the information which are needed to differ their different types. There is a great variety of features which have been used in the literature such as [10]:

- Amplitude values of EEG signals,
- Band Power (BP) values of EEG signals,
- Power Spectral Density (PSD) values of EEG signals,
- Auto Regressive (AR) and Adaptive Auto Regressive (AAR) parameters,
- Time-frequency features and
- inverse model-based features

To extract the features, often "Dimensionality Reduction Methods" or "Time/Frequency and Space Methods" are necessary.

Dimensionality Reduction Methods The dimension of the feature space that contains from raw EEG signals extracted features is often very large and not all the information provided by the measured channels is generally relevant [10]. If there are too many irrelevant and/or redundant features, learning methods tend to over-fit. Moreover, high dimensionality increases the time and space requirements for processing the data. A common way to resolve this problem is dimensionality reduction. Techniques to reduce the Dimension and to remove irrelevant and redundant information are the Principal Component Analysis (PCA) and the ICA, which is a generalization of the PCA. The use of both methods can lead to higher accuracies in the classification.

Time/Frequency and Space Methods The EEG Signals have information in the Time/Frequency as well as in the Space. Matched Filtering (MF), Wavelet Transformations (WT) and Common Spatial Pattern (CSP) are common methods to extract features in these dimensions [2].

2.4.3 Translation Algorithm

To control a BCI application the system needs to interpret the user's intentions and translate this to control signals. To enable the interpretation of the user's intention, BCIs normally classify the pattern according to its extracted features into two or more classes. The Classifiers can be linear, nonlinear or generative models and be assigned as follows [2]:

- Linear classifiers: Linear Discriminant Analysis (LDA), Support Vector Machines (SVMs)
- Nonlinear classifiers: SVMs, k-Nearest Neighbors (k-NNs), Artificial Neural Networks (ANNs)
- Generative models: Bayesian Statistical Classifiers

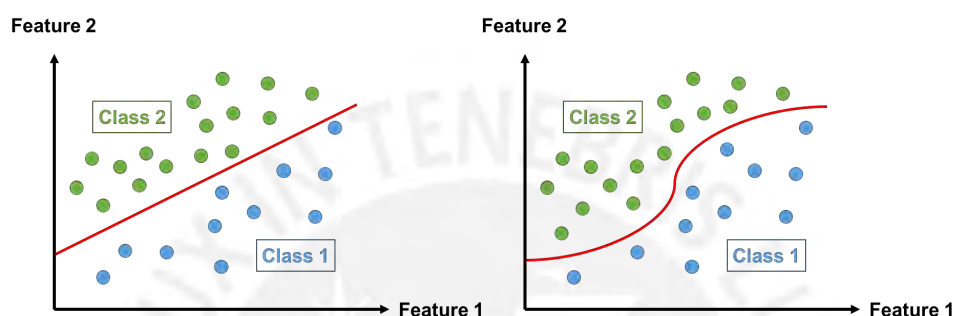


Figure 2.6: Classification. The figure shows examples for a linear (left) and a nonlinear (right) classification of feature vectors into two classes. The green and the blue dots represent the extracted feature vectors of a two-dimensional feature space.

To improve the performance of the Classifiers, which means a reduction of the number of false detections, a signal post-processing can be done [21].

2.4.4 Disadvantages of conventional Motor Imaginary-based BCIs

Conventional MI-based BCIs, also known as SMR BCIs, typically enable the control of different devices by classifying the feature vectors created by imagined motor execution. However, since classification performance is crucial, the scientists are forced to use the best classifiable MIs and not the MIs the movement is most similar to [5]. For this reason SMR BCIs often require an artificial association between the MI and the movement functionality. Often used MIs are the movement of the right arm, left arm, feet and tongue [6]. Hence, the users have to learn new mental strategies to control devices like neuroprostheses or robot arms by conventional SMR BCIs, what often require an extended training period of weeks or months. Furthermore, although there are some SMR BCIs which use a MC classification in a multi-dimensional feature space, the most successful paradigms are based on only two mental states. This means that these kinds of BCIs need to deal with a very limited number of control signals. Another disadvantage of (MC) SMR BCIs is that these BCIs are suitable for the decoding of a certain number of end target positions, however decoding of a trajectory is not possible with this technique [12].

2.5 Motion Trajectory Prediction by a Brain Computer Interface

2.5.1 Differences to conventional Motor Imagery-based BCIs

There is a relatively new approach to develop MI-based BCIs, which enable in contrast to (MC) SMR BCIs the reconstruction of imagined movement trajectories, including the velocity vectors. Korik et al. [23] called this technique Motion Trajectory Prediction (MTP).

In contrast to conventional SMR BCIs for MTP BCIs no classification is used, but a regression. The principle is that there is usually a correlation between brain and kinematic data calculated, which can subsequently be utilized for the reconstruction of trajectories only from brain data.

For the prediction of motion trajectories it is not essential to find a direct correlation between brain and kinematic data, e.g. Choi [24] showed that it is also possible to predict EMG data from brain data, which can be used to deduce the position of the limbs at specific time points and hence the trajectories itself.

Commonly, investigated MTP BCIs involve decoding of a single upper limb movement in 3D space like done by Korik et al. [12], Choi [24], Bradberry et al. [25] or Antelis et al. [26]. However, MTP BCIs have also been investigated for complex movements like finger movement [27] or walking [28].

2.5.2 Experiments

The literature shows some different experiments to compute the correlation between brain and kinematic data. In the most experiments the participants had to move their dominant right arm to touch some target points [25] or [26], some points on a screen [24], some subjects in the space [12] or the subjects had to connect some points with a pen on a screen [29]. For all experiments, it is important that during the execution of the movements eye movements, as well as blinking are reduced as much as possible.

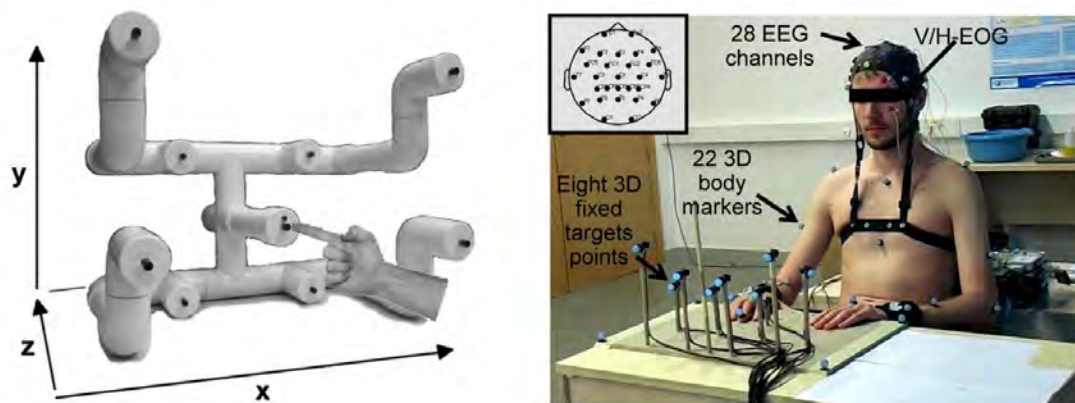


Figure 2.7: Basic experiments for the development of a MTP BCI (left [25], right [26]). Both pictures show targets, which have to be touched by the participants. The right picture shows also the kinematic and EEG data recording systems.

2.5.3 Specific Data Acquisition

Compared to EEG, ECoG (or implanted micro) electrodes have a higher spatial resolution, greater sensitivity for activity at higher frequencies and a higher signal-to-noise ratio (SNR) [30]. However, some studies show that EEG systems are also suitable for the use in MTP BCIs. Very often electro-caps with 64 sensors are used, e.g. in [24], [27], [25] or [29]. Additionally to the EEG electrodes often EOG electrodes are used. The EOG electrodes enable later an easier elimination of artifacts resulting by eye movements.

The Kinematic Data can be recorded by a 3D position measurement systems like MacReflex [24], Kinect [7], [12] or a data glove like the CyberGlove [27]. 2D positions can e.g. be measured on a digitizing tablet [29].

2.5.4 Specific Signal Processing

The Signal processing for the prediction of trajectories differs partially from the signal processing of conventional SMR-based BCIs.

Specific EEG data Preprocessing

The basics of the preprocessing (bandpass/band-stop filtering and signal re-referencing) for the prediction of trajectories are the same like for conventional SMR BCIs. However, since a part of the processing can be done offline there is a greater choice of filters to improve the quality of the signals.

Independent Component Analysis (ICA) The ICA algorithm calculates the Independent Components (ICs) from highly statistically correlated EEG signals without regard to the physical location or configuration of the source generators [31]. After the ICA, ICs like EOG or EMG can be removed and thus the quality of the signals be improved.

Baseline Correction If a time-series of EEG BP values (BTS) are used as features for the calculation of the correlation, it seems recommendable to do a baseline correction, which is performed by subtracting the average value of the EEG data, which were measured in a particular time window, from each data point. The baselines of the re-referenced EEG signals $X(n)_t^{ref}$ can be corrected for all time points t and all channels n according the following equation, in which M is the number of all measured time points:

$$X(n)_t^{BC} = X(n)_t^{ref} - \frac{1}{M} \sum_{l=1}^M X(n)_l^{ref} \quad (2.1)$$

Threshold filtering Threshold filters can be used to remove brain data intervals with high noise from further analysis to improve the SNR.

Splitting in different Frequency Spectra For the preparation of the feature extraction the EEG signals are separated in non-overlapping frequency bands. Bandpass filters are usually used to do this.

Downsampling At the end of the EEG data preprocessing the signal need to be downsampled in all frequency bands to the usually lower kinematic data sampling rate. However, it is important to remember the Nyquist–Shannon sampling theorem, which says that frequencies above half the sampling rate (frequency) cannot be reconstructed [32].

Kinematic data preprocessing

The preprocessing of the kinematic data is less extensive than the preprocessing of the EEG data. To reduce random noise it is recommendable to use a Moving Average (MA) filter.

A MA filter operates by averaging a number of points from the input signal to produce each point in the output signal [33]. This can be written according the following equation, in which M is the span of the filter:

$$x[i]^{MA} = \frac{1}{M} \sum_{j=-\frac{M-1}{2}}^{\frac{M-1}{2}} x[i+j] \quad (2.2)$$

Feature Extraction

Usually MTP BCIs employ a time series of bandpass-filtered EEG potentials for reconstructing the trajectory of a 3D limb movement. Interestingly for this model the best results are reported in the low frequency ($< 4\text{Hz}$) time-domain, e.g. in [7], [25] or [34]. For a long time it was assumed that the traditional mu and beta bands used in SMR-based BCIs are rather associated with general movement activity but contain only little information about movement trajectories. However, Korik et al. proved in [35] that the mu and beta bands provide good information about the trajectories, when using instead of a time-series of EEG potentials a time-series of power spectral values as features. With the replacement of the standard model by this feature Korik et al. could even increase the accuracy of MTP BCIs. Because of the results of Korik et al. and the insight, that these results are consistent with the extensive literature on traditional SMR-based MC BCI studies, which report the best accuracy of limb movement classification using power values of mu and beta frequency bands in the following is only the BTS model described.

The BP is calculated separately for the different separated frequency spectra and channels of the EEG according to the following equation:

$$B_{fn}[t] = \frac{\sum_{m=1}^M |S(m)_{fn}[t]|}{M} \quad (2.3)$$

In this equation represents $B_{fn}[t]$ the calculated BP value from EEG channel n and bandpass filter f . t means the time window, M the number of samples in this time window and $S(m)$ is the m 'th bandpass-filtered sample within the time window. The time windows are overlapping and shifted for a specific range to match the kinematic sample rate.

After the calculation of the BP values, the values were standardized. The standardized difference results as the quotient of the BP values with the standard deviation of the BP values:

$$S_{fn}[t] = \frac{B_{fn}[t]}{\sigma_{B_{fn}}} \quad (2.4)$$

The most common used kinematic feature is the velocity, which can be calculated from the measured points, according to the following equation, in which $v_i[t]$ is the velocity in i direction at the time point t :

$$v_i[t] = \frac{x_i[t] - x_i[t - 1]}{\Delta t} \quad (2.5)$$

2.5.5 Development of a Trajectory Decoder

Prediction of Trajectories

The prediction of the motion trajectories takes place in two steps:

- first, finding a correlation between the kinematic and brain data and
- second, reconstructing the trajectory by using the found correlation

To enable a prediction of trajectories, the data set need to be separated in a training set, which is used to find the correlation between the brain and the kinematic data, and in a test set, which is used to apply the results from correlation to predict the trajectories. Often the data are separated by a k-fold Cross-Validation (CV). In this method, the data set is divided into k subsets, which can be redistributed in randomized subintervals [36]. Each time, one of the k subsets is used as the test set and the other k-1 subsets form together a training set. After every calculation, another subset is defined as test set. At the end, the average error across all k trials is computed. The advantage of this method is, that the variance of the estimated results from new predictions decreases. The higher the number of folds, the lower the variance, however with a larger number of folds increase the computational effort.

For the prediction of the trajectories mostly the model presented by Bradberry et al. in [25] is used. In this model a linear relationship between the three orthogonal velocities and the standardized and differenced voltages is calculated for all sensors in all frequency spectra separately by using a multiple linear regression (mLR). In the BTS model of Korik et al. [12], the standardized temporal difference from bandpass-filtered EEG potentials was replaced with the standardized BP values, according to the following equation:

$$v_i[t] = a_{if} + \sum_{n=1}^N \sum_{k=0}^L b_{ifnk} S_{fn}[t-k] + \varepsilon[t] \quad (2.6)$$

In this equation the in Equation 2.4 calculated standardized differences of the BP $S_{fn}[t]$ with the timelags k (temporal difference between kinematic and brain data) are the independent input variables and the velocity components $v_i[t]$ for the three spatial dimensions i are the dependent output variables. a_{if} and b_{ifnk} are regression parameters that learn the relationship between the input and the output in the training sets, while $\varepsilon[t]$ is the residual error.

Practically does this mean that firstly in the training sets with the included features "standardized velocity" and "standardized BP" the regression parameters a_{if} and b_{ifnk} are calculated and then, with these parameters in the test sets the dependent velocities can be predicted from the independent BP components.

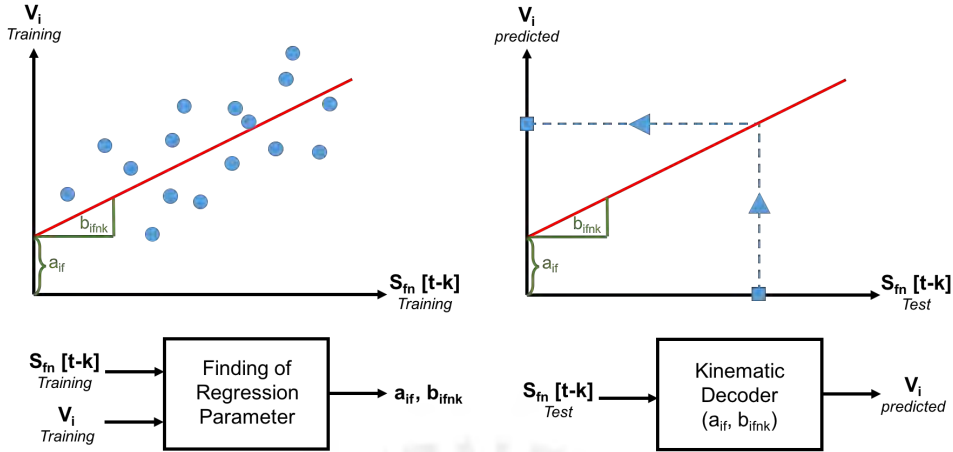


Figure 2.8: Two steps of the trajectory prediction. The figure shows the two steps to predict a trajectory from EEG data. First, in the training stage regression parameters are calculated, then in the test set, the trajectories can be reconstructed using the calculated regression parameters. For a better understanding the example is shown for a single linear regression where a one-dimensional regression line in a two-dimensional feature space is calculated. In a multiple linear regression, a $n-1$ -dimensional surface is calculated in a n -dimensional feature space.

Optimization of the Trajectory Decoder

An optimization of the settings can enhance the results a lot. In this postprocessing the optimal timelag distance and number of timelags (embedded dimensions) should be found out and used for the prediction [12]. In general, a high amount of EEG channels is important to get as much information as possible about the relation between the brain and the kinematic data. However, it is shown that the model tends to overfit if there are too many channels used [25], so it is also recommendable to find an optimal EEG channel montage.

To find the optimal settings it is necessary to know about the decodable quality of the trajectories. To assess this quality the Pearson's Correlation Coefficient (CC) r can be used. The Pearson's CC r can be calculated between the known measured signal and the predicted decoder's output according to the following equation [28]:

$$r(x, \hat{x}) = \frac{\text{cov}(x, \hat{x})}{\sigma_x \sigma_{\hat{x}}} \quad (2.7)$$

In this equation x are the actual measured values, \hat{x} are the predicted values, and σ_x as well as $\sigma_{\hat{x}}$ are the standard deviations of x and \hat{x} , respectively.

2.5.6 Expectable accuracies

The accuracies (CC between the predicted and real trajectories) are difficult to compare because of the different movements that were predicted and the different features that were used. E.g.:

- Bradberry et al. [25] reached a mean accuracy of 0.19 in x, 0.38 in y and 0.32 in z direction by reconstructing hand movement from a time-series of EEG potentials.
- Paek et al. [27] reached a median accuracy of 0.36 for the reconstruction of finger movements from a time-series of EEG power values.
- Ofner et al. achieved in [7] mean values for 3D hand movement in x direction of 0.70, in y direction of 0.77 and in z direction of 0.62 and in [5] an average value of 0.64 of imagined movements in horizontal or vertical direction, the values were all calculated from a time-series of EEG potentials.
- Korik et al. [12] achieved a median accuracy of around 0.2 from a time-series of EEG potentials and around 0.45 from a time-series of EEG power values

The results by using of other calculation methods like the reconstruction from EMG signals or other non-invasive neuro imaging methods like MEG seem to be a little bit better:

- Choi [24] achieved an accuracy of around 0.8 for reconstructed joint angles from EMG signals.
- Yeom et al. [37] reported an overall accuracy of higher then 0.7 for the reconstruction of hand coordinates from MEG and

The following figure shows how the results of a prediction could be represented, when calculating the trajectory from the predicted velocities.

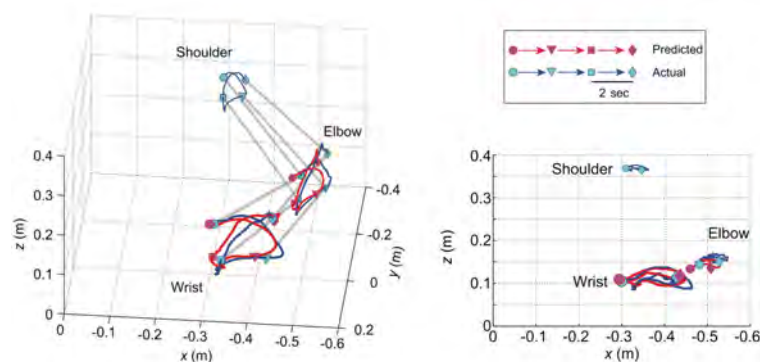


Figure 2.9: Predicted trajectories from ECoG data (adapted from [38]). The pictures show the comparison between actual and predicted trajectories for the three joints "shoulder", "elbow" and "wrist". In the left picture the trajectories are shown in a 3D space and in the picture at the bottom right the trajectories in a x-z plane.

2.5.7 Applications and future prospects

A long time the researchers focused mainly on the enhancement of conventional BCIs using classification. One reason for this lack of attention could be that the researchers were a long time satisfied with the results they got from the conventional technique. Another reason could be that for a long time it was thought that the most practical system for data acquisition - the EEG - does not provide sufficient SNR, bandwidth, and information content to decode kinematics [25]. For these reasons, applications that use from MI predicted trajectories are not known yet. However, some studies (see above) have shown that the concept is working and that it is possible to predict trajectories even by EEG signals.

For the future, a non-invasive position decoding system could be the basis to control e.g. a neuroprostheses in a natural manner, because with this technique the users don't need to learn new mental strategies to control the devices. Scientists like Ofner et al. [7] expect that the learning period should be substantially reduced.



3 Methodology

3.1 Introduction Methodology

In the Methodology chapter, an experiment similar to those already described in subsection 2.5.2, is carried out in order to find a correlation between movement and EEG data, which can subsequently be used for the prediction of motion trajectories. To make these results later useful for a PC application, the movements are performed within a field that is smaller than a 21" PC screen. In the experiment, vertical and horizontal movements are carried out since the prediction of alternative trajectories, is assumed to be calculated from the superposition of a vertical and a horizontal motion. To make the experiment more realistic with respect to the development of an application for drawing shapes, the participants take a pencil into their hands while executing the movements. When executing such drawing movements in the vertical plane the movements are almost exclusively from the shoulder joint while the elbow and the wrist are stiff, it is assumed that the correlation between EEG and kinematic data is higher when only a single joint is moved, hence it is expected that the accuracies of the predicted trajectory are also higher.

3.2 Description of the experiment

The goal of the experiment is to get a correlation between the kinematic and the brain data. To get this correlation, as it was explained in the chapter "State of the art", the participants must do real movements while the kinematic and brain data are recorded.

In this experiment, the participants are sitting comfortable on a chair in front of a plate with targets. The participants are holding a pen in their right hand and do self-initiated movements from a center point to a target and back to the center point with slightly angled right arm. The left arm lies banded in a relaxed position on the left thigh. The plate is located in around 1.50 m distance to a kinematic data acquisition system. For the recording of the EEG data, the participants have a cap with EEG electrodes on their heads. To reduce the artifacts the participants are instructed to stare at the center point of the target plate and to avoid any other movements than the instructed ones.

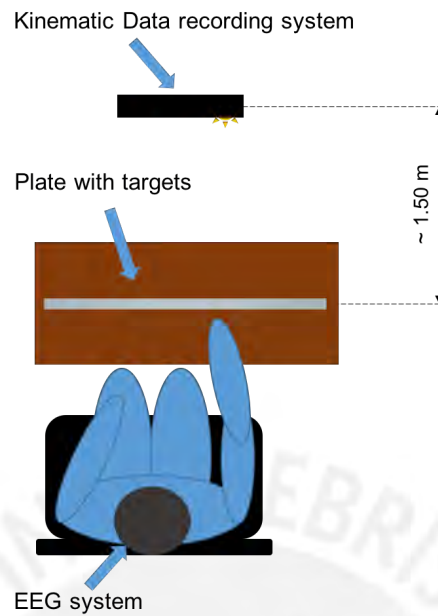


Figure 3.1: Principal structure of the experimental setup. The experimental setup consists of a plate with targets, to which the user have to do self-initiated movements, a kinematic data recording system in a distance of around 1.50 m, and a participant with an EEG cap on his/her head.

The target points, as well as the center point are placed on an acrylic glass plate. Two targets are placed on the right and left side of the center point in a horizontal distance of 10 cm to the center point each. The other two targets are placed above and below of the center point in a vertical distance of 10 cm each.

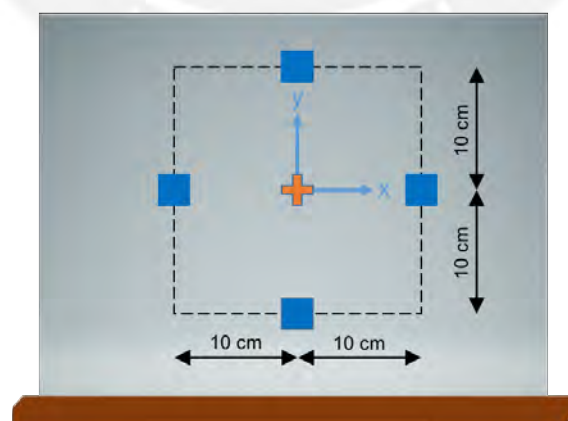


Figure 3.2: Plate with targets. On a plate of acrylic glass are 4 target points (blue squares) and 1 center point (orange cross) placed. The target points are located at a horizontal or vertical distance of 10 cm to the center point.

3.3 Participants of the experiment

In this experiment participated, voluntarily a right-handed male with an age of 25 years. The participant had no medical history that might interfere with the task. The study was approved by the *Comité de Ética de la Investigación* of the *Pontificia Universidad Católica del Perú* (see subsection A.5.4). The participant gave a written informed consent prior to participation (see subsection A.5.3).

3.4 Experimental Task

To synchronize the movements, the participant had to do center-to-target and target-to-center movements, each in 0.5 s. Between the movements the participant had 0.5 s to rest. The center-to-target movements were indicated by a 6 kHz tone, the target-to-center movements by a 4 kHz tone. The tones came from the loudspeaker of the computer. In the resting phases there were no tones played by the computer.

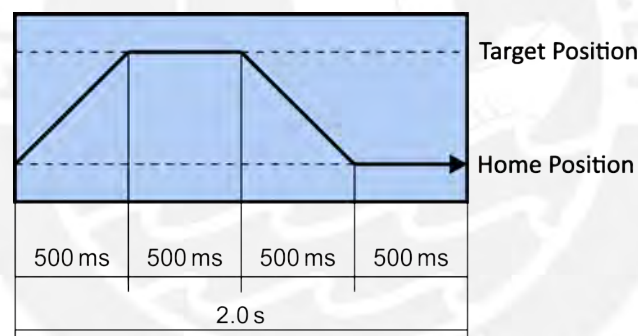


Figure 3.3: Movement Cycle. The figure shows the time course of a Movement Cycle. The participants have 0.5 s to move the hand from the center position to a target position, 0.5 s to rest, 0.5 s to go back to the center position and finally 0.5 s to rest again.

A Movement Block (MB) consists of 12 Movement Cycles and last 24.0 s hence. During this time the participant was not allowed to blink, to move his eyes or to make any other limb movements.

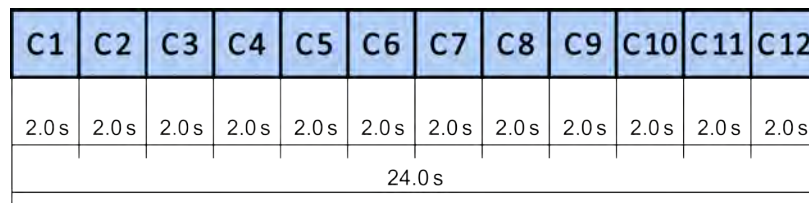


Figure 3.4: Movement Block. A MB consists of 12 Movement Cycles (C), which last 2.0 s each. Hence, the resulting time of a MB is 24.0 s.

The experimental session consists of 8 MBs. Before every MB there were a 8 s lasting initialization phase, which were indicated by a 5 s durable *initialization sound*. In this phase the participant had to make two waves with both arms over his head. Immediately afterwards the participant had to take the target position, relax and wait for the start of the experiment. The waving over the head was necessary because otherwise the used kinematic tracking system wouldn't have recognized the skeletal points. Before the initialization phases, there were breaks of 20 seconds. In the first 17 s of these phases a relaxing melody was played. The participant should use the break to relax his eyes. After the MBs, there were phases in which the metadata of the Kinect had to be saved. The total time of the experimental task had a duration of 8 min. The reason why these numbers of MBs and Movement Cycles per block were chosen is explained in section A.3.1.

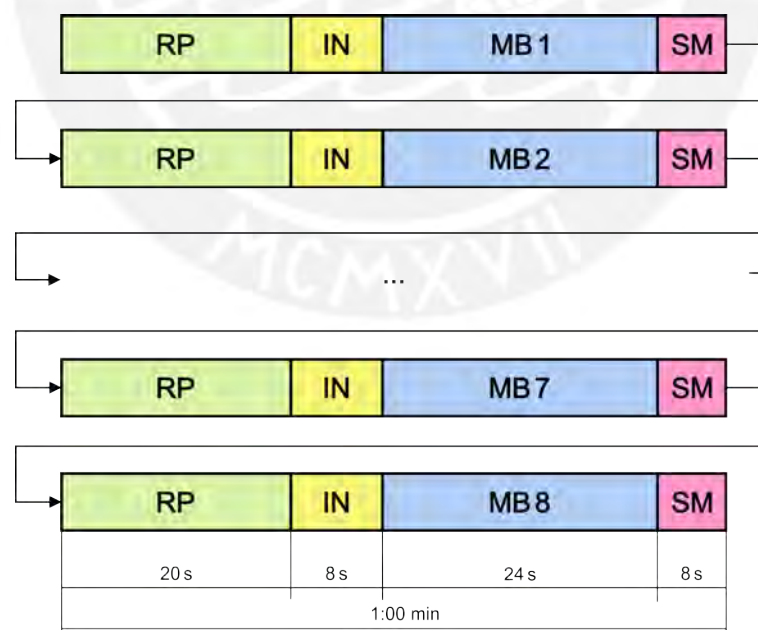


Figure 3.5: Time course of the experiment. The experiment consists of 8 MBs (MBX), which last 24 s each. Before every MB there are a 8 s durable Initialization Phases (IN) and before that, 20 s lasting Relaxing Phases (RP). After the MBs are 8 s lasting phases to save the metadata (SM) from the Kinect. Hence, the total duration of the experiment is 8 min.

3.5 Data Acquisition

3.5.1 EEG Data Acquisition

The EEG data were recorded with the g.Nautilus Research Headset from g.tec [39]. The system consists of 32 active dry electrodes with 8 pin gold-alloys (g.SAHARA), which are prefixed mounted on an elastic cap (g.GAMMAcap) and positioned according to the 10-20 method.

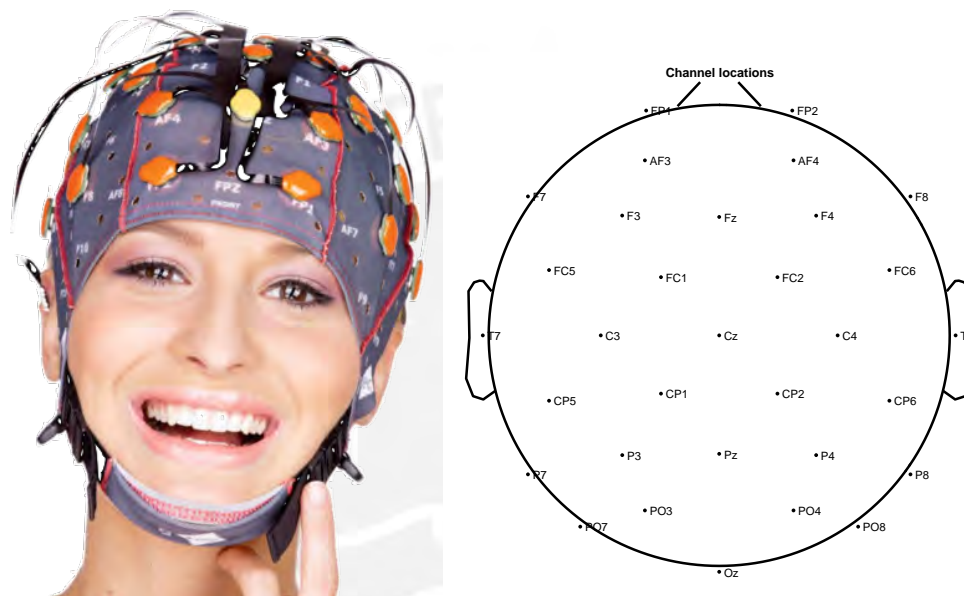


Figure 3.6: Used EEG System [39]. The figure shows on the left the g.Nautilus Research Headset with the g.GAMMAcap and g.SAHARA electrodes and on the right the available electrodes for the used 32 channel version.

The EEG data were recorded with 32 active dry electrodes with an impedance higher than $100\text{ M}\Omega$, an input sensitivity of 562.5 mV , a sampling rate of 250 Hz and (according to [40]) a 24 Bit resolution, which leads to an oversampling of 4096, yielding a high SNR. The reference and the ground electrode were positioned behind the participants ears. The signals were low-pass filtered with the amplifier at a frequency of 10.23 kHz [40]. No other filter were used. The digitized data were sent via a wireless data link to a Base Station that was connected to the PC [40].

Before the use of the EEG system, the participant was asked to remove his electronic devices from his pockets and to touch a metal grounded object to protect from electrostatic discharge (ESD).

3.5.2 Kinematic Data Acquisition

For the acquisition of the kinematic data the Kinect[®] for Windows[®] v2 system was used. This system consists of the Kinect for Xbox One sensor and the Kinect Adapter for Windows [41]. The Kinect for Xbox One sensor includes a [42]:

- Depth sensor, which has a resolution of 512 x 424 pixels, an image frequency of 30 frames per second (fps) and works in a distance from 0.5 to 4.5 m.
- Color camera, which has a full HD resolution of 1920 x 1080 pixels, and an image frequency of 30 fps (in low light 15 fps).

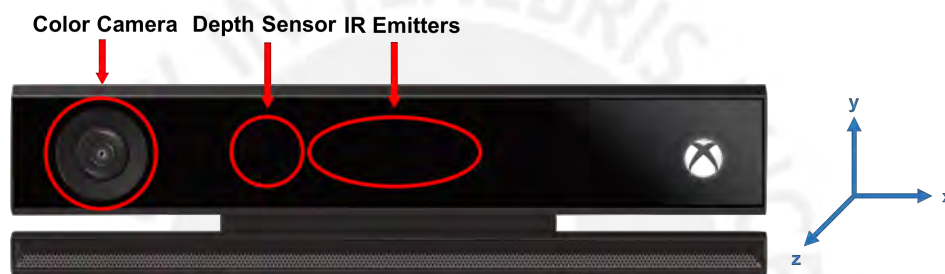


Figure 3.7: Kinect for Windows v2 (adapted from [43]). The Kinect System has, among other components, a color camera and a depth sensor, which works with three infrared light emitters. The orientation of the measured coordinates is according to the coordinate system on the right.

With the depth sensor it is possible to track 25 skeletal points with a high stability and anatomically correctness of up to 6 people [42]. The trackable skeletal points are [44]:

- | | | | | |
|------------------|-----------------|------------------|------------------|---------------|
| • spine base | • left shoulder | • left thumb | • right hand tip | • left foot |
| • spine mid | • left elbow | • right shoulder | • right thumb | • right hip |
| • spine shoulder | • left wrist | • right elbow | • left hip | • right knee |
| • neck | • left hand | • right wrist | • left knee | • right ankle |
| • head | • left hand tip | • right hand | • left ankle | • right foot |

According to the results of the preliminary tests (see subsection A.3.2), the best kinematic results for the experiment have been achieved when tracking the right hand skeletal point.

3.6 Implementation of the experiment

The available EEG system from g.tec (see section 3.5) is designed to be controlled by Matlab[®] and Simulink[®]. Since the Kinect system can also be controlled relatively easy with the Matlab

Image Acquisition ToolboxTM, it seems optimal to implement the entire data acquisition as well as the playing of the necessary sounds and tones for the synchronization of the movements in the Matlab environment.

Since both data recording systems are very computationally intensive (see section A.3.1), the EEG and the Kinect data acquisition were done on two different computers.

For the experiment two computers were used; each with an i7 processor up to 3 GHz and 8 GB random access memory (RAM). The EEG data acquisition via Simulink was done on one computer; and the Kinematic data acquisition, as well as the play of the tones and sounds for the movement synchronization using the Kinect v2 system via Matlab were done on the other computer. To enable a later synchronization of the data, the clocks from both computers were before the start of the data acquisition synchronized with the time server of the "Physikalisch-Technische Bundesanstalt" in Braunschweig (Germany), which uses an atomic clock [45].

The Simulink model, shown in Figure 3.8 was created for the EEG data acquisition. The model uses the g.Nautilus Highspeed block, that provides a graphical interface to the g.Nautilus hardware, which can be used to specify the amplifier properties and to acquire the data [46]. The "unbuffer" and "Data Type conversion block" is necessary to write the data provided from the "g.Nautilus" in a Matlab variable. The lower part of the model was created to save a time stamp since the g.Nautilus block does not provide the absolute time. At the simulation time point 0.004 s (1/250 Hz), a "step" block creates a step, which is detected and converted to "1" from the "detect change" block. From this value, a constant value of 0.5 is subtracted, thus a value of +0.5 reaches a triggered subsystem at the time point 0.004 s. At the time point 0.000 s, there is no step detected, which means that a value of -0.5 reaches the triggered subsystem. Because of the change from -0.5 at time point 0.000 s to +0.5 at time point 0.004 s, the "trigger" in the subsystem effects that at the time point 0.004 s the absolute time is queried from the system and then written into a Matlab array.

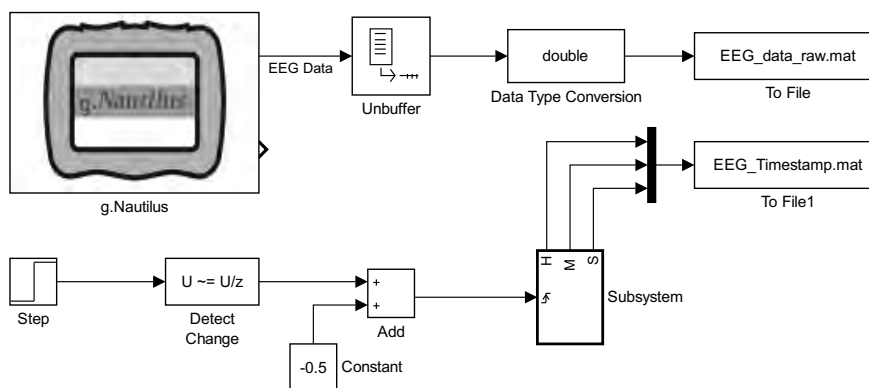


Figure 3.8: Simulink model for the EEG data acquisition. The upper part of the model provides the acquisition of the data and the transfer into a Matlab array; the lower part is to take a time stamp at the beginning of the acquisition and to copy this time stamp into another Matlab array.

From the 32 acquired EEG channels all up to the two most frontal electrodes *FP1* and *FP2* were used. These two electrode channels were excluded since the signals are resulting from their location particularly vulnerable to EOG artifacts [26].

Since the processing can be done offline and hence practically no limits exist for the selection of the frequency filters, there was no need for using the implemented 8th-order Butterworth digital filters of the g.Nautilus EEG [46] while recording the EEG data.

The script to acquire the Kinect data and to play the sounds for the movement synchronization was written according to the following flow chart.

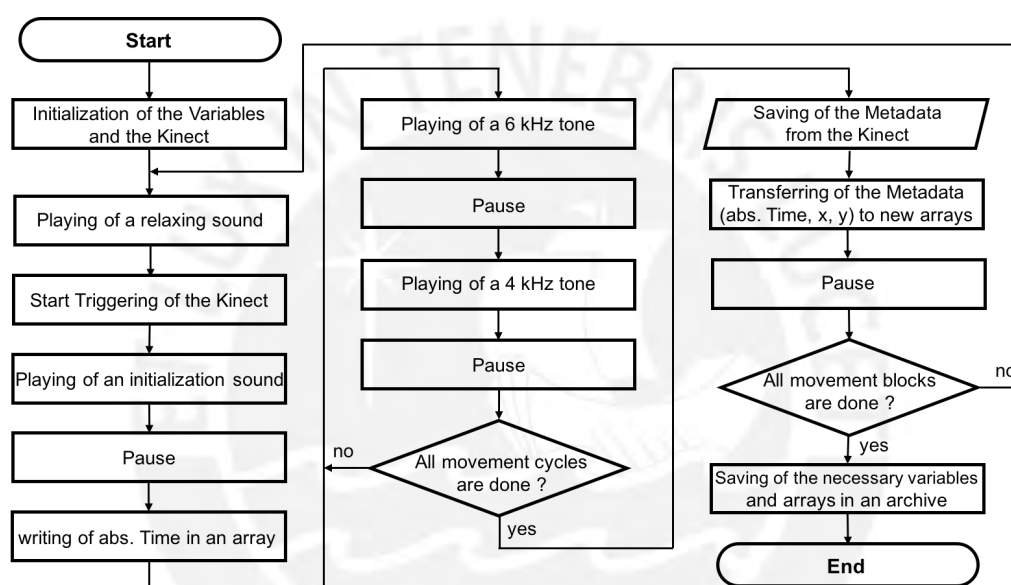


Figure 3.9: Programming scheme for the experiment.

The experimental setup was constructed according to the preliminary test results (see section A.3.3).

The target plate was clean, it was not in a parallel position to any active screens, it was located in a right angle compared to the windows and shielded from punctual light. The participant sat close with his back to a bright wall and he was not allowed to wear loose clothes. The plate was subsequently horizontal, parallel to the Kinect, shifted till there was no more reflection of the infrared light from the Kinect depth sensor (see Figure A6).

The distance between the Kinect and the target plate were estimated. The horizontal level of the Kinect and the plate has been adjusted by a Carpenter's level. Finally, the plate was fixed with vises on the table to reduce vibrations if the plate is inadvertently touched during the experiment.

Figure 3.10 shows the theoretical structure of the experimental setup and Figure 3.11 shows its implementation.

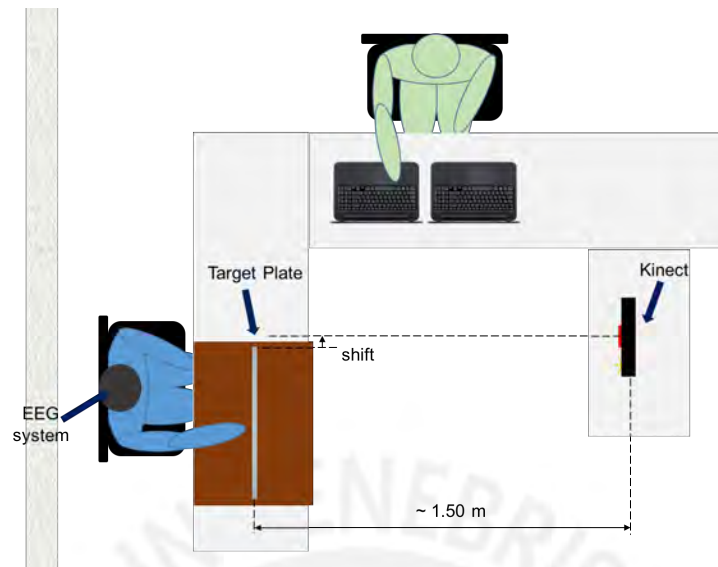


Figure 3.10: Theoretical structure of the experimental setup The figure shows that the Kinect should be placed in a distance of around 1.5 m and parallel shifted to the target plate. Furthermore the participant (blue person) should be close to a bright wall and the computer screens should not be directed toward the target plate as this can produce reflections or distract the participant.



Figure 3.11: Implementation of the experimental setup. The two pictures were taken during preliminary tests for the experiment.

3.7 Signal Processing of the experiment

3.7.1 Overview of the Signal Processing

The Signal Processing of the experimental data was done according to Figure 3.12. The steps are explained in detail in the following.

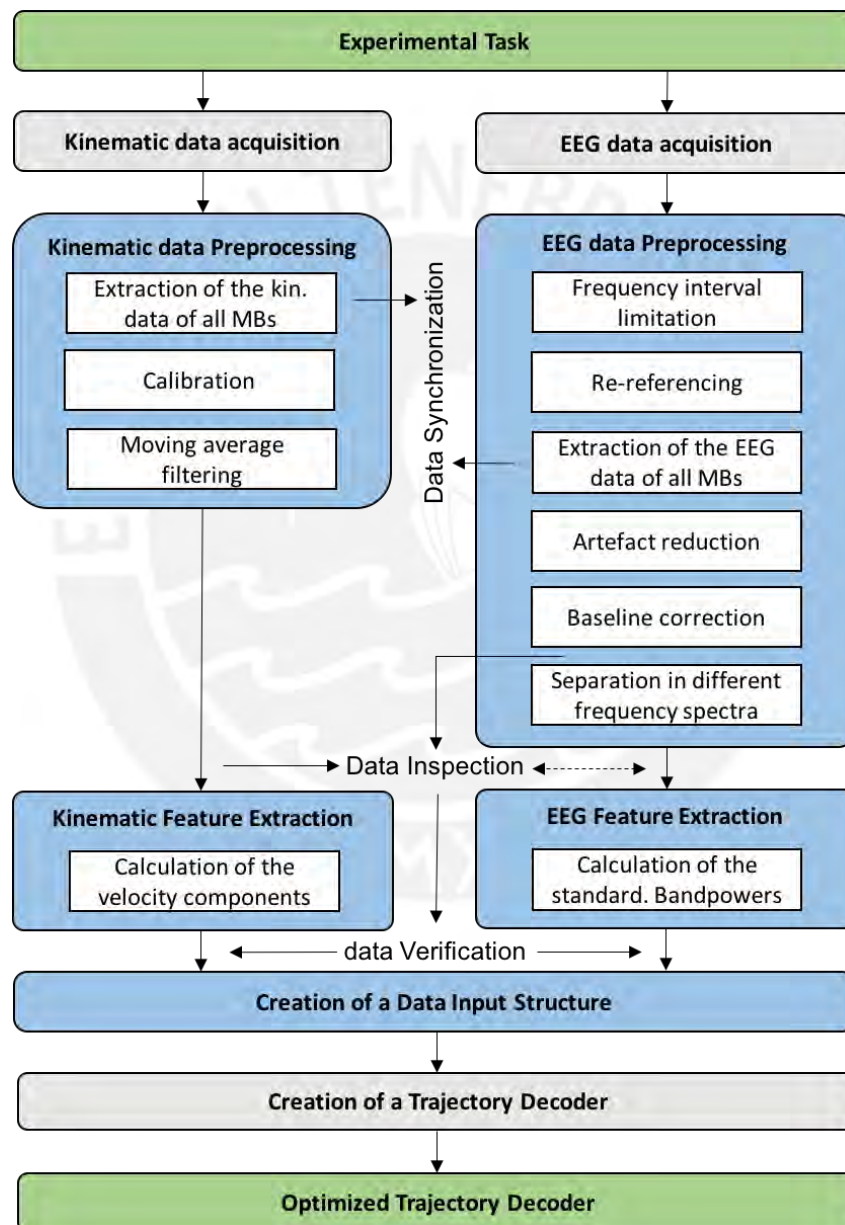


Figure 3.12: Signal Processing scheme for the experiment. The scheme shows all the steps in order from the Experimental Task to reach an optimized Trajectory Decoder. The steps in the blue boxes are the Signal Processing steps, which are explained in this section, the gray boxes above were already explained in section 3.5 and the gray box below will be specified in section 3.8.

3.7.2 Kinematic Data Preprocessing

Extraction of the kinematic data of all Movement Blocks

The first step of the kinematic data preprocessing was to extract the kinematic data for all MBs. To enable this, the start times, written immediately before the first beep of every MB (see Figure 3.9) were used.

Calibration of the kinematic data

A calibration for the kinematic data is not necessary, however it makes the visual inspection of the data easier. To calibrate the system, the mean values of the last 15 measurement points of the initialization phases were calculated for each data block (initialization phase + movement block) and after that these values were subtracted from all measured values of the data blocks.

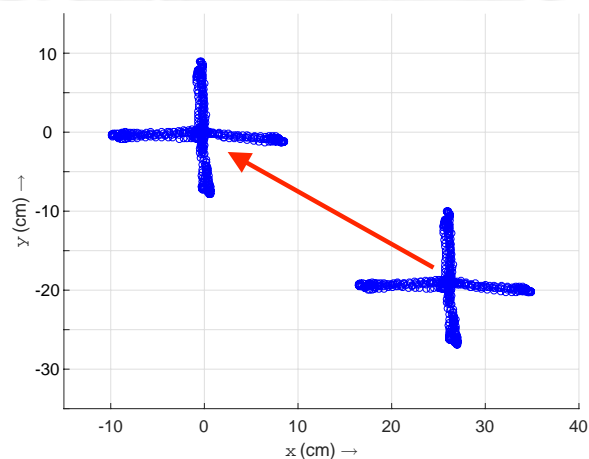


Figure 3.13: Calibration of the kinematic data. The figure shows the measured points of the first MB in an x-y plane before and after the calibration.

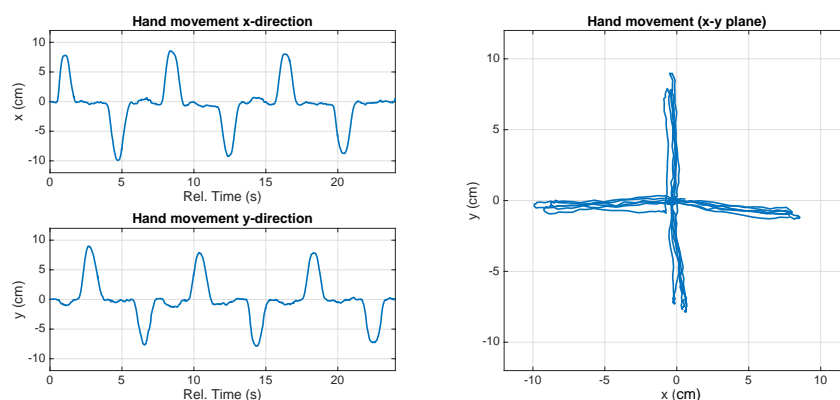


Figure 3.14: Calibrated kinematic data. The figure shows the kinematic data of the first MB after the calibration in time-courses and in an x-y plane.

Moving Average filtering of the kinematic data

The kinematic data in Figure 3.14 don't look noisy, however, to prove if the Kinect's data really don't include kinematic noise, the data were transformed into the frequency domain and their plots were examined.

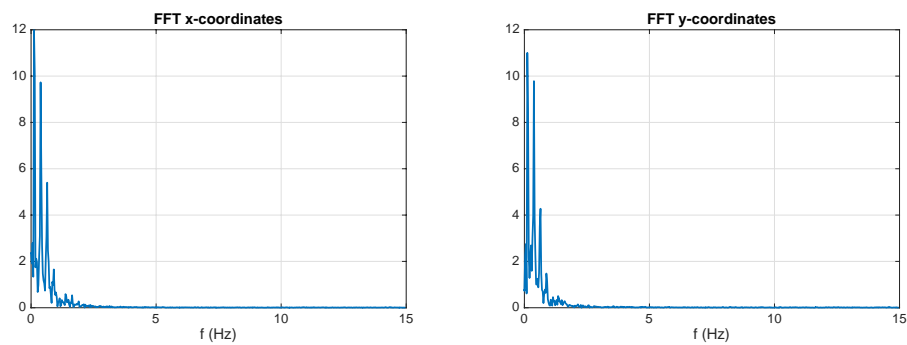


Figure 3.15: Fourier-Transformation of the kinematic data. The plots show the FFT of the data from the first MB. There were no movement data with a frequency higher than 2 Hz detected, what means that the recorded data of this MB do not have any higher-frequency kinematic noise.

As you can see in Figure 3.15, in this MB, there was no signal higher than 2 Hz recorded, what proves a good quality of the recording. However, when examining a plot of the trajectory in the x-y plane in detail, you can see that the signal makes small peaks, which presumably lead to a poor correlation between kinematic and EEG data.

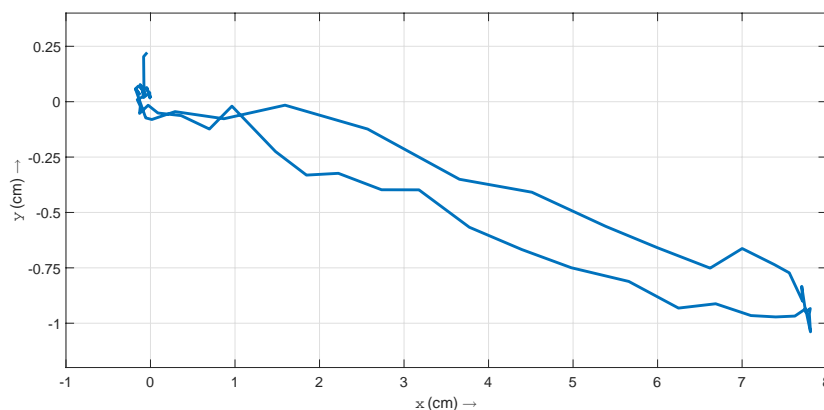


Figure 3.16: Original trajectory of a Movement Cycle. The figure shows the original trajectory of the first Movement Cycle of the first MB.

A way to smooth these peaks is by filtering the signal with a MA filter. A MA filter calculates the mean value of a value with its preceding and following values. To find out which span (number of preceding values + number of following values + 1) for the MA filter is best suited

for the actual problem, the trajectory to the first target point and back to the center point was plotted in the x-y plane and overlaid by MA smoothed versions of this trajectory.

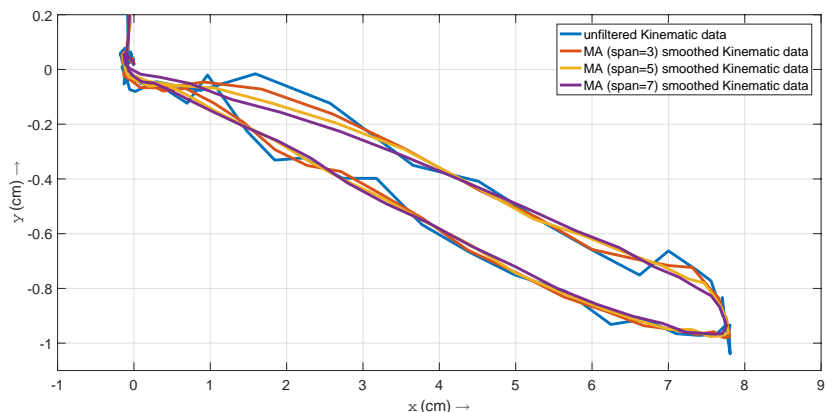


Figure 3.17: Comparison of Moving Average smoothed movement trajectories. In the figure the original trajectory for a Movement Cycle is compared with the results of by Moving Average filters of different spans smoothed trajectories .

The by a MA filter with a span of 5 smoothed trajectory seems to be optimal, because it is smoother than the trajectory filtered by a MA with a span of 3 and it is similarly smooth as the trajectory filtered by a MA filter with a span of 7 but closer to the original trajectory. In order to be able to recognize the result in a better way, in the following figure there is only the by a MA filter with a span of 5, smoothed trajectory plotted.

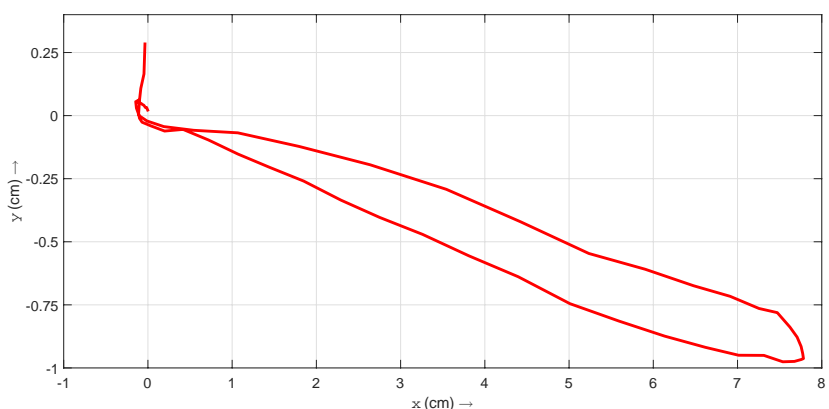


Figure 3.18: Final Moving Average smoothed movement trajectory. The figure shows the final movement trajectory, which was filtered with a MA filter of a span of 5.

3.7.3 Kinematic Data Feature Extraction

As kinematic feature for the calculation of the correlation between the kinematic and EEG data the velocity of the movements is used. The velocity was calculated outgoing from the

preprocessed kinematic data according to Equation 2.5.

When looking at the plots of the time-courses of the velocity components, the signal looks noisy.

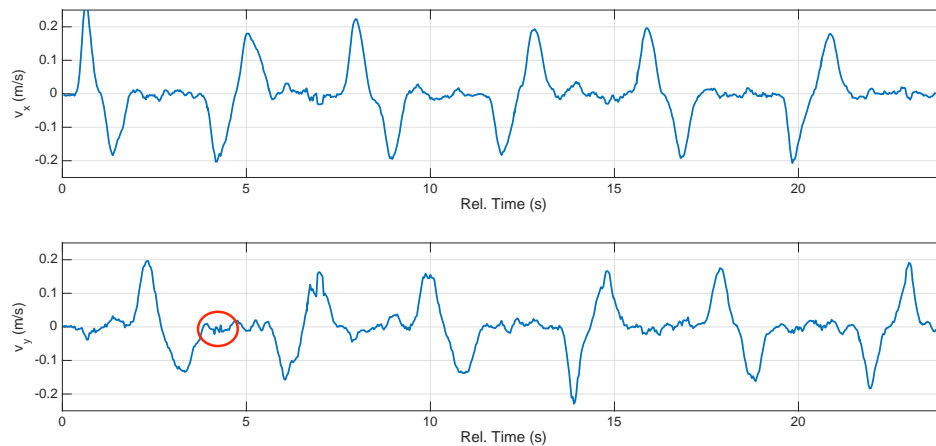


Figure 3.19: Time-course of the velocity data. The time course of the velocity data shows a little noise, e.g. in the red marked area.

For this reason, the data of the velocity components were smoothed again with a MA filter of a span of 5.

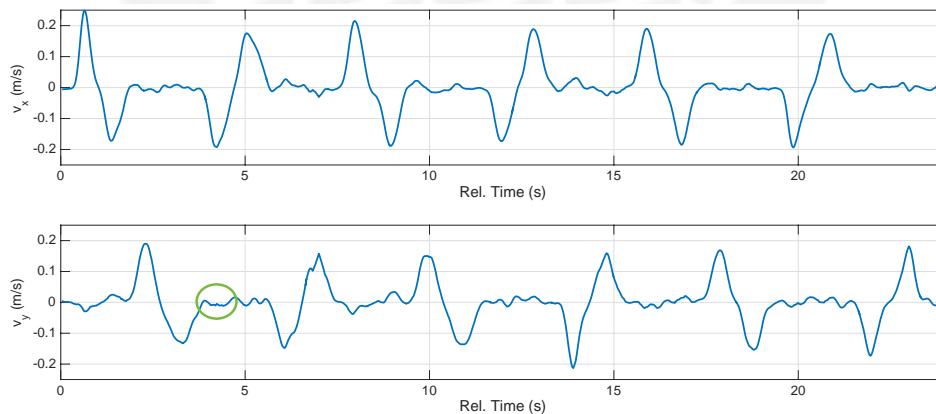


Figure 3.20: Time-course of the smoothed velocity data. Smoothing of the velocity data has reduced the noise as seen in Figure 3.19.

This second kinematic filtering does not seem to be imperative, however when reconstructing the trajectory of the data and comparing it with the trajectory after the first filtering in an x-y plane it does not seem to bring any disadvantages.

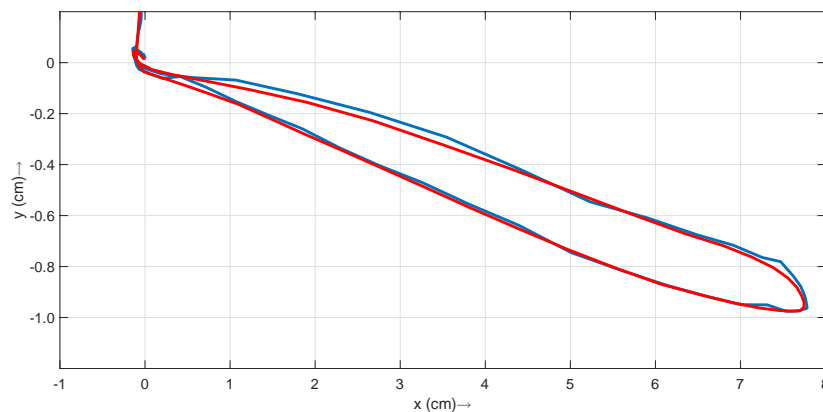


Figure 3.21: Comparison of the trajectories of a Movement Cycle. The trajectory in blue is the trajectory of Figure 3.18 and the trajectory in red are the reconstructed velocity components after the second MA smoothing. The red trajectory is smoother but still very close to the original trajectory.

3.7.4 EEG data Preprocessing

Frequency interval limitation

As the first step of the EEG data preprocessing, the frequencies below 0.5 Hz and the frequencies above 40 Hz were eliminated. Since the processing can be done offline practically no limits exist for the selection of the frequency filters. Due to their higher slope between the pass and stop band, it was assumed that FIR filters are more suitable for the offline processing. However, after using an FIR filter, it turned out that these filters could not filter frequencies below 1 Hz.

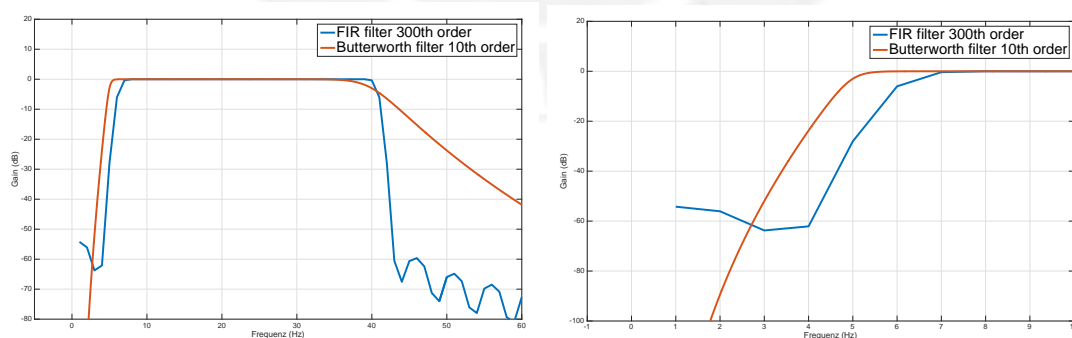


Figure 3.22: Comparison of an FIR bandpass and a Butterworth bandpass filter. The figure shows that the FIR filter cannot filter out frequencies below 1 Hz.

When applying IIR and FIR bandpass filters, with cutoff frequencies at 0.5 and 40 Hz (which are often used in the processing of EEG data) and comparing the results, it becomes clear that the FIR bandpass filter with a lower cutoff frequency at 0.5 is absolutely useless since by far the

largest part of noise of EEG signals is close to 0 Hz, like the Fast Fourier Transformation (FFT) shows. Hence it is necessary to have almost a IIR high-pass component.

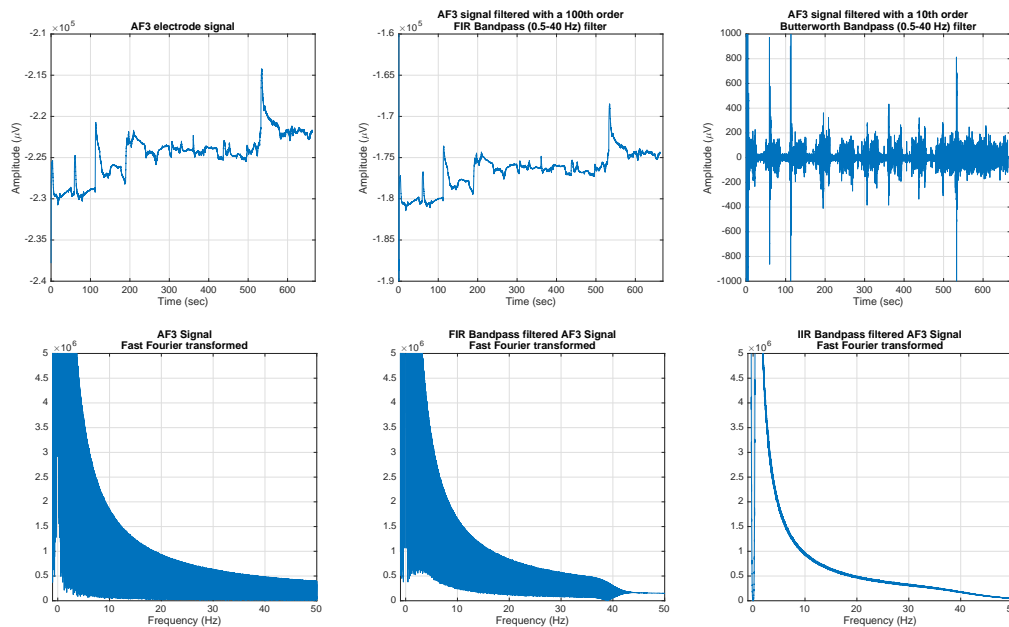


Figure 3.23: Results when filtering the EEG raw data with a FIR bandpass and a Butterworth bandpass. The figure proves that FIR filter, which cannot filter out frequencies below 1 Hz are not suitable for the filtering of EEG data.

Since the Butterworth bandpass has a weak slope between the pass-band and the second stop-band, it seems to be optimal to use a combination of a Butterworth high-pass with a cut-off frequency of 0.5 Hz and a FIR low-pass with a cut-off frequency of 40 Hz instead of a Butterworth bandpass.

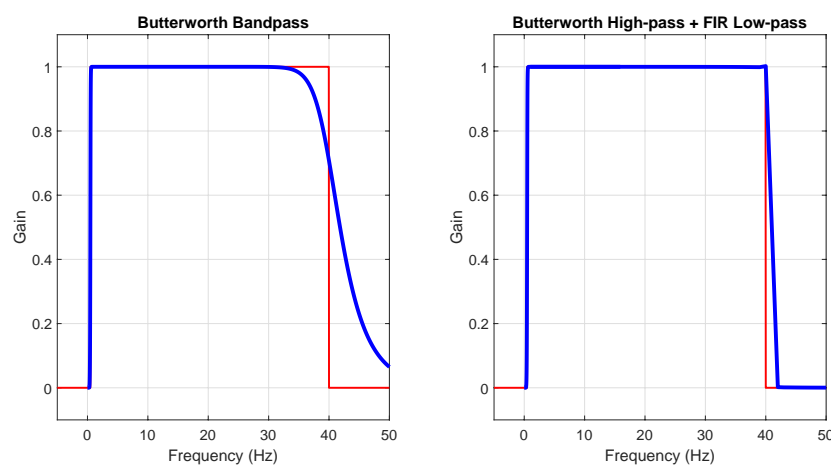


Figure 3.24: Comparison of a bandpass filter with a high- and low-pass filter in series. With a Butterworth high-pass and a FIR low-pass better filter properties as with a Butterworth bandpass can be reached.

A problem of FIR filters seems to be that these filters produce a high time delay because of its high number of filter coefficients, which would aggravate the calculation of the correlation between the EEG signals and the kinematic data. However, FIR filters have usually a linear phase [47], which leads to an overall frequencies constant group delay, which can be compensated easily.

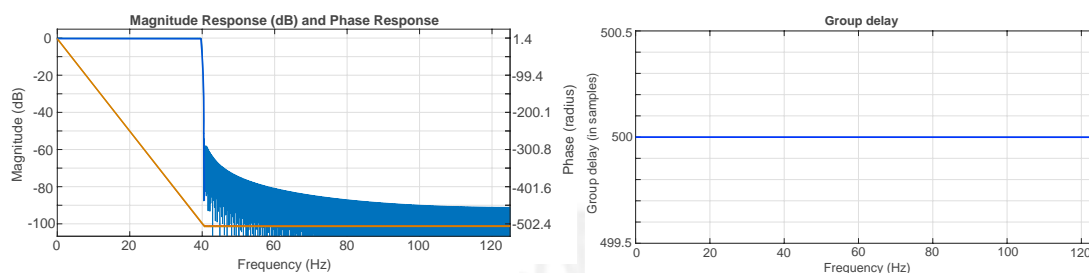


Figure 3.25: Properties of a FIR filter with 1000 filter coefficients. The figure shows the properties of a FIR low-pass filter with 1000 filter coefficients and a cutoff frequency of 40 Hz. In the left picture, the gain (blue line) and the linear phase (orange line) of the filter can be seen. In the right picture, the resulting linear group delay can be seen.

A way to compensate the time delays is to filter the signal first and switching the filtered signal in time afterwards. A more elegant way is to filter the signal with a zero-phase filter, which can be called by the matlab command "filtfilt" [48]. A zero phase filter reverses the filtered sequence and runs it back through the filter automatically.

As you can see in the following figure and in Figure 3.25, FIR filters have a constant time group delay of samples, which corresponds to the half number of filter coefficients. Here, a FIR filter with 1000 filter coefficients produce a time delay of 500 Samples, which is equal two a delay of 2 s at a Sampling Rate of 250 Samples/s.

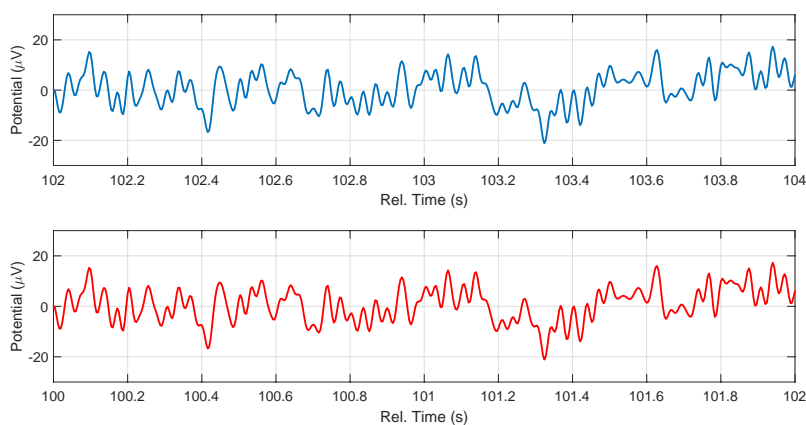


Figure 3.26: Comparison of a linear-phase and a zero-phase FIR filtered signal. The amplitudes of the signals are identical; the group delay is exactly two seconds for the linear-phase filtered signal over all measure points.

In contrast to FIR filters, Butterworth filters have a non-linear phase, which lead to non-linear time group delays. Normally the time delays of Butterworth filters are not high. However, when filtering close to 0, the time delay increases enormously. When, like here, a Butterworth high-pass filter of 8th-order with a cut-off frequency of 0.5 Hz is used, the time delay at 0.5 Hz after filtering is around 750 Samples, which means a time delay of 3(!) s at a Sampling rate of 250 Hz.

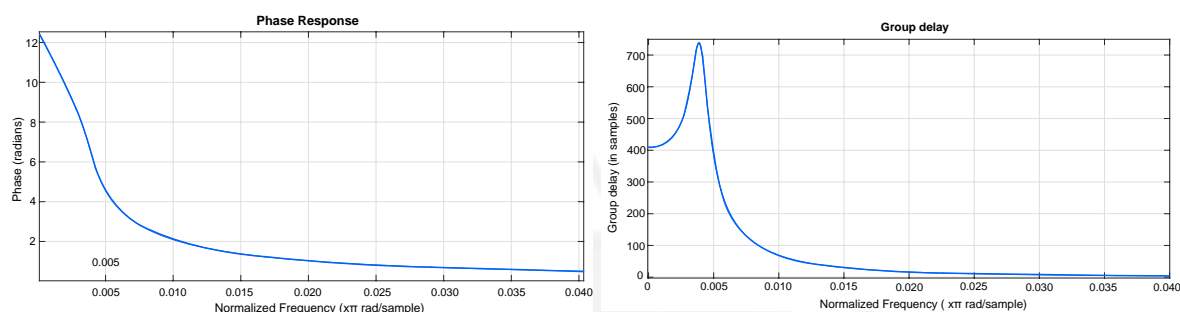


Figure 3.27: Properties of a Butterworth high-pass filter of 8th-order. The figure shows the properties of a Butterworth high-pass filter with an order of 8 and a cutoff frequency of 0.5 Hz. The picture on the left shows that Butterworth filters have a non-linear phase and resulting non-linear group delays (right picture).

IIR filters can, like FIR filters, also be constructed as zero-phase filters. However, when using this filter the values of the amplitudes can differ. In the following figure, a EEG raw signal can be seen, which were parallel filtered by a Butterworth high-pass non-linear and by a Butterworth high-pass zero-phase filter with cut-off frequencies of 0.5 Hz each. When comparing the both results, it can be seen that the amplitudes at around 60 Hz (power supply artifact) differ.

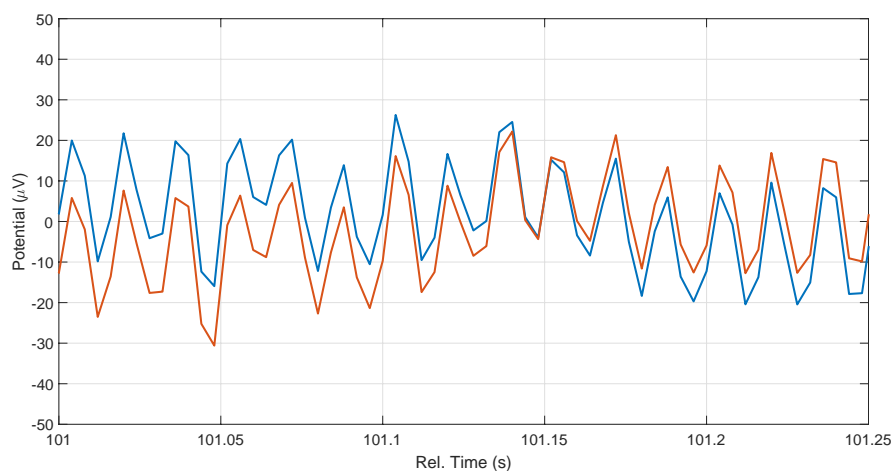


Figure 3.28: Comparison of the results of a zero-phase and a non-linear-phase FIR filtered signal. The figure shows that the amplitudes of the zero-phase filtered signal (orange line) differ to the non-linear-phase filtered signal (blue line).

The results of the filter tests showed that for the elimination of EEG signals below 0.5 Hz the signals need to be high-pass filtered with a Butterworth filter. Since a zero-phase Butterworth filter falsify the amplitude a normal (non-linear-phase) Butterworth filter was used instead. As a compromise of a high-slope between the pass- and stop-band, which requires a filter with a high filter order and a low time-delay, what is only guaranteed when using filters with low filter orders, a Butterworth high-pass filter with an order of 8 was used to limit the range below 0.5 Hz. Afterwards this elimination, the range higher than 40 Hz was limited with a window-based zero-phase low-pass FIR filter with 1000 filter coefficients.

Re-referencing

To enhance the focal activity from the local sources the signal was re-referenced. As re-referencing method re-referencing with a CAR was used. A CAR is the mean of all electrodes for every measured time. These values were subtracted from every electrode channel, according to the following equation:

$$X(t)_n^{CAR} = X(t)_n - \frac{1}{N} \sum_{k=1}^N X(t)_k \quad (3.1)$$

In this equation are $X(t)_n^{CAR}$ the re-referenced signals and $X(t)_n$ the signals before the re-referencing for the channels n at the time point t .

The difference between an original signal and a CAR re-referenced signal can be seen in Figure 3.29.

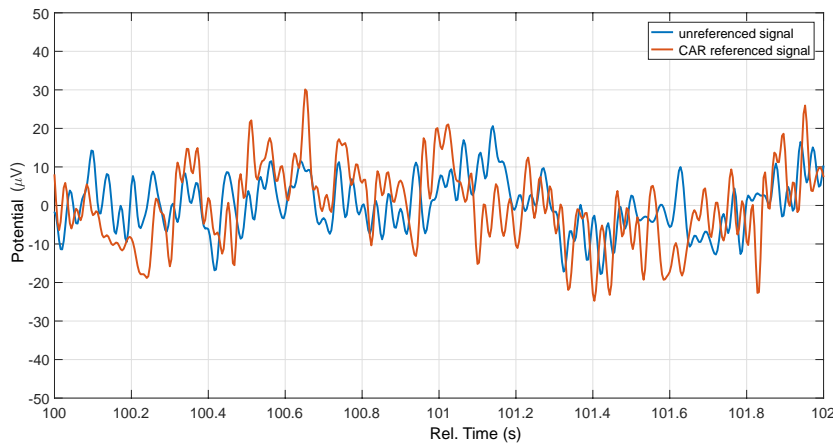


Figure 3.29: Re-referencing with a CAR. The figure compares a signal before (blue line) and after (orange line) the re-referencing with a CAR.

Extraction of the EEG data for all Movement Blocks

After the re-referencing, the EEG signals were extracted for all MBs using the EEG data time stamp (see Figure 3.8) and the start times of every MB written immediately before the first beep of every MB (see Figure 3.9).

Artifact reduction

After the extraction of the EEG data for all MBs the data could be visually checked for paradoxical phenomena.

One finding here was that when plotting the FFT of the EEG signals for a MB a peak at 30 Hz could be seen. Since the peak is relatively higher when observing only the data of the MBs as when observing the data of the whole measured time, it is assumed that it is an artifact, which occurs only or more intensively during the experiment. Due to the characteristic of the artifact (high peak at exactly 30 Hz) it can be assumed that this artifact is generated by the Kinect. Another finding was that the artifacts written by hand during the recording can be retrieved in the time course.

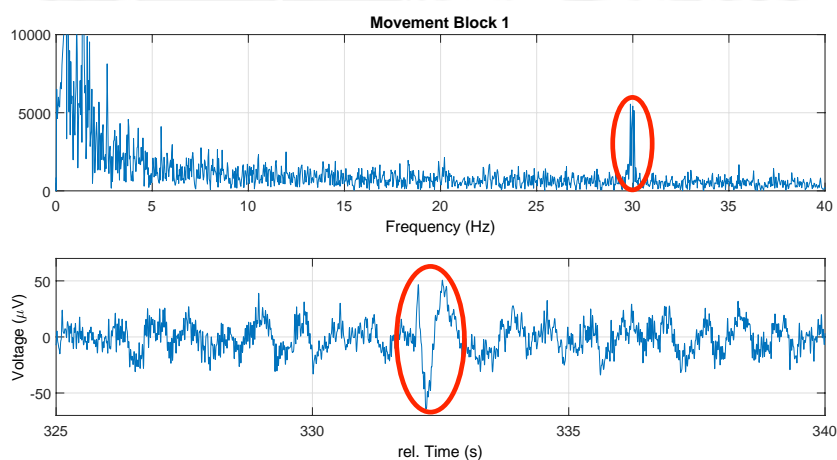


Figure 3.30: EEG artifact findings. The figure shows two EEG artifacts, evoked by the Kinect system (upper part, frequency course) and evoked by blinking (lower part, time course).

Since the Kinect artifact also occurred, when the with the Kinect connected PC was far away from the EEG system, it can be assumed that the artifact is directly produced of the Kinect system, for this reason it cannot be well shielded. Also, sometimes a blink cannot be avoided.

A possibility to deal with these artifacts is to make an ICA. In an ICA decomposition, the signals are separated into maximal temporal independent components (ICs). After an ICA ICs, which present noise, blinking artifacts etc., can be subtracted. For this project the ICs were calculated with the "runica" algorithm using the Matlab Toolbox "EEGLAB" [49].

Normally, in an ICA decomposition the number of ICs corresponds to the number of used EEG channels. However, in these datasets the rank (29) and the number of channels (30) differed. Since with EEGLAB it didn't work to reduce the number of ICs with a PCA to the number of rank in order to obtain proper results with an ICA, one channel was excluded from the ICA manually. Without doing this, the ICA would add noise to the datasets when subtracting an IC.

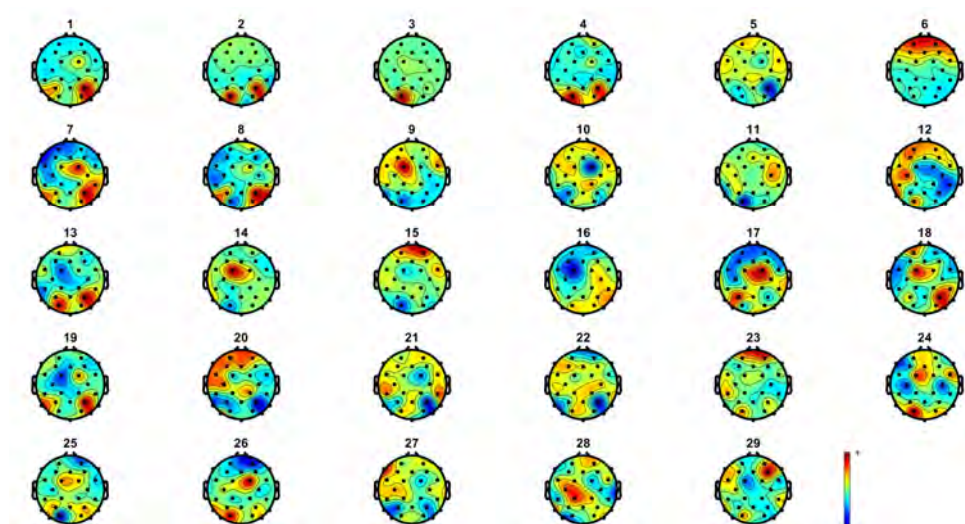


Figure 3.31: Calculated ICs by an ICA. The figure shows the 29 calculated ICs with its spatial occurrence.

IC 6 of Figure 3.31 can easily be identified as a blinking artifact because of the smoothly decreasing EEG spectrum and because of the strong-far-frontal projection shown in the scalp map (see Figure 3.32, left) [50]. To prove whether the IC is actually a blinking artifact, the plot of the channel activation (see Figure 3.32, right) can also be checked. Like you can see, the blink can be clearly identified at 13 - 14 seconds, (which is the same than in Figure 3.30 at the relative time of around 332 s).

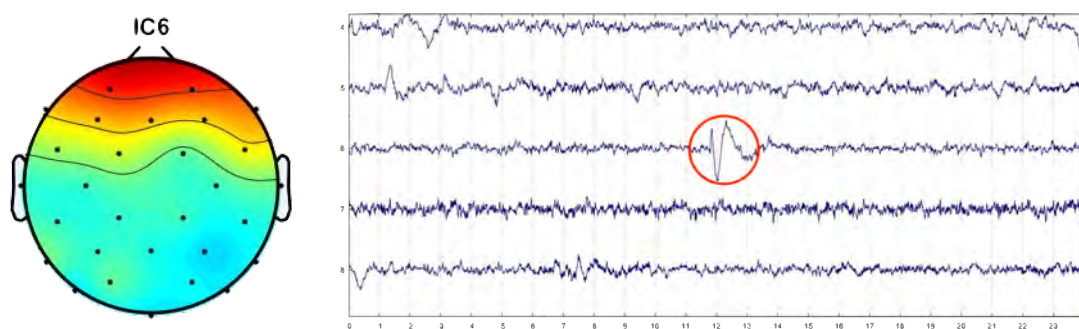


Figure 3.32: Channel activations of different ICs. The channel activation shows a strong impulse at IC 6 between the relative time from 11.5 to 12.5 s. Since at that time an artifact was suspected after writing down all times of blinking, this confirms the assumption that IC6 is a blinking artifact.

In the PSD (see Figure 3.33) can be seen that a portion of the Kinect artifact is presented in all ICs, which means that this kind of artifact is not temporal independent and hence, it cannot be subtracted by the use of an ICA.

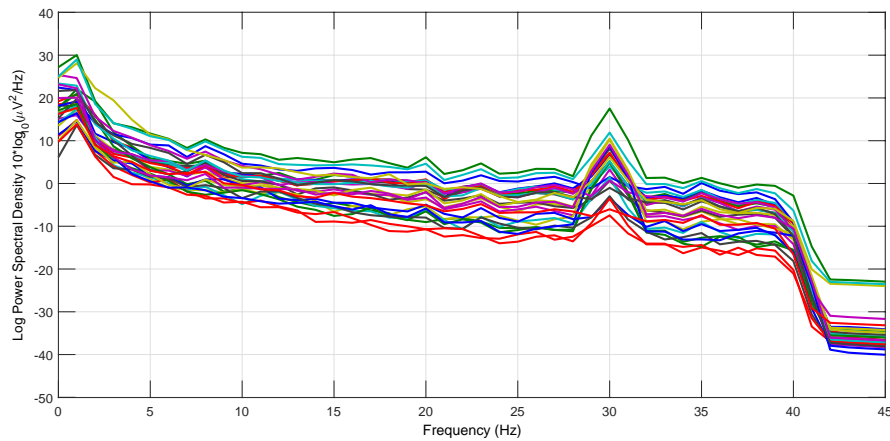


Figure 3.33: Power spectral density of the ICs. The figure shows the PSD of the 29 calculated ICs of the EEG signals for a MB. It is striking that the proportion of the Kinect artifacts is distributed over all ICs.

To reduce the artifacts, due to the results of the investigation of the ICA, the IC for the blinks were removed and the ICs showing Kinect artifacts were kept. Since it is expected that the most information necessary for the movement prediction can be found in the SMR, which are in the mu and low beta frequency band, the frequency space of around 30 Hz was excluded from further investigation. The following figure shows the same detail than the previous figures, before and after subtracting the IC of the blink.

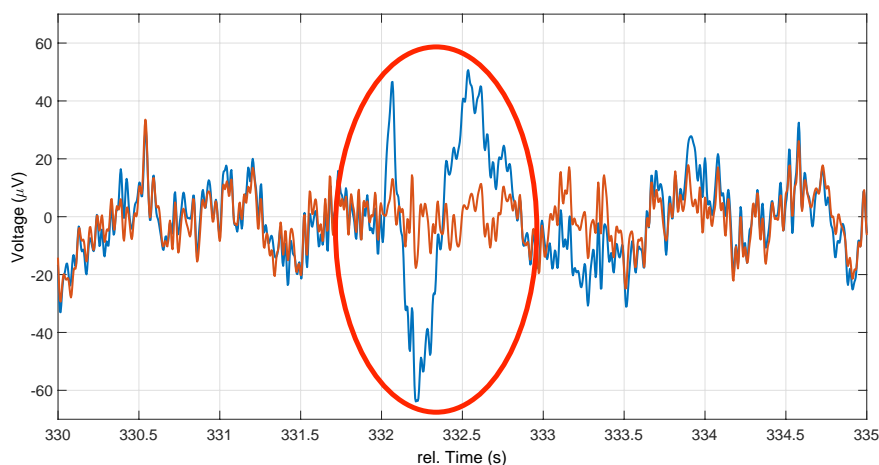


Figure 3.34: Blinking artifact reduced EEG signal. The figure shows an EEG signal with a blinking artifact (blue line) and the same signal after the removal of this artifact (orange line) by an ICA.

EMG and ECG artifacts could normally also be made visible with an ICA and subsequently be removed, however, to recognize these kind of artifacts is much more difficult and could not be done within this Master's Thesis.

Baseline Correction

To correct the baselines (DC offsets), the mean value of all time points were calculated for each EEG channel and subtracted from all EEG points in all MBs according to Equation 2.1.

Separation into different frequency bands

It can be assumed, that the CCs between the EEG data and the kinematic data are higher, when calculating the correlation separately for different frequency bands. For this reason the last step in the EEG data preprocessing is the separation of the signals in six non-overlapping frequency bands.

According to subsection 2.2.1 the signals were separated in the following frequency bands:

- Delta waves (0.5 - 3.5 Hz)
- Theta waves (3.5 - 7.5 Hz)
- Mu (Alpha) waves (7.5 - 12 Hz)
- Low Beta waves (12 - 18 Hz)
- High Beta waves (18 - 29 Hz,)
- Low Gamma waves (31 - 40 Hz)

The frequency space at around 30 Hz was excluded because of the artifact generated by the Kinect (see section 3.7.4).

To separate the signals in the different spectra, they were parallel filtered. Since the spectra was already limited from 0.5 to 40 Hz (see section 3.7.4), the lowest spectra were separated by a low-pass filter with a cut-off frequency of 3.5 Hz and the highest spectra were separated with a high-pass filter with a cut-off frequency of 31 Hz. All the other spectra were separated with bandpass filters. All the used filters were (like in section 3.7.4) zero-phase FIR filters with 1000 filter coefficients.

The following figure shows a section of the recorded signal separated into the six different, non-overlapping frequency bands.

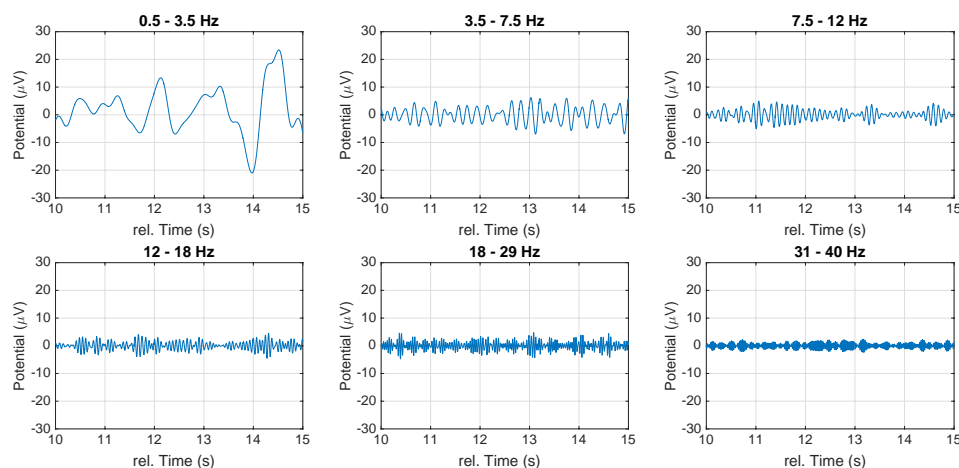


Figure 3.35: Six non-overlapping EEG frequency spectra. The figure shows the during the experiment recorded EEG signal at electrode *CP1*, separated in six non-overlapping frequency spectra.

3.7.5 EEG Data Feature Extraction

According to the results of Korik et al. [12], the standardized BP was chosen as the EEG feature for the Calculation of the correlation between the kinematic and EEG data. The standardized BP was calculated for every frequency spectra separate in time windows of 500 ms, according to equation 2.3 and subsequently standardized according to equation 2.4. To match the kinematic data sampling rate of 30 fps, the BP time windows were overlapped and switched for 33.33 ms. Since with the provided recording frequency (250 Hz) of the used EEG system it was not possible to switch the windows exactly of 33.33 ms, which are 8.33 ($250/30$) points, the windows were switched in an order of "8-9-8-8-9-8-..." points. Since the BP is calculated for time windows of 500 ms symmetrically around a time point no BP values can be calculated for the first and last 250 ms.

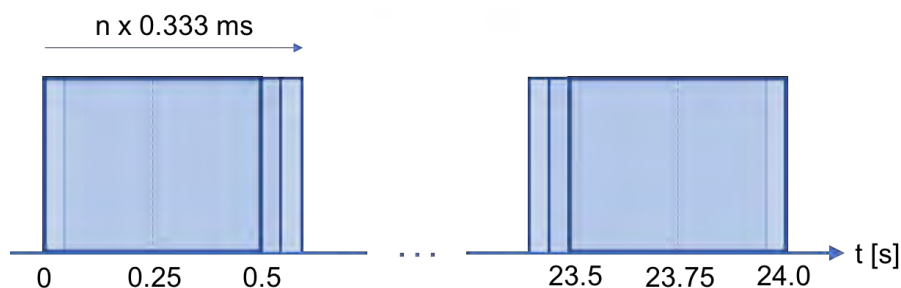


Figure 3.36: Band Power Time Windows. The figure shows how the BP Time Windows of 500 ms have been shifted in steps of $1/30$ s from one end to the other.

The following figure shows the result of the BP calculation for the same section as in Figure 3.35.

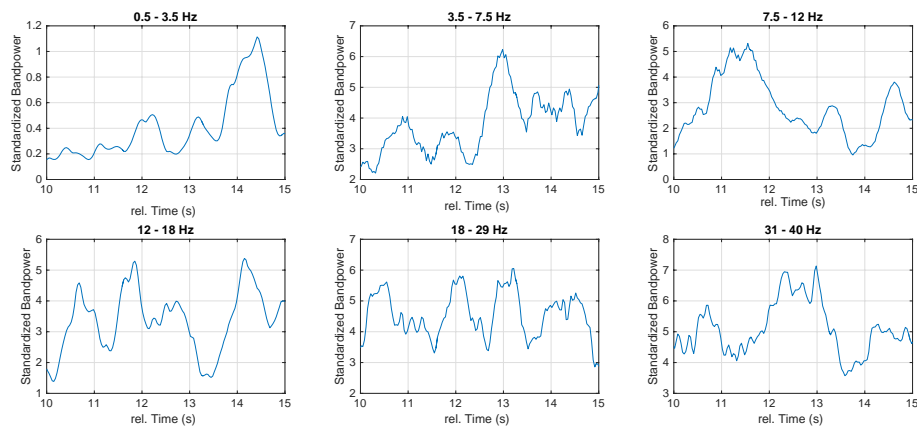


Figure 3.37: Standardized BP values. The figure shows the calculated standardized BP values of the same data as in Figure 3.35.

To get a feeling about what data are used to calculate the correlation for the prediction of motion trajectories, the BPs of Figure 3.37 corresponding velocity data were plotted below.

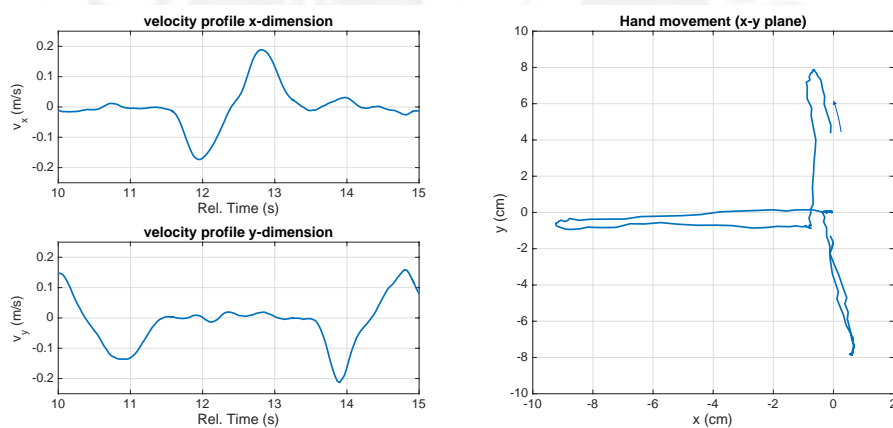


Figure 3.38: Corresponding kinematic data. The figure shows the to Figure 3.37 corresponding velocity data (left) and the original trajectory in an x-y plane (right).

3.7.6 Data verification, data synchronization and creation of a Data Structure

Verification of the kinematic data

For the verification of the kinematic data plots of the time courses of the motion data before the feature extraction were visually inspected for any paradox values, separately for all MBs. Although there were no errors in the kinematic data recording at the end of the preliminary-tests, some errors appeared in the actual experiment. The errors were noise, which couldn't be filtered out with an MA filter and recording errors during the movement to the lower target point. Since both types of errors only occurred in two MBs, however continuously in both MBs, these MBs, as you can see in the following figure, were completely excluded from further analysis.

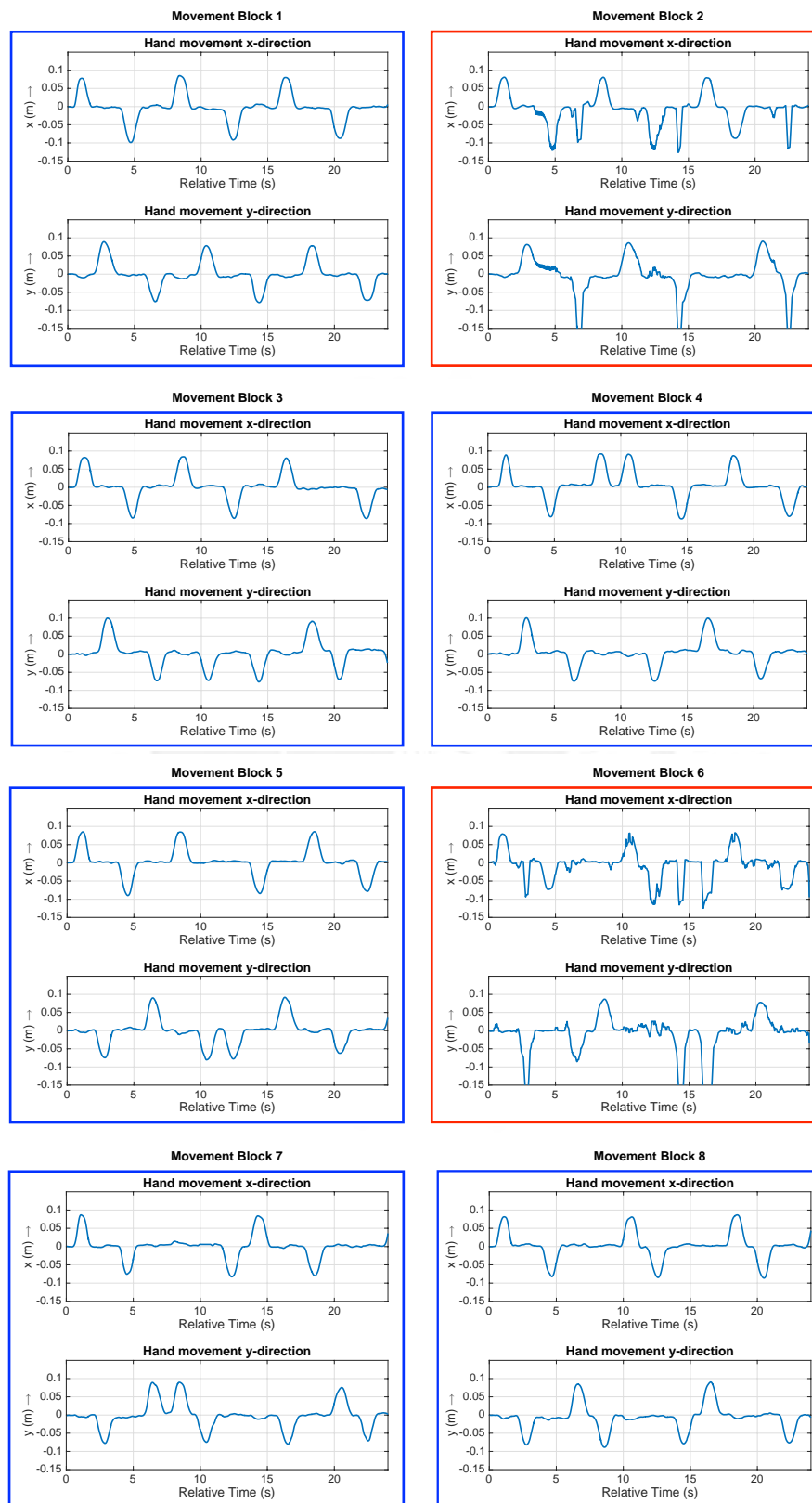


Figure 3.39: Verification of the kinematic data. The figure shows the preprocessed kinematic data for all MBs in a time course for x and y coordinates separately. The data in the red-framed MBs show some errors and were completely excluded from further analysis.

Verification of the EEG data

For the verification of the EEG data, the data before the separation into the different frequency spectra were visually inspected. To avoid the artifact produced by the Kinect in this inspection, the data were filtered with a zero-phase FIR band-stop filter with a cutoff frequency of 30 Hz before.

Since transients resulting from the movements of the initialization phases could be found up to the first 4 s of nearly each MB, the first 4 s of all MBs were excluded from further analysis. Also, the data of the last 0.25 s were excluded as for these times no BP values could be calculated (see subsection 3.7.5).

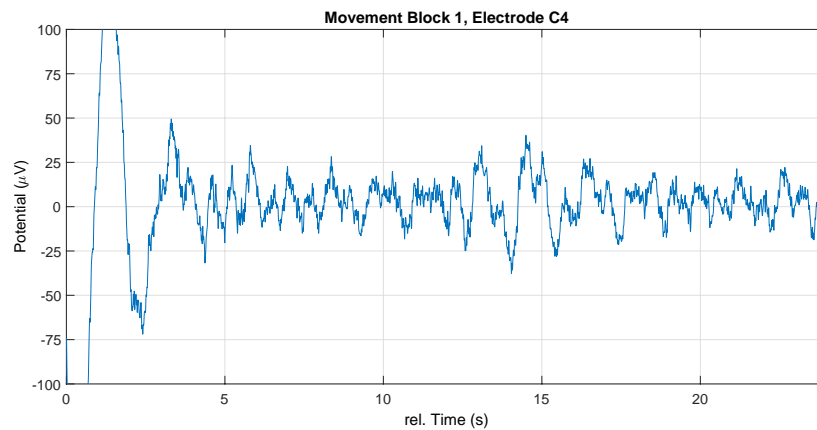


Figure 3.40: Transients at the beginning of the Movement Blocks. The figure shows a transient phase at the first 3 - 4 s of a MB resulting from the movements in the initialization phase before.

Synchronization of the data

To match the kinematic data sampling frequency, the EEG BPs were calculated in time windows that were shifted for 33.33 ms (see subsection 3.7.5). The datasets were already synchronized at the extraction of the EEG and Kinematic data in the preprocessing part, however since the first BP values are at 250 ms because of the symmetrical calculation in a window around a time point, is a time-shift of 7 points between the BP and the velocity components existing.

Creation of a Data Input Structure

For the calculation of the correlations using a mLR it was necessary to create a Data Input Structure, in which each computed velocity component (dependent data) can be assigned to the computed BP components (independent data) for each channel n at the same time, and further times in a time lag distance k according to Equation 2.6.

The investigated timelag distances were chosen from 0 to 500 ms, which yields an embedding dimension $(L + 1)$ of 16. The consideration of a time lag is important because of different reasons:

- The action potentials occurring in the brain during the preparation of the movements are passing over the spinal cord to the motoneurons, which lead to a contraction of the muscles and to a movement. This chain of action takes some time.
- Filtering the signals cause time shifts which, however, have been reduced due to the selection of optimal filters (see section 3.7.4).
- Since the BP is calculated with values that are symmetric to a time point, future values are included, which may have to be compensated by a time-shift.

The investigated numbers of EEG channels n are 30, as already described.

These parameters cause the input structure, which is shown in the following figure. This input structure was created for every investigated time point and separately for the both investigated velocities and the six investigated frequency spectra.

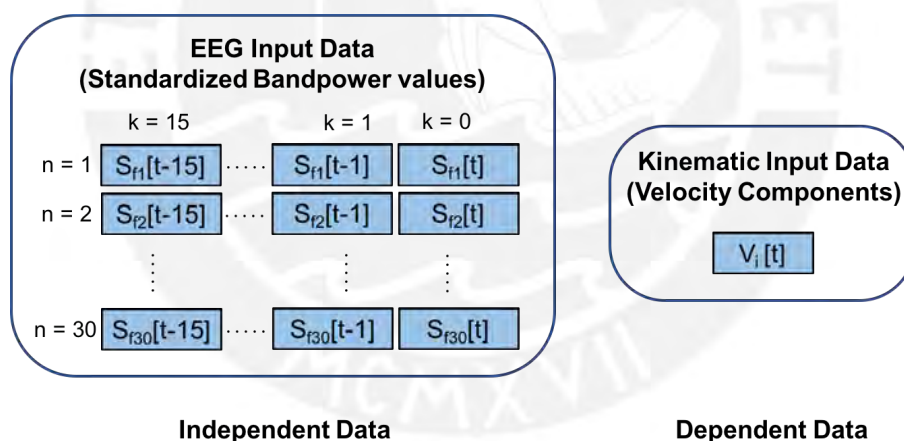


Figure 3.41: Data Input Structure. For all six frequency bands, each computed velocity component is assigned to the computed BP components of 30 EEG channels within 16 time lag distances.

3.8 Development of a Trajectory Decoder

3.8.1 Prediction of trajectories

Overview

For the prediction of trajectories, it is necessary to have a training and a test set of the extracted velocity data in x and y direction and BP data of the six frequency spectra data. With the training data, the regression parameter between the velocities and the BPs, can be calculated. The regression parameter can subsequently be used to predict the trajectories from the BP of the test set. At the end with the Pearson's CC the strength of the correlation between the original velocity data of the test set and the predicted velocity trajectories can be calculated.

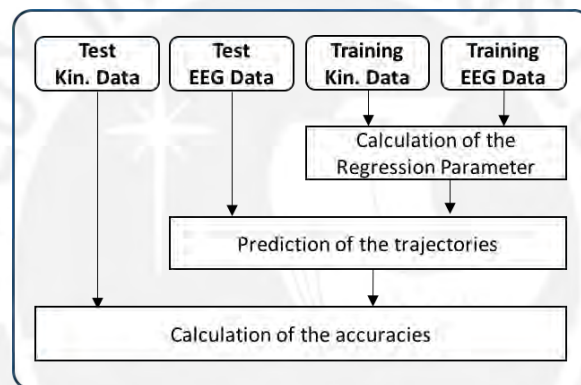


Figure 3.42: Overview of the prediction of trajectories and the calculation of the prediction accuracies. The figure shows how trajectories can be predicted and how the accuracies of the predicted trajectories can be calculated.

Data validation

In order to get a proper evaluation of the results, the training data should not be used as test data. To separate the data into an independent training and test set, a validation is necessary. For this experiment, the data were validated manually; the data of the first MB were defined as (outer-fold) test set and the data of the other seven MBs were defined as (outer-fold) training set.

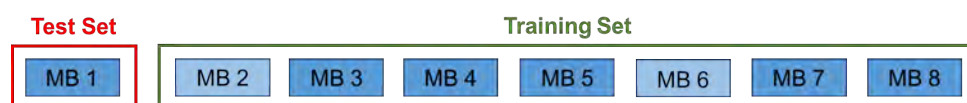


Figure 3.43: Creation of an outer-fold training and test set. The data of the first Movement Block were used as outer-fold test set, the data of the other seven Movement Blocks were used as outer-fold training set. The data of the MBs 2 and 6 were already excluded at the verification of the data (see Figure 3.39).

Calculation of the initial outer-fold trajectories

Like above described, with the full dataset of 16 embedding timelag distances and 30 embedding EEG channels, the regression parameter between the (outer-fold) velocity and EEG BP data of the training sets were calculated for all frequency spectra in both velocity dimensions using the matlab function "regress".

With this regression parameter and the EEG BP data of the test sets, the test set trajectories were predicted and the CCs between the reconstructed trajectories and the original test set trajectories were calculated. The CC was defined as the accuracy of the reconstructed trajectories. The results can be seen in the following figure.



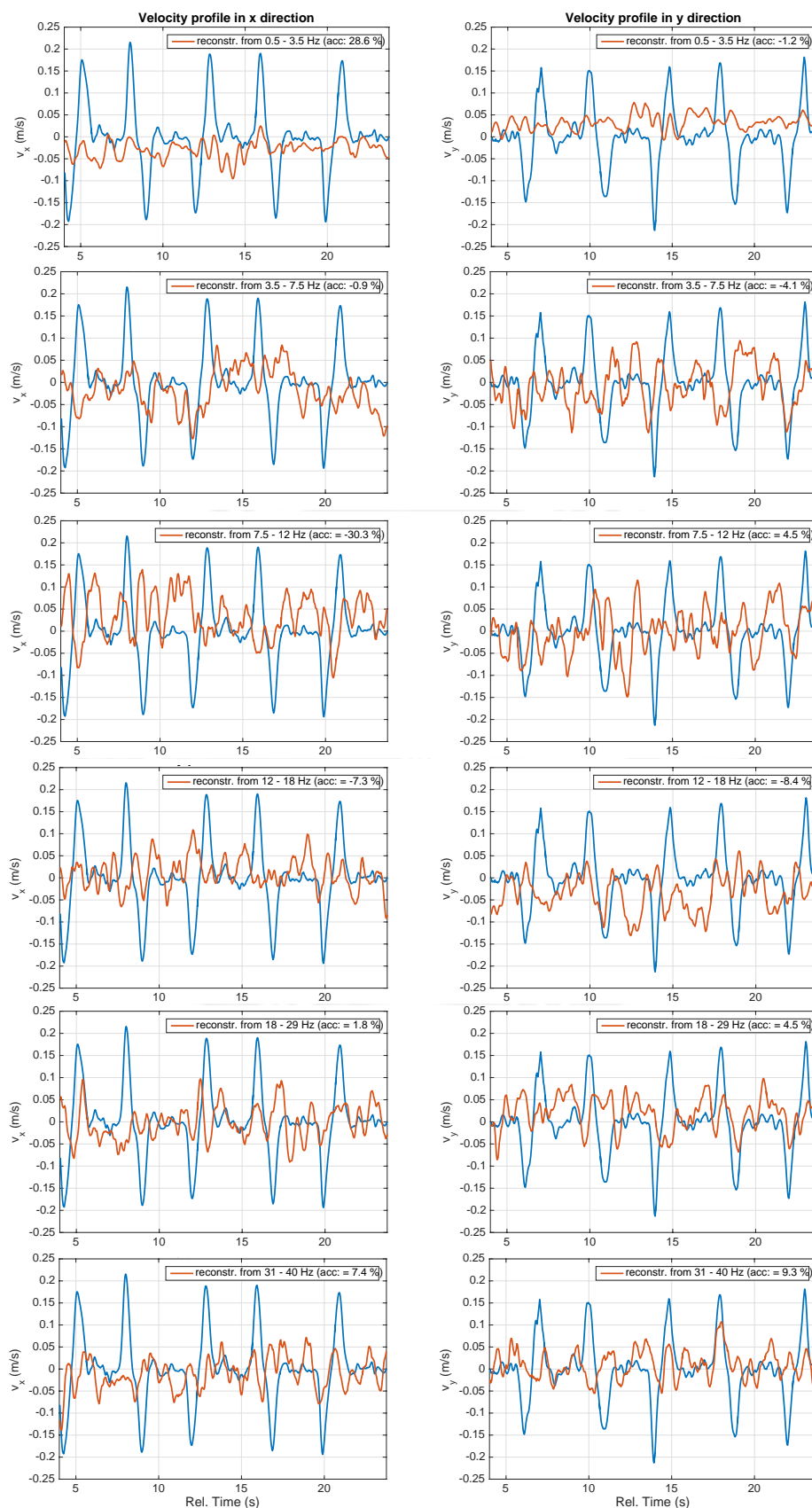


Figure 3.44: Predicted initial outer-fold trajectories. The figure shows the measured and reconstructed velocity profiles of the hand movements in x and y direction separately. For the reconstruction for all frequency spectra the full dimensions of EEG channels and timelags were used.

3.8.2 Improvement of the Trajectory Decoder

Overview

As you can see in the legends of Figure 3.44, the accuracies of the velocity profiles are very low and often negative, hence they cannot be used for the control of a BCI device or application. The reason for these low accuracies is that the used datasets for the calculation of the regression parameter contain many dimensions (16 timelag and 30 EEG channels) with a low level of information, what decreases the quality of the decoder. For this reason to get a good Trajectory Decoder it is necessary to find the optimal timelag and EEG channel combinations.

To find these optimal combinations, it is necessary to separate the outer-fold training set into k inner-folds since the ecological validation, resulting by the self-selection of the targets is not high enough. For these inner-folds, one fold is always used as test set, while the others build the training sets.

The process to improve the Trajectory Decoder is the following:

- For all constellations of test and training sets, the trajectories are predicted with all channels for each timelag separately and averaged over all folds. This approach makes it possible to rank the timelags for their accuracies.
- In a new calculation, the number of timelags sorted according to their ranks is varied and the trajectories are predicted for different numbers of timelags and the accuracies averaged over all folds. With this process the optimal number of timelags can be found.
- after finding the optimal timelags, for the constellation of the EEG channels the same procedure is repeated, however, this time the accuracies over all (optimized) timelags is calculated for all EEG channels separately.
- When for the inner-folds an optimal constellation for the timelags and EEG channels is found, this setup is used to optimize the outer-fold training set, what hence improves the Trajectory Decoder.

A graphical overview of the optimization process of the Trajectory Decoder is shown in the following figure.

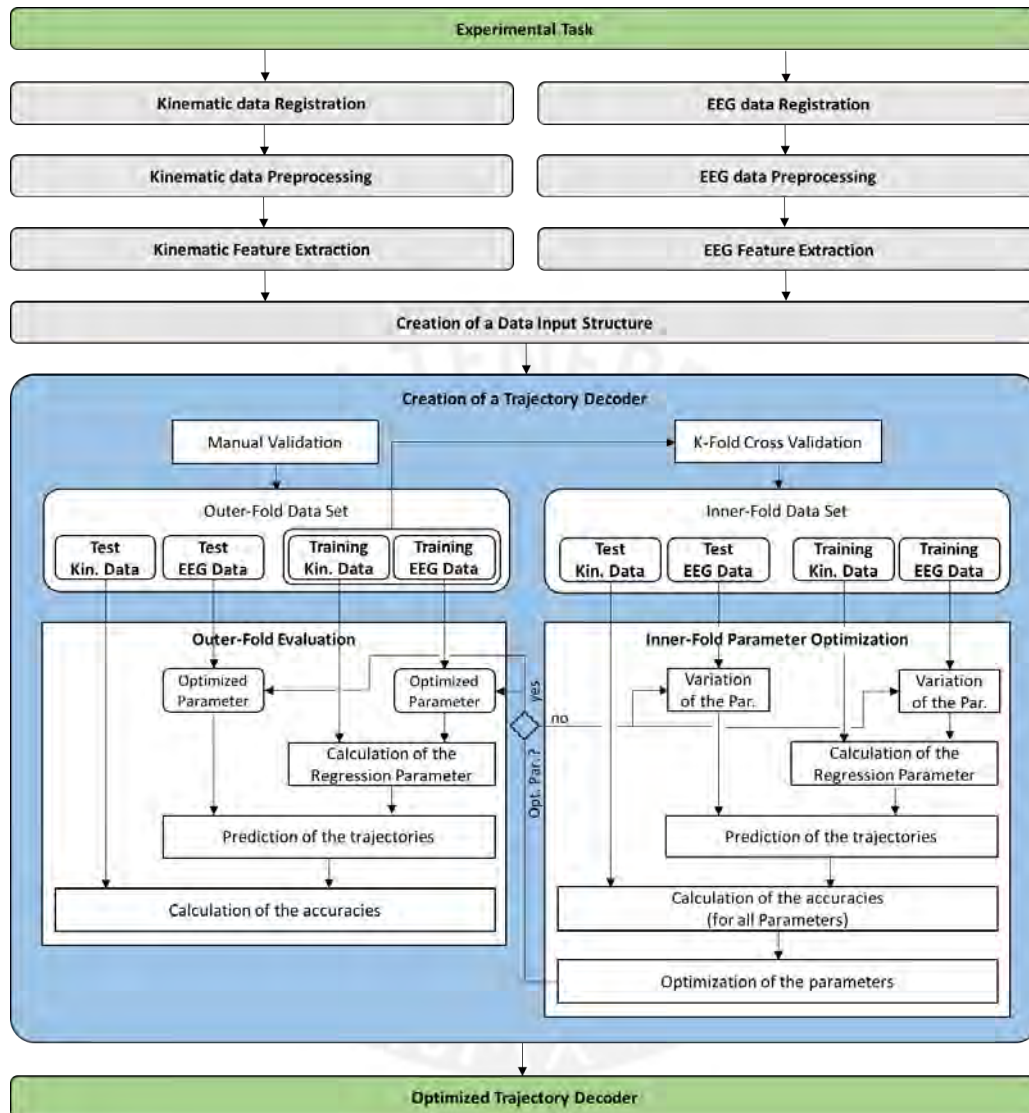


Figure 3.45: Processing scheme for the optimization of the Trajectory Decoder. In the inner-fold level is used to find an optimal setup of timelags and EEG channel montage, and to improve the Trajectory Decoder. The outer-fold level is used to evaluate the results of the Trajectory Decoder.

Validation

The higher the number of inner-folds, the better the decoder can be improved, however with the number of folds the computational effort increase linearly. Here, the inner-folds were created by a 6-fold CV.

Since Matlab is not able to separate the used kind of dataset by a CV, a manual CV was carried out. The steps to do this were the following:

- the data of the MBs, which were used for the outer-fold training set were separated in six equal sized sub intervals.
- With the computer a random sequence of numbers from 1-6 was created, here "4-2-6-1-5-3".
- The six numbers were in the generated sequence assigned to the sub intervals.
- With the numerated sub intervals the six inner-folds were created.

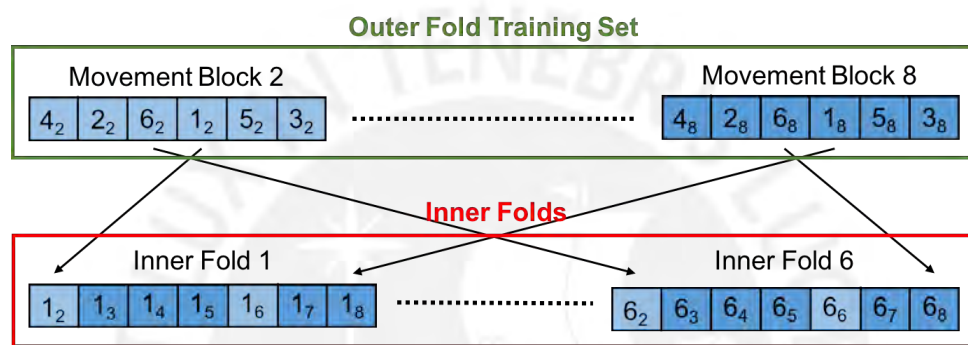


Figure 3.46: Creation of an inner-fold data structure. The inner-folds were created from the outer-fold training set. For the participant MB 2 and MB 6 (light blue) have already been excluded in the outer-fold training set (see Figure 3.43).

As already described above, each inner-fold were used once as test set while the other five folds were used together as training set. Because of the six different combinations of training and test datasets, this procedure is called 6X6 CV.



Figure 3.47: Inner-fold training and test set combinations. In the inner-fold training, each inner-fold is used once as test set while the other five inner-folds build together the training set.

The velocity profiles of all inner-folds can be seen in the following figure.

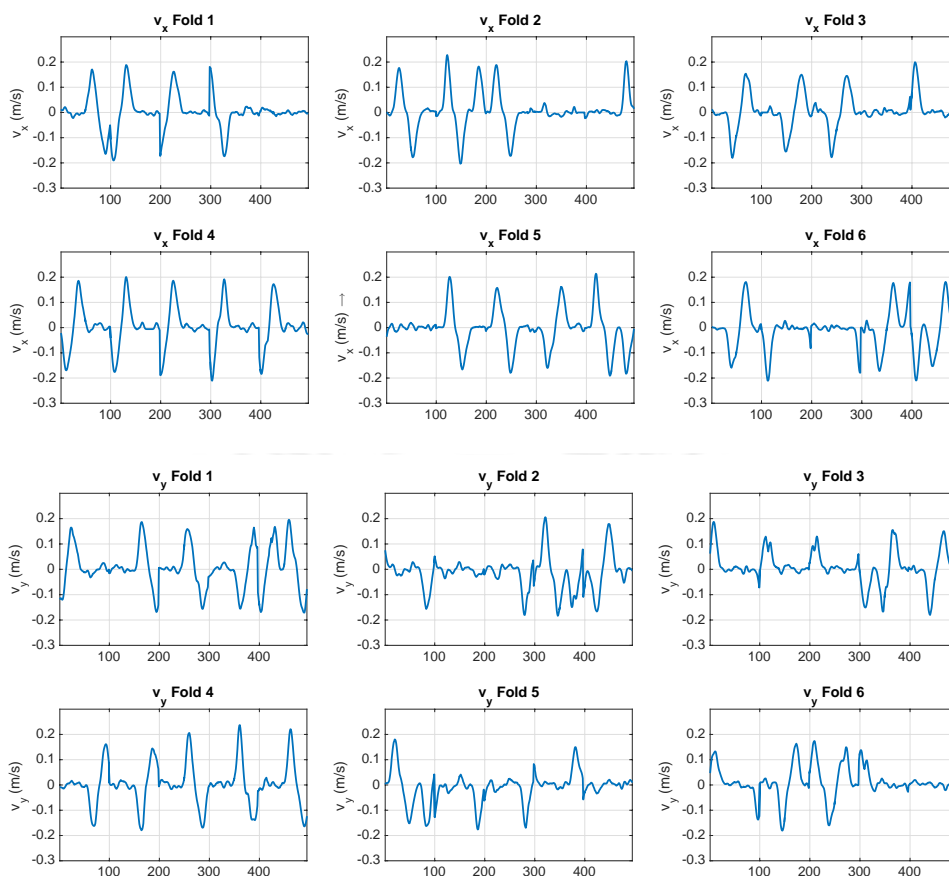


Figure 3.48: Inner-fold velocity profiles. The figure shows the velocity profiles for all six inner-folds in the x and y dimension. These profiles were used for the training of the Trajectory Decoder.

Calculation of the initial inner-fold trajectories

The first step in the inner-fold optimization stage was to calculate the accuracies for the predicted trajectories in each fold and the averaged values over all six folds; these results were subsequently compared with the results, got from the outer-fold calculation.

The result of this evaluation (see Table 3.1) is that the calculated accuracies for the averaged inner-folds and the outer-fold differ enormously, as well as the accuracies between all the inner-folds differ enormously. It is assumed that the results, which are random, have been caused by an overfitting of the model with its 481 dimensions.

Accuracy v_x (%)	Fold 1	Fold 2	Fold 3	Fold 4	Fold 5	Fold 6	Average	Outfold
0.5 - 3.5 Hz	7.5	- 11.5	- 9.2	4.4	- 1.9	19.1	1.4	28.6
3.5 - 7.5 Hz	2.4	- 3.5	- 16.1	7.5	- 3.1	- 1.2	- 2.4	- 0.9
7.5 - 12 Hz	14.2	- 21.0	18.5	1.1	13.3	7.5	5.6	- 30.3
12 - 18 Hz	8.6	- 0.0	6.1	- 0.9	10.9	13.0	6.3	- 7.3
18 - 29 Hz	19.5	- 4.7	11.2	- 17.0	- 31.6	10.7	- 2.0	1.8
31 - 40 Hz	- 2.3	9.4	- 18.2	0.5	10.4	22.3	3.7	7.4

Accuracy v_y (%)	Fold 1	Fold 2	Fold 3	Fold 4	Fold 5	Fold 6	Average	Outfold
0.5 - 3.5 Hz	- 3.2	- 11.2	-18.4	- 8.8	- 29.4	- 7.4	- 13.1	- 1.2
3.5 - 7.5 Hz	- 8.9	- 13.0	4.7	- 4.5	7.8	1.1	- 2.1	- 4.1
7.5 - 12 Hz	23.6	20.8	- 4.1	21.5	6.5	11.9	13.4	- 4.5
12 - 18 Hz	24.9	10.9	- 25.8	- 14.5	- 1.6	- 15.0	- 3.5	- 8.4
18 - 29 Hz	- 6.6	- 31.4	- 17.8	- 10.0	- 12.0	- 7.0	- 14.3	4.5
31 - 40 Hz	11.6	- 11.4	- 9.8	1.6	- 3.8	14.6	0.5	9.3

Table 3.1: Prediction accuracies for trajectories predicted with initial Parameters

Optimization of the timelags

The dataset seems too big for a practical one-step optimization, for this reason the timelags and the EEG channels were optimized separately, beginning with the timelags. To optimize the timelags first the trajectories over all 30 EEG channels were calculated for each timelag separately in all six folds. Then, the accuracies for each fold were calculated and finally the accuracies were over all six folds averaged.

It was assumed that the "accuracy courses" have a similar shape to a downwardly opened parabola or to a sinus function (because of the periodic character of the movements) with peaks at different timelag distances. Furthermore, it was assumed that the accuracy courses calculated from the mu (7.5 - 12 Hz) and low beta (12 - 18 Hz) frequency spectra have the best results and that the curve shapes of the accuracies in the x and y dimension are similar. Figure 3.49 shows the actual results.

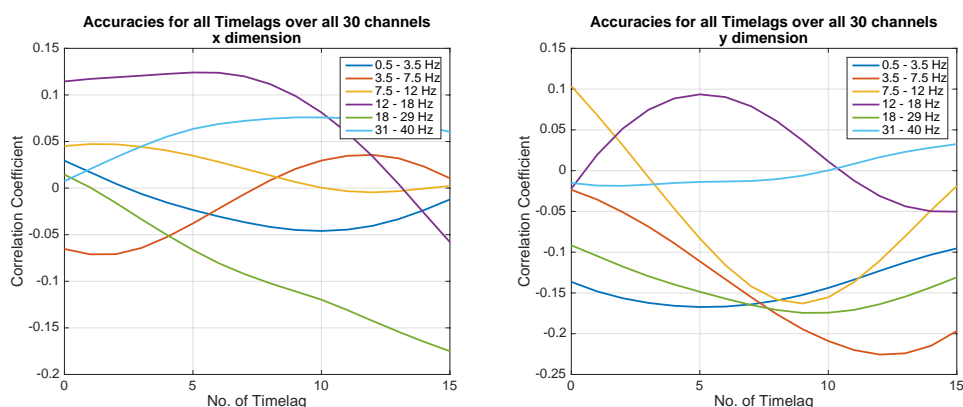


Figure 3.49: Timelag-accuracy-courses using all 30 EEG channels (sep. in x and y dim.). The figure shows expected accuracy courses with the highest maximum in the x dimension for the low beta (violet) frequency band and in the y dimension for the mu (yellow) frequency band.

The figure shows that, as assumed, the most curves have a sinusoidal appearance. Also, the accuracies calculated from the mu and low beta band are the highest, as expected.

Since it is assumed that the final timelag distances are independent of the movement directions, the over the x and y dimension averaged results are used for the optimization. The averaged values of the last evaluation are shown in the following figure.

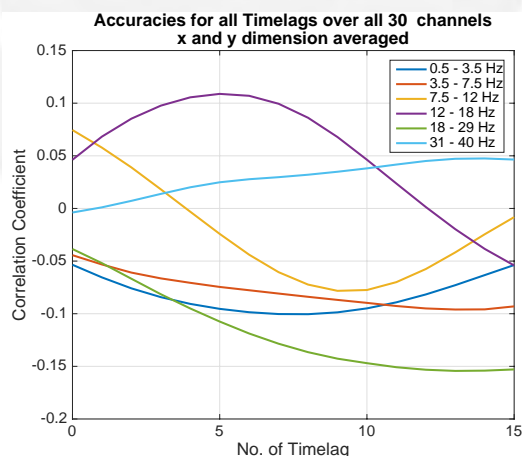


Figure 3.50: Timelag-accuracy-courses using all 30 EEG channels (av. in x and y dim.). The figure shows that the accuracies for the mu (yellow) and low beta (violet) frequency bands have still the highest maximums when the x and y values are averaged.

The results from the last evaluation were particularly as expected, however, the medium and maximum accuracy values are very low for all frequency spectra. To check if these low values are due to too many channels with low information content, the same procedure like above described

was repeated, however this time the number of electrode channels was reduced from 30 to the six channels that are placed over the motor cortex. The used channel montage can be seen in the following figure.

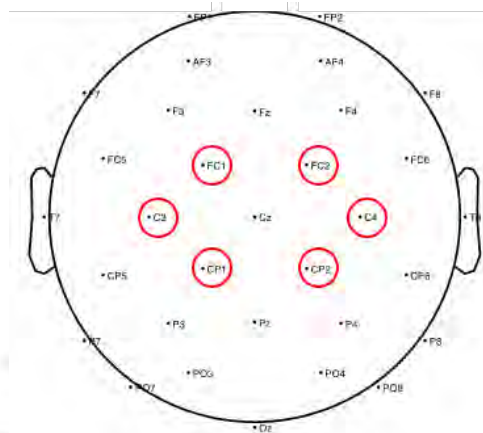


Figure 3.51: Reduction of the EEG channels to six over the motor cortex placed electrodes. For the following evaluation were just the data produced by these six marked EEG electrodes used.

The evaluation (see Figure 3.52) shows very different results regarding the shapes of the curves, the timelags and also the highest maximum.

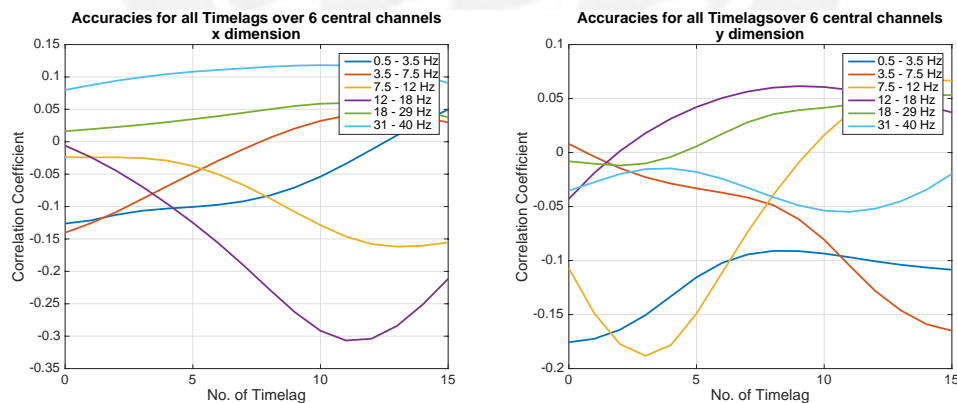


Figure 3.52: Timelag-accuracy-courses using six central EEG channels (sep. in x and y dim.). The results calculated from six central channel differ particularly enormous from the results calculated from all 30 EEG channels (see Figure 3.49)

The over the x and y dimension averaged results are plotted in the following figure.

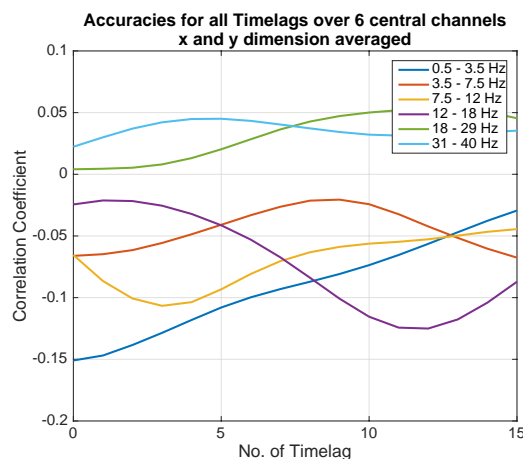


Figure 3.53: Timelag-accuracy courses using six central EEG channels (av. in x and y dim.). The figure shows, that the accuracies for the mu (yellow) and low beta (violet) band have deteriorated compared to Figure 3.50.

When comparing the results from the over x and y dimension averaged accuracies for the predicted trajectories over all 30 EEG channels (see Figure 3.50) and over six central EEG channels (see Figure 3.53), it can be seen that the mu and low beta band have their highest maximum, when they were calculated from all 30 EEG channels and the other four frequency bands have their highest maximum, when they were calculated from the six central channels. This is other than expected, because the SMR which include the mu and low beta spectra is particularly found over the motor cortex, while other frequency spectra are often found in other brain regions.

Due to the results of both evaluations, the timelags for the mu and low beta band were ranked according to Figure 3.50 and the timelags of the other four frequency bands were ranked according Figure 3.53. Thereby, the timelag with the best accuracy was assigned to rank 1 and the timelag with the worst accuracy was ranked as 16.

After ranking the timelags the optimal number of timelags has been determined. To do this, the accuracies were calculated for the trajectories from a varying number of channels, sorted by its ranks. This means, that a trajectory predicted by 5 timelags is calculated by the timelags with the ranks 1-5. The results for the optimization of the timelags are shown in Figure 3.54.

Optimization of the channel montage

After the timelags, the EEG channel montage had to be optimized. To optimize the channel montage, the averaged accuracies for each channel were calculated in a similar way as the optimization of the timelags. For the calculation of the accuracies, the determined optimized timelags were used. Also, like in the optimization of the timelags, the channels were first ranked and after the optimal number of channels were calculated using the ranks of the channels. The results for the optimization of the EEG channel montage are shown in Figure 3.55.

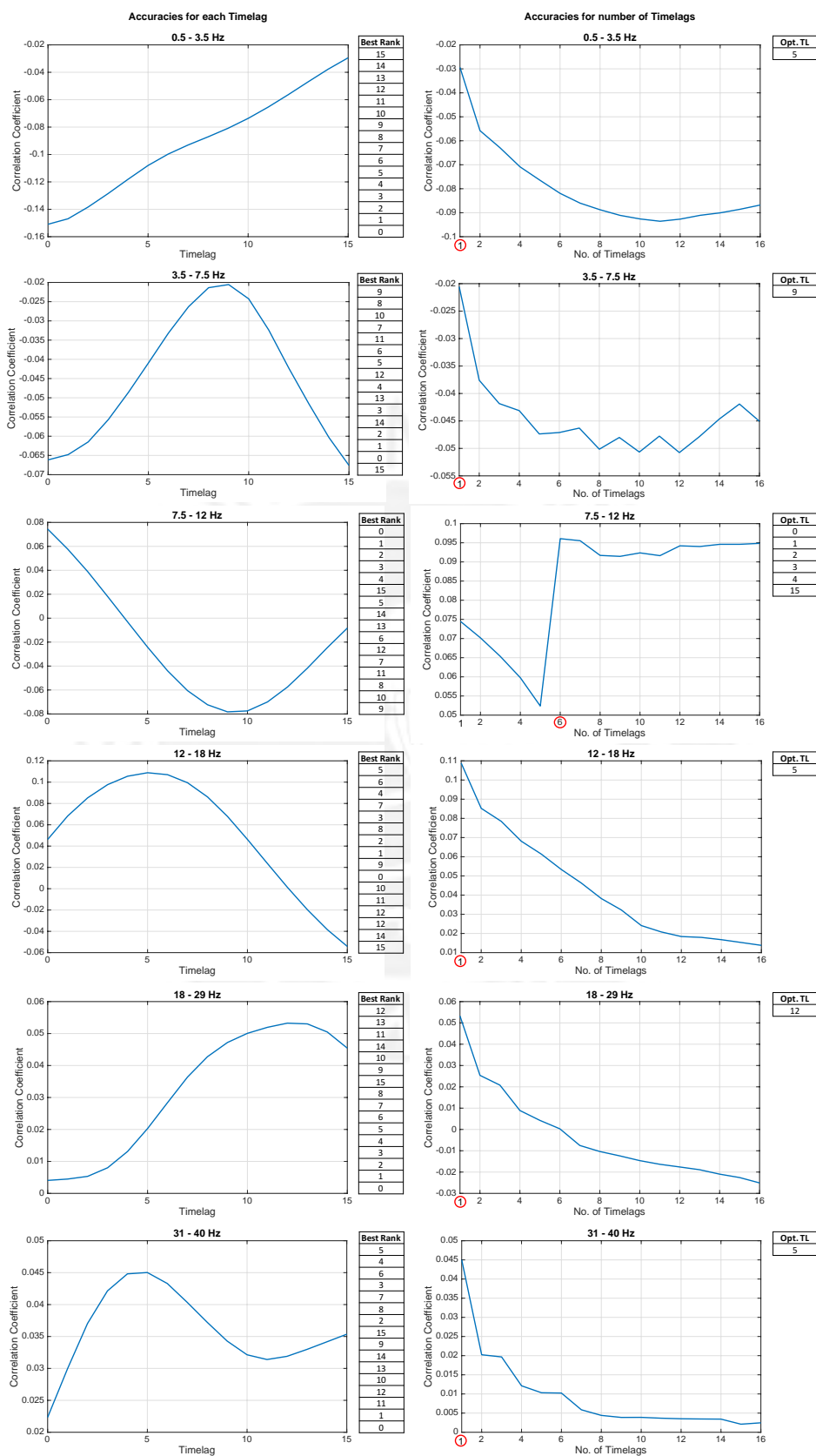


Figure 3.54: Optimization of the timelags. On the left side you can see the accuracies for each timelag, which were subsequently ranked according to this evaluation. On the right side are the accuracies that are depending on the number of timelags from the timelags with rank 1 to the timelags with rank x.

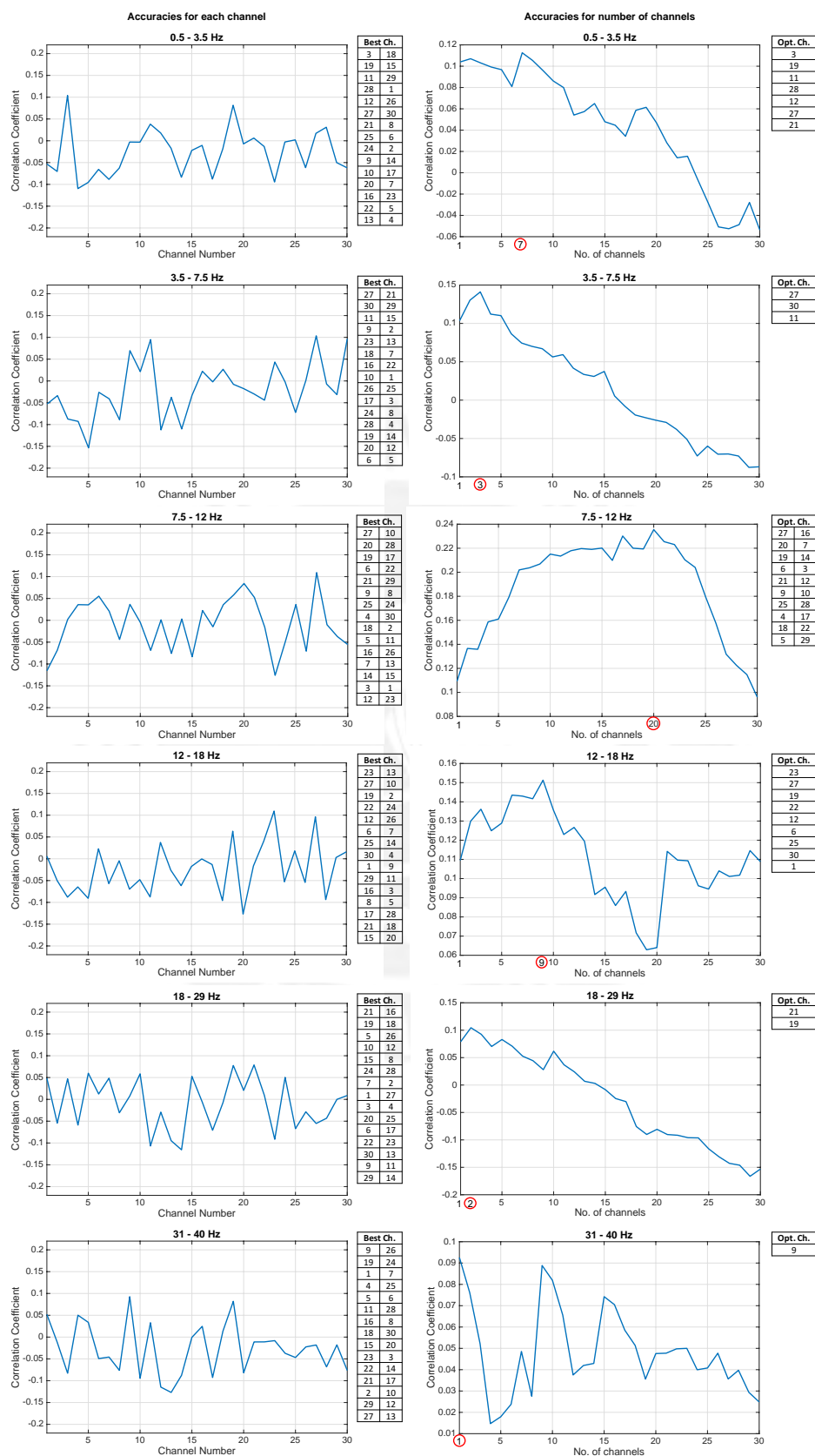


Figure 3.55: Optimization of the EEG channel montage. On the left, the accuracies for each EEG channel, which were subsequently ranked according to this evaluation can be seen. On the right are the accuracies depending of the number of channels from the channel, with the rank 1 to the channel with the rank x.

After the optimization of the EEG channel montage, the timelags were re-optimized. To do this, the procedure described above was repeated. However, this time the determined optimized channel montage was used. This procedure improved the results for the frequency spectras 7.5 - 12 Hz, 12 - 18 Hz, 18 - 29 Hz and 31 - 40 Hz, for the frequency spectras of 0.5 - 3.5 Hz and 3.5 - 7.5 Hz the results stayed the same.

In the following figure, the process of the re-optimization of the timelags for the four frequency spectra, which were improved, is plotted.

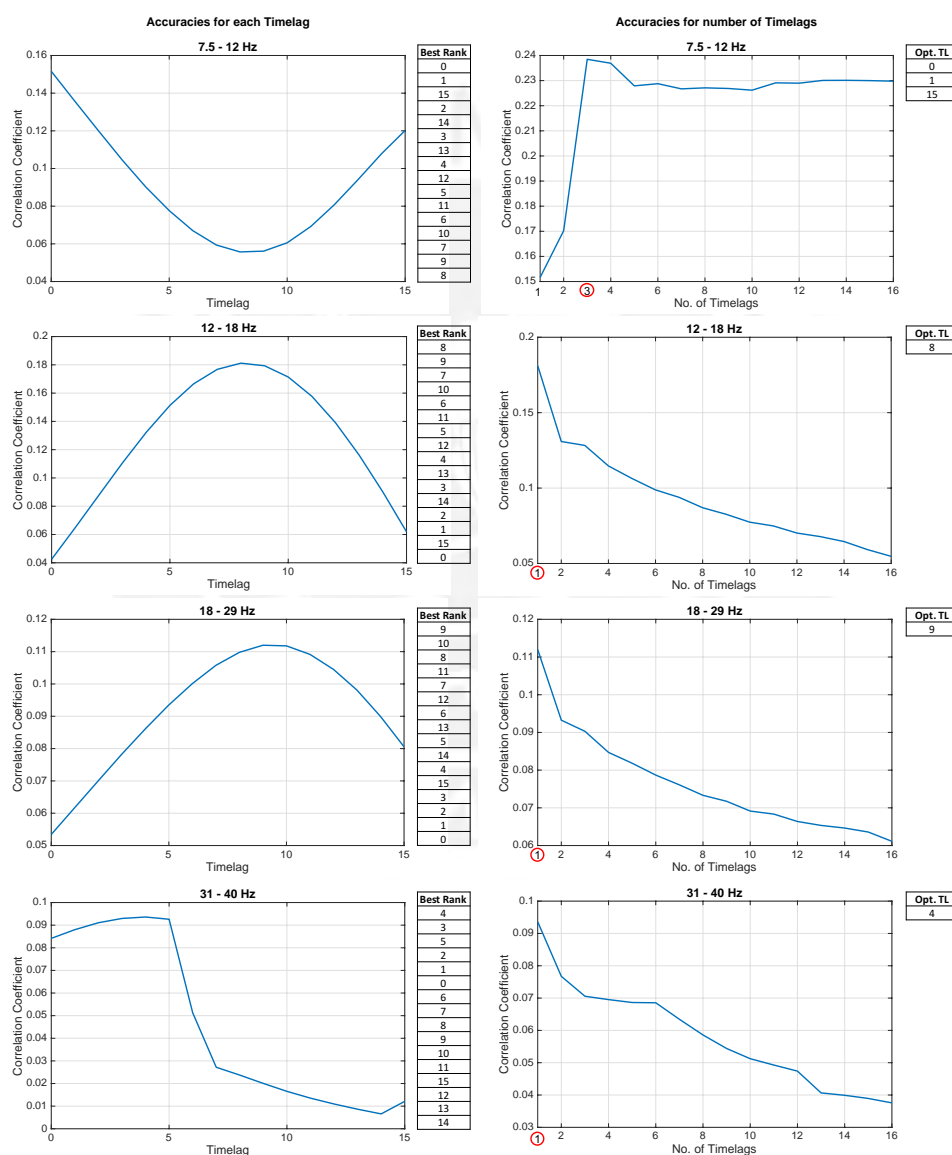


Figure 3.56: Re-optimization of the timelags. On the left are the accuracies for each timelag, which were subsequently ranked according to this evaluation. On the right are the accuracies depending on the number of timelags from the timelags with rank 1 to the timelags with rank x.

After the re-optimization of the timelags the EEG channel montage can also be re-optimized using the re-optimized timelags. The process of alternating optimization of the timelags and channels can be continued as desired. Here, the process was terminated if no further improvement of the accuracies resulted. However, since it is a process to find a local and not a global maximum it is possible that the results will deteriorate but will reach a new maximum at a later point.

The final results of the optimization are shown in the following section.



4 Results

4.1 Achieved results

The results of the inner-fold optimization (see Table 4.1) is that the accuracies over all six inner-folds and both spatial dimension averaged has improved for each frequency band, what confirms that the chosen optimization process is working. Furthermore, the results show that the highest accuracies were calculated from the mu and low beta band, where it was expected. It was also assumed that the optimal timelag distances would be at around 200 - 300 ms for all frequency bands higher than 3.5 Hz. For the delta frequency band (0.5 - 3.5 Hz) a higher timelag distance was expected because of the time delay of lower frequencies resulting from the non-linear phase of the Butterworth filter (see Figure 3.27). All timelag distances determined, except for the mu band (7.5 - 12 Hz) are according the assumption. The course of the Accuracy depending on the timelags, see also Figure 3.54 and Figure 3.56 seem surprising.

Results Inner-folds	0.5-3.5 Hz	3.5-7.5 Hz	7.5-12 Hz	12-18 Hz	18-29 Hz	31-40 Hz
Optimal TL dist.	500 ms	300 ms	0 ms, 33 ms, 500 ms	267 ms	267 ms	133 ms
Optimal no. of Ch.	7	3	20	9	3	1
Acc. optimized	11.3 %	14.1 %	23.9 %	18.1 %	13.2 %	9.4 %
Acc. before opt.	-5.8 %	- 2.3 %	9.5 %	1.4 %	- 8.1 %	2.1 %

Table 4.1: Averaged inner-fold accuracies after the parameter optimization

The optimized channel montages shown in Figure 4.1 are a bit surprising. While the optimized montage for the mu band is very symmetrical, the montages for the other frequency bands are very unsymmetrical and especially for the low beta band it is surprising that only one of the nine optimal calculated electrodes is placed of the central cortex.

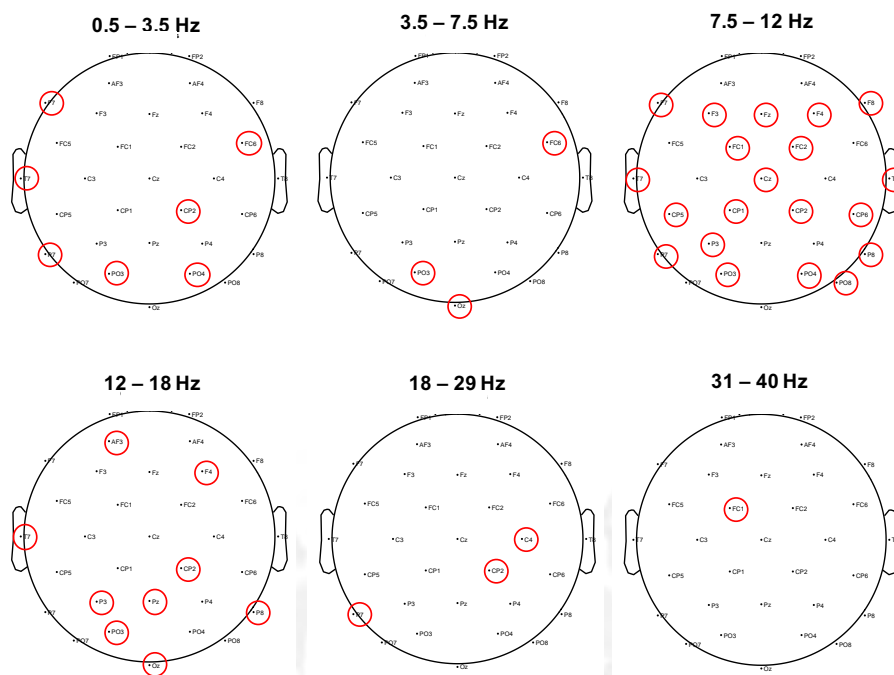


Figure 4.1: Optimized EEG channel montage. The red circles mark the determined optimal EEG channels which are necessary to calculate the highest possible accuracy.

The following figure shows what accuracies are predictable for each channel in each frequency spectra when using the optimized timelags.

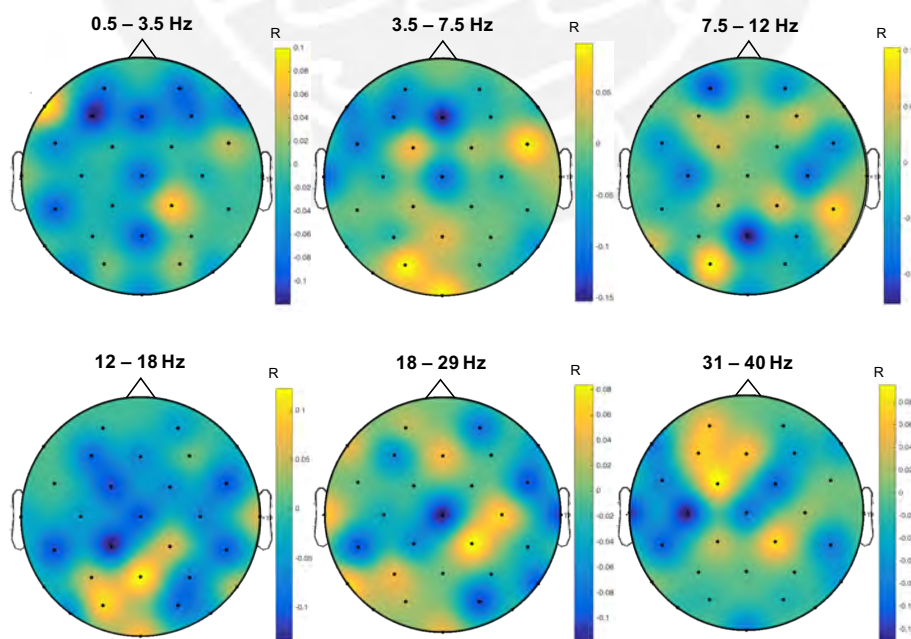


Figure 4.2: Topographic map of the predicted accuracies for each channel. For this evaluation 2D Gaussian functions were multiplied with the calculated accuracy for each channel, shifted to the channel positions and subsequently overlaid.

The plots of the topographical maps show that the EEG channels above the motor cortex can not be used to calculate trajectories with higher accuracies, and that the majority of the channels produce negative accuracies. This could possibly indicate a problem of the selected optimization method.

In order to see if this has negative effects, the accuracies in the outer-folds using the optimized combination of timelags and EEG montage were calculated and with the outer-fold values before the optimization as well as with the values of the optimized inner-folds themselves compared. The results of this evaluation separately for the x and y dimension can be seen in the following table.

Results, x dim.	0.5-3.5 Hz	3.5-7.5 Hz	7.5-12 Hz	12-18 Hz	18-29 Hz	31-40 Hz
aver. Inner-folds	16.5 %	19.3 %	22.7 %	20.1%	11.9 %	13.4 %
Outer-fold bef. opt.	28.6 %	- 0.9 %	- 30.3 %	- 7.3 %	1.8 %	7.4 %
Outer-fold aft. opt.	7.8 %	12.2 %	- 34.4 %	- 2.2 %	0.2 %	17.0 %

Results, y dim.	0.5-3.5 Hz	3.5-7.5 Hz	7.5-12 Hz	12-18 Hz	18-29 Hz	31-40 Hz
aver. Inner-folds	6.0 %	- 0.3 %	25.0 %	16.2 %	14.6 %	5.3 %
Outer-fold bef. opt.	- 1.2 %	- 4.1 %	4.5 %	- 8.4 %	4.5 %	9.3 %
Outer-fold aft. opt.	- 7.1 %	15.0 %	-4.0 %	9.2 %	0.7 %	19.2 %

Table 4.2: Outer-fold accuracies after optimization

Table 4.2 shows that there is a huge difference in the results between the optimized inner-folds and the optimized outer-fold test set. A huge variance between the results can be a sign that the number of k in the k-fold CV is not sufficient, however a variance as huge as shown in the previous table cannot be attributed to the number of k folds. Since also only the outer-fold accuracies calculated from three frequency spectra improved in both dimensions while the accuracies calculated from the other three frequency spectra decreased, it seems that the chosen optimization process is not transferable from the inner-fold level to the outer-fold level. The reasons are explained in the following section.

4.2 Discussion of the results and problems

The chosen optimization method is a method to find a local maximum. That means that the found local maximum could theoretically differ significant from the global maximum. A method to find a global maximum would need to calculate independently of the ranks all combinations of timelags including the number and the chosen timelags, and all combinations of EEG channel

montages, including the number of channels and the chosen channels itself. For an optimization of 480 parameters the computational effort would be enormous. It can be assumed that the local maximum after the optimization of the time lags, the optimization of the channel montage and the re-optimization of the timelags are close to the global maximum.

The reason why the chosen optimization method cannot be transferred from the inner-fold to the outer-fold level seems to have its origin in the chosen ranking method of the timelags. To understand the problem the kinematic and EEG feature vectors for a training set are plotted in the following figure.

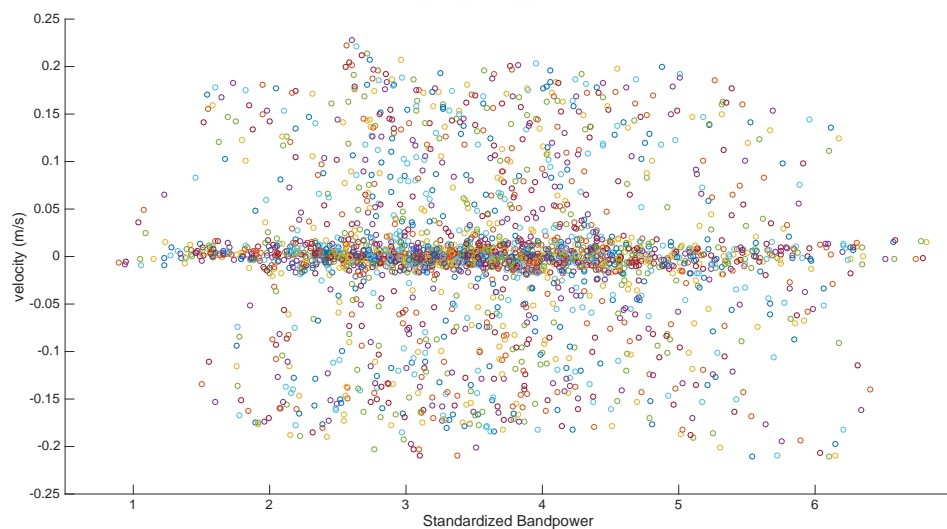


Figure 4.3: Correlation between the EEG BP and associated velocity data. In this figure, for the training set of inner-fold 1, the feature vectors of the velocity in x dimension and the EEG BP of channel *CP2* in the low beta band with a timelag distance of 267 ms are plotted.

First, it can be seen, no matter which regression line is plotted, the reproduction of an original trajectory in the test set is with this line hardly possible since the variance of the data is extremely high. For this reason, the method of multiple linear regression has been applied, since this method can be used to combine information from different dimensions (timelags and EEG channels), and thus the overall variance can be reduced during optimization what improves the CC.

Second, without applying a regression line, it can be seen that this line would have a slope of almost zero. The problem that arises is that some single points could convert a positive slope of the straight line into a negative slope or a negative slope of the straight line into a positive slope. It seems very probably, that for many training sets negative (positive) slopes (equal to the regression parameter b) were calculated while for the test sets positive (negative) regression parameter were determined.

The effect of a different sign of the CCs can be understood better when understanding better the meaning of the CC. The CC measures the strength of the contemporaneous linear association between two series [51] and can have values between -1 and 1. Figure 4.4 gives an example of correlations between contemporaneous datasets and Figure 4.5 gives an example of correlations between a sinus function and time shifted sinus functions, what means that the datasets are time shifted and not contemporaneous.

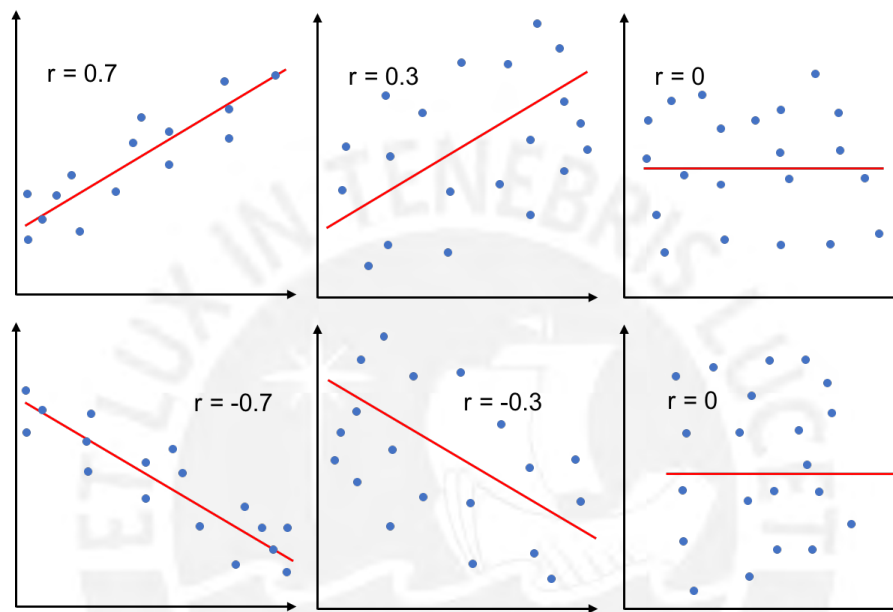


Figure 4.4: Examples of correlations between contemporaneous datasets (adapted from [52]).

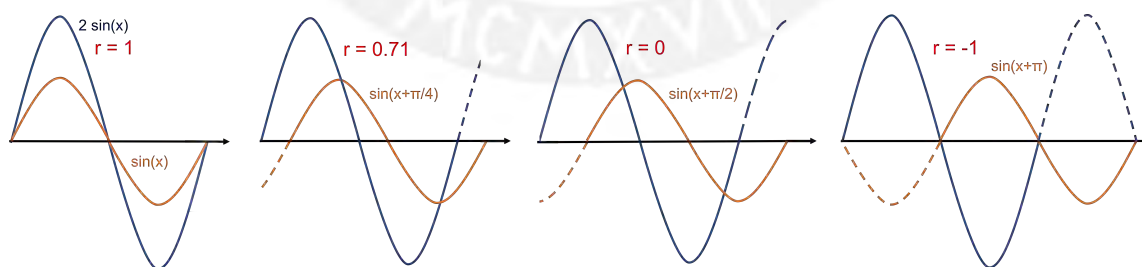


Figure 4.5: Examples of correlations between time-shifted datasets.

As you can see in Figure 4.5 in the left graphic, the amplitude of the sin functions don't have an effect on the CC respectively the r value, however a time-shift, as you can see in the other three graphics, has a huge impact. Although there is a 100% linear dependency between the two functions in the second graphic from the right, the CC is 0 and in the right graphic the CC is -1.

Transferred to the analysis of the correlation between the kinematics and EEG datasets does this mean that regression parameter with different signs in the training sets leads to predicted trajectories which are mirrored on the time axis although there is no time-shift between both datasets.

This effect can be observed in the inner-fold level many times between two neighbor timelag distances. In the following, a visualization of this effect is done by the data from electrode *CP2*, which predicts in the low beta frequency range at a time interval of 8 (267 ms) a trajectory with a relatively high accuracy compared to the other electrode channels.

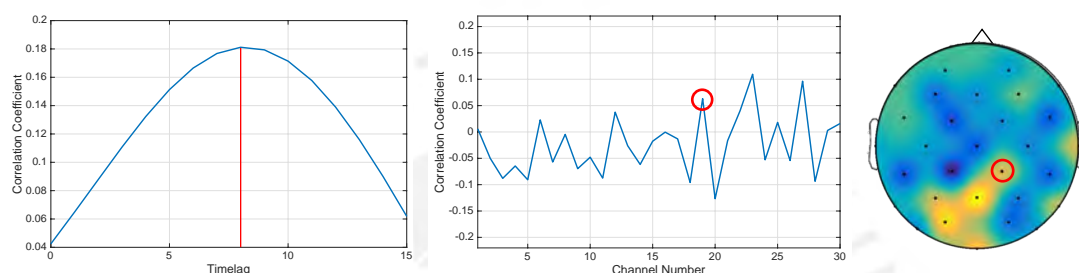


Figure 4.6: Investigated EEG channel. The over the motor cortex placed EEG channel *CP2* shows a relatively good prediction accuracy in the low beta band.

For the electrode channel *CP2*, all predictable accuracies were calculated for each timelag separately in all six folds and two spatial dimensions, averaged and plotted in the following figure on the right. As can be seen, there is a huge jump in the accuracy course between the timelags 10 and 12. This jump can be made even clearer in the x dimension in the inner-fold 1, see the following figure on the right.

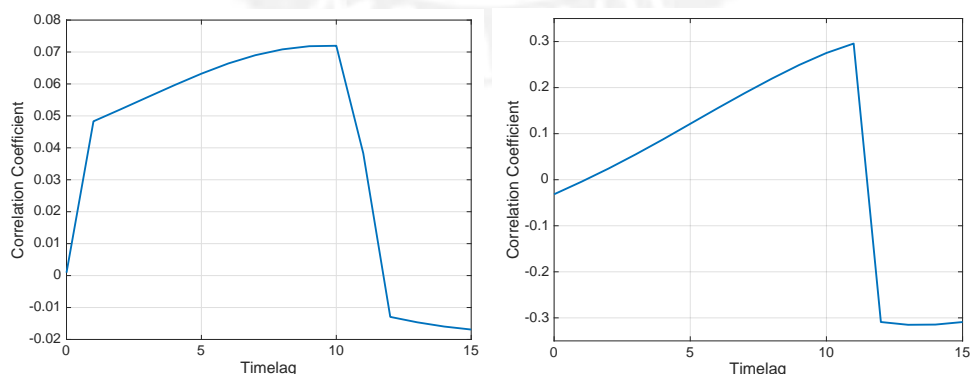


Figure 4.7: Timelag-accuracy-courses for EEG channel *CP2* in the low beta band. On the left is the timelag accuracy course averaged over all six inner-folds and both spatial dimensions on the right is the timelag accuracy course for timelag 1 and the spatial dimension x to detail the accuracy jump in the timelag accuracy course.

As can be seen in the previous figure on the right, there is a jump in the prediction accuracy

course of about $+0.3$ to slightly below -0.3 between the timelags 11 and 12. This jump results since the regression parameter b changes from -0.000149 in timelag 11 to $+0.000584$ in timelag 12.

In the following figure, the training and test sets of fold 1 with its feature vectors are plotted. The feature vectors are the BP data in the low beta spectra created from EEG channel *CP2* with timelags of 367 and 400 ms with its corresponding velocity data in the x dimension. In the training sets calculated regression lines were added to the plots of the training and corresponding test sets.

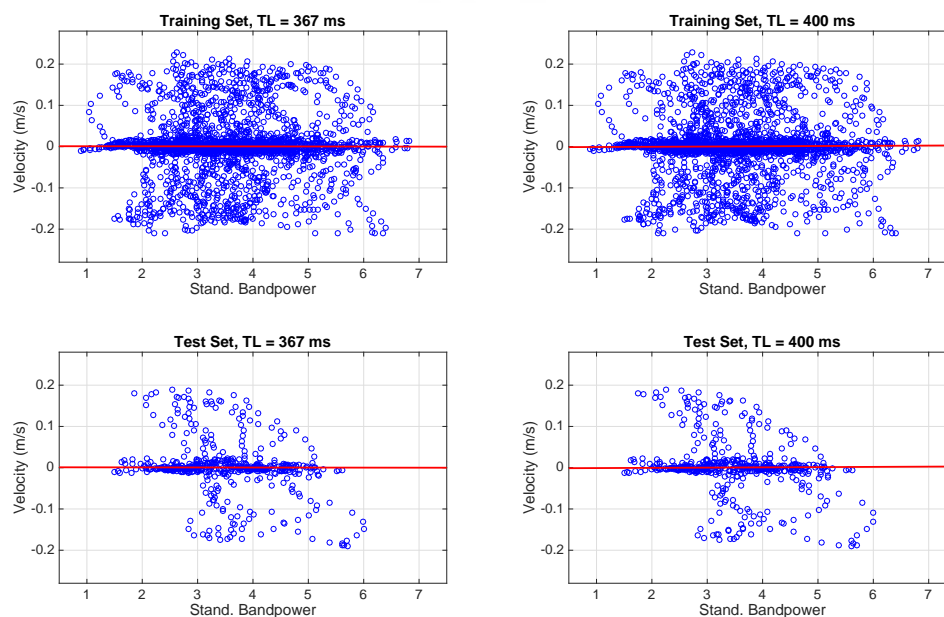


Figure 4.8: Feature vectors of training and test sets with a timelag distance difference of 33 ms. The figure shows the high similarity between the feature vectors in the training and test sets of neighbor timelags. Also the regression lines look nearly exactly the same.

The kinematic data of the training sets as well as the kinematic data of the test sets are the same. The EEG BP data differ marginally between the two timelags. For this reason it could be expected that the predicted trajectories of both timelags are very similar, however as in Figure 4.7 was supposed, in the following figure is confirmed that the trajectories predicted from the timelag distances 267 ms and 300 ms are more or less mirrored at the time axes.

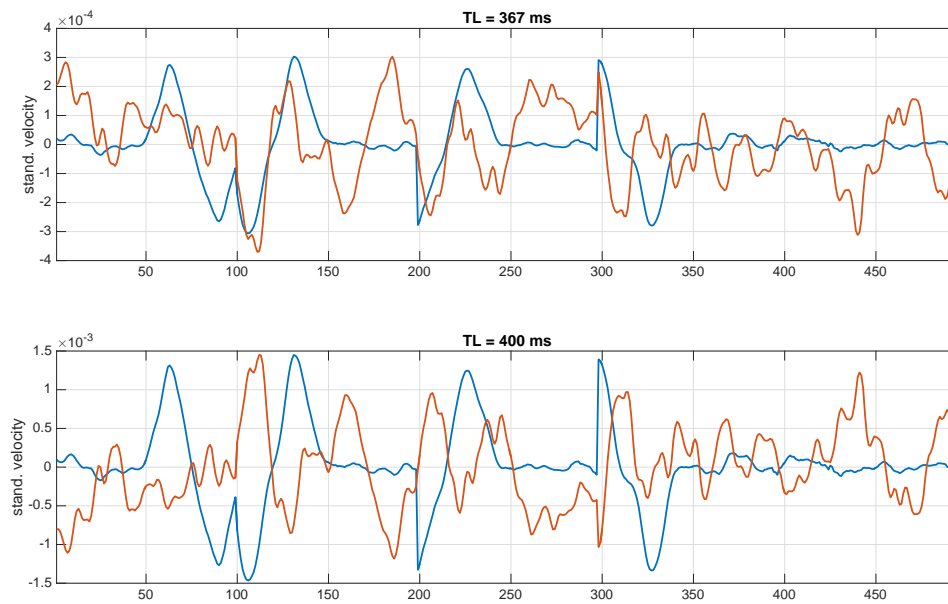


Figure 4.9: Predicted trajectories from two timelags with a difference of 33 ms. The figure shows that the trajectories predicted from two neighbor timelags can be mirrored on the time axes when the sign of the regression parameter change.

It was shown in an example that if the regression parameter b is very small the accuracy of the predicted trajectory can be reversed by the change of a single timelag, this means that the timelags, which produce small regression parameter are very sensitive timelags. In the chosen optimization method it is not clear whether a timelag is sensitive or not. As can be seen in Figure 4.6, the timelag twelve has a good ranking; although there is this effect like shown before.

Besides the fact that sensitive timelags are not shown in the chosen ranking method, the problem is that if the functions which are compared are periodic, a negative CC does not give any information about, whether this was due to a time-shift or due to a wrong sign of the regression parameter in the training sets. The method is successful in the inner-folds because when averaging the values over all folds negative values in the folds can be eliminated, however if in the outer-folds the parameter differ only a little bit, the in the parameter optimized in the inner-folds have no value in the outer-folds. An approach to solve this problem is given in subsection 5.2.1.

Figure 4.9 shows another problem, the problem that only standardized velocities can be predicted, that means that the velocity values from the test set need to be divided by the standard deviation to make both sets comparable. The standardized value decreases with the decrease of the regression parameter. Converting the standardized velocity into the real velocity is possible, however it seems very challenging in a real time prediction.

Besides all the shown problems it is assumed that the main reason for the low accuracy is a very low SNR. There are some reasons to suggest that:

- The used EEG system has dry electrodes, which effect very high impedances between the electrodes and the skin and thus the quality of the measured signals is impaired.
- The experiment was not carried out in a shielded BCI laboratory, but in an electronic laboratory with many electronic devices around and WiFi connection. This makes the measured signals susceptible to artifacts.
- With an ICA, EOG artifacts were removed, however other components like EMG or noise couldn't be identified and removed.



5 Summary and Future Prospects

5.1 Summary

The aim of this Master's Thesis was to develop a naturally controllable BCI that can predict motion trajectories from the imagination of motor execution. The approach to reach this aim was to find a correlation between movement and brain data, which can subsequently be used for the prediction of movement trajectories only from brain signals. To calculate this correlation, an experiment was carried out, in which a participant had to do triggered movements, synchronized by beep tones, to four different targets and back to the start position. The four targets were placed on an acrylic plate in a horizontal or vertical distance of 10 cm to a center point. For a high ecological validity the order of the targets to which the participant made his movements was self-selected by the participant. While the participant executed 10 MBs with 12 center-to-target and target-to-center movements each, the positions of the hand were tracked by the Kinect camera system with a frequency of 30 fps and the brain data were recorded by the g.nautilus EEG system with 32 active and dry electrodes at a frequency of 250 Hz. In a preprocessing stage, the qualities of the kinematic and EEG data were improved when applying different filters. After the preprocessing, features of the kinematic and EEG data were extracted for the calculation of the correlation. As kinematic features the velocities, separately in x and y direction, and as EEG features a standardized BTS in six different frequency spectra in overlapping time-windows of 500 ms were calculated. To make the data of the kinematic and EEG features comparable, the time-windows for the calculation of the EEG BP were respectively shifted by 33.33 ms. For all six EEG frequency bands, datasets were created which include the BP data of 30 EEG channels in 15 timelag dimensions from 0 to 500 ms. The EEG and kinematic datasets were serial divided into two different levels. First, in an outer-fold level, the kinematic and EEG data of the first MB were defined as outer-fold test set and the data of the other MBs together were defined as outer-fold training set. Second, the data of the outer-fold training set were defined as inner-fold set and separated into six folds by a 6-fold CV. In this inner-fold level, in change, the data of five folds together were defined as training sets and the data of the one fold left were defined as test sets. In the training sets regression parameter between the kinematic and EEG data were calculated using a multiple linear regression. Subsequently, with the calculated regression parameter of the training set and the EEG data of the test set, trajectories were predicted. The predicted trajectories were compared with the original trajectories of the kinematic test sets and the correlation coefficient between the original and predicted trajectories were calculated. The

CCs were averaged for all six frequency spectra over all six folds and both spatial dimensions. To avoid overfitting, the setup of timelag and used EEG channels were optimized. To calculate an optimized timelag distance, the accuracies were calculated for each timelag separately with a fixed EEG channel montage. According to these results, the timelags were ranked. At the end of the timelag optimization, the optimal numbers of timelags were calculated; to do this the accuracies for varying numbers of timelags, sorted by its ranks, were calculated while the EEG channel montages were kept fix. After the optimization of the timelags, the EEG channel montages were optimized. This was done in the same way like the optimization of the timelags, however, with varying channels and a fixed time lag distance.

With an optimized setup the inner-fold accuracies were improved and the best results were as expected shown in the mu and low beta spectra with accuracies up to 25%. When calculating the outer-fold test set accuracies using the optimized setup from the inner-folds, there was no significant improvement. The problem has been that the regression parameters b are very low, this makes some timelag distances very sensitive for high changes in the accuracies. Beside the problem of the high sensitivity of the results between the timelags, it is assumed that the SNR is not high enough for a good prediction. The assumed reasons for the low SNR are that the used EEG system has dry electrodes with high impedances between the electrodes and the skin, that the experiment was carried out in a not-shielded laboratory and that EMG, ECG and noise were not removed in an ICA. As further problem, it was shown that the system could only predict trajectories with standardized velocities.

For this reasons, the developed BCI system can actually not be used for the control of an application. However, in the last part of this thesis some future prospects, which show how the developed system can be improved and how the system could be used for a future application, are given.

5.2 Future Prospects

5.2.1 Improvements to the current system

It can be expected, that with some changes in the execution of the experiment, in the processing and in the evaluations, the prediction accuracies of the trajectory decoder could be improved enormously.

The EEG data basic could be improved when using an EEG system with wet electrodes instead of dry electrodes. This would lower the impedances between the electrodes and the skin of the participants. Furthermore, some artifacts could be avoided when examining the experiment in a shielded BCI laboratory.

With an extended ICA, other components like EMG artifacts or noise could be reduced from the signal and thus the SNR could be improved. Also, the variance of the results could be reduced

if the number of k folds in the CV is increased. However, if the number of k folds is increased, it seems advisable also to higher the number of MBs to keep the same number of measurement points in all folds.

To make the good inner-fold results transferable to the outer-fold level, it is necessary to include the sensitivity of the timelags in the inner-fold optimization. An approach to solve this problem is shown in the following figure. In this figure the timelag course of the regression parameter is compared with the timelag course of the predictable accuracies. The courses were made for six central channels (see Figure 3.51) in the low beta spectra. For the timelag courses of the regression parameter, the absolute values of the regression parameter were averaged over the six inner-folds and both spatial dimensions.

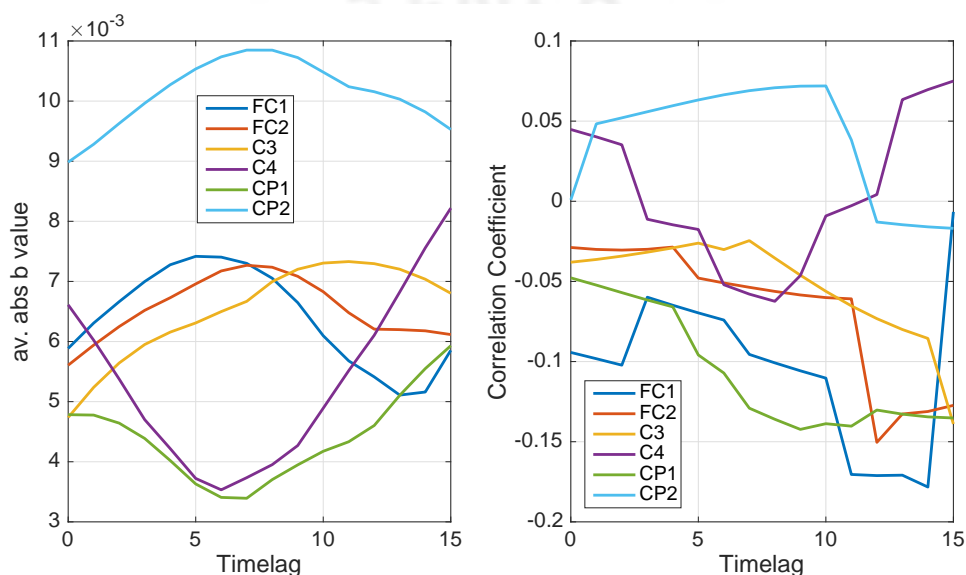


Figure 5.1: Comparison of the timelag courses of the regression parameter and the predicted accuracies. For the timelag courses of the regression parameter (on the left side) the absolute values were taken. For both courses the values for the six calculated channels over all six folds and both spatial dimensions were averaged.

The figure shows, that the courses of the timelag sensitivity and the courses of the predictable accuracies are similar for all channels. However, the timelag-sensitivity courses are much smoother and differ enormously at some timelag distances. As it can be seen, for channel *FC1*, the highest accuracy value is at timelag 15 while the sensor activity has one of its lowest values for the same channel at this timelag.

Since both courses are related, maybe the regression parameter alone could be used as criterion for the ranking. This would make sense because only regression lines with higher slopes could guarantee low variances in the datasets.

A total different approach to improve the accuracies could be to change the regression method. Since it is not sure if there is a linear correlation between movement and brain data, the regression

could be done by an ANN, that also can calculate non-linear correlations [53].

5.2.2 Concept for the practical use of the Trajectory Decoder

If the BCI system can be improved according to the previously mentioned improvement suggestions and a solution is found to calculate real velocities instead of standardized velocities, it is recommendable to develop an application for this system. The BCI system was designed to be optimized for a PC application, however, before the system can be used for a computer application, it is need to be made online-capable. This could be done in the Matlab environment with a Simulink model as it is shown in a simplified manner in Figure 5.2. For the online-capable system, the frequency interval could be limited between 0.5 and 40 Hz by the EEG system block integrated bandpass filter as well as the re-referencing with a CAR can be done within this block. An artifact reduction, as well as a baseline correction is not possible in the online-processing model. That means that the system could only work reliable as long as the users don't make any blinks. After the optimizations in the offline system, it is not necessary to separate the signal in the online-capable system into all six frequency spectra, it is sufficient and useful when the signal is only separated in the frequency range where the best results were shown in the offline model. The main parts; the calculation of the standardized BP, the prediction of the velocity from the BP and the prediction of the position from the velocity can be done in Matlab functions within a Simulink block. Finally, the calculated positions can be transferred to an application.

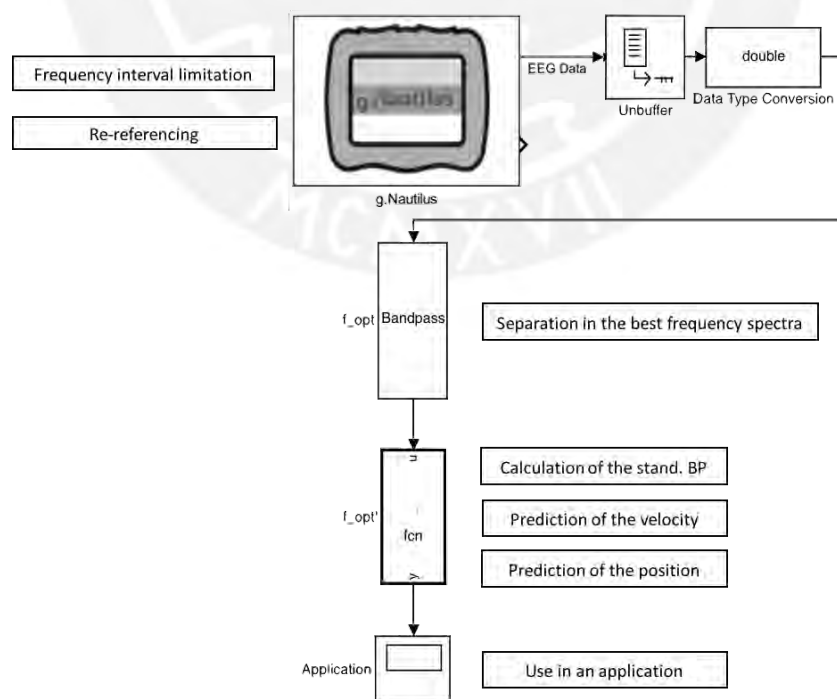


Figure 5.2: Simplified model of the online-capable BCI system. In the Simulink model it is shown which blocks could take over which functions.

In the application, patterns could be shown with a movable cursor placed on it. The BCI users could then move this cursor by MI and trace the pattern as it is shown in the following figure.



Figure 5.3: Example for an application for the BCI system. The application could show pattern which could be traced by MI of the BCIs user.

With such a system, a neurofeedback training could be enabled, in which the users learn to generate MIs. Later, when the users are accustomed to create the necessary MIs for the control of the cursor, they could draw more difficult shapes which are not shown on the screen and communicate by this way.

5.2.3 Finding of suitable participants

A look to the results of BCIs that can predict motion trajectories, developed by other researchers show that the reached accuracies between the different subjects differ enormously. This applies to common systems that use time series of EEG potentials for reconstructing trajectories, like in Bradberry et al. [54], as well as it applies to systems that use time series of EEG power spectral values, as used in this thesis and in Korik et al. [12].

The enormous differences between the individual participants in the same experiments suggest that there are some participants more suitable for the use of such a BCI system than other participants. The reason for this phenomenon might be that because of the low spatial resolution of EEG systems some signals that correlate with the execution or imagination of movements cannot be measured. As Korik et al. have shown in [12] and in this thesis confirmed, MTP BCIs that use BTS as features have the best results for trajectories predicted from the mu and low beta band. To the movements correlating changes in the BPs is in the mu band a result of ERD and in the low beta band a result of ERS.

It can be assumed, that already before adjusting a MTP BCI system that use BTS, the predictable accuracies for a particular person can be estimated when having a knowledge about how strong ERDs and ERSs can be calculated for a particular person.

An approach to find out the strength of ERDs and ERSs that can be measured for a participant is that the participant does some triggered movements (e.g. the finger to thumb opposition, as shown in the following figure) and afterwards, the to the movements correlating ERDs and ERSs

from the EEG BPs according to Figure 2.3 are calculated. The maximum of the ERD and ERS could be used as criteria for the strength.



Figure 5.4: Finger to thumb opposition [55]. In the finger to thumb opposition, the participant has to move one finger after the other to the thumb and back in a triggered sequence.

Appendix

A.1 Commissioning of the EEG system

The g.nautilus Research set requires a actual version of Windows 10 Pro and a Matlab Version of 2015 or newer. After the installation of all necessary software and drivers, paths had to be set in Matlab in order to put the system into operation.

The first test with the system was to check the electrode-skin-impedance with an equipped internal impedance check. The result of this test should be that for all the electrodes up to "Cz", which is used for the impedance calculation and cannot measure its own impedance, have higher impedances than 10 M Ω . The reason for this high impedance is that the used electrodes are dry electrodes. However, the measured signals have a good quality.

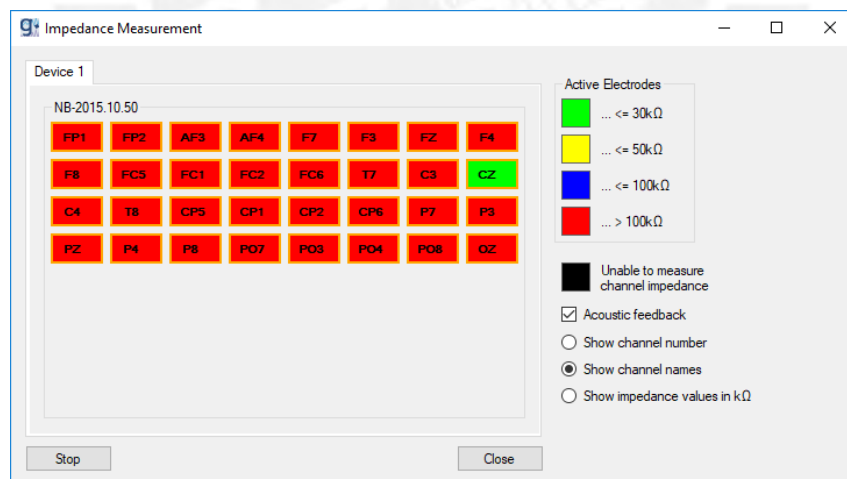


Figure A1: Measuring of the EEG electrodes impedance. The figure shows the expected result for the measuring of the electrode impedance. Channel "CZ" is green because it is used for the calculation of the impedance and cannot measure its own impedance; all the other channels have impedances higher than 100k Ω , which are normal values for active electrodes.

According the high impedance, it is recommended to set the sensitivity level for all channels up to 562.5 mV, which allows higher DC offsets as normally seen with dry electrodes [46]. In order to enable an optical test of the voltage with a scope for all channels at least a bandpass filter

had to be set. With the scope certain signal components e.g. created at blinking or jumping are visible.

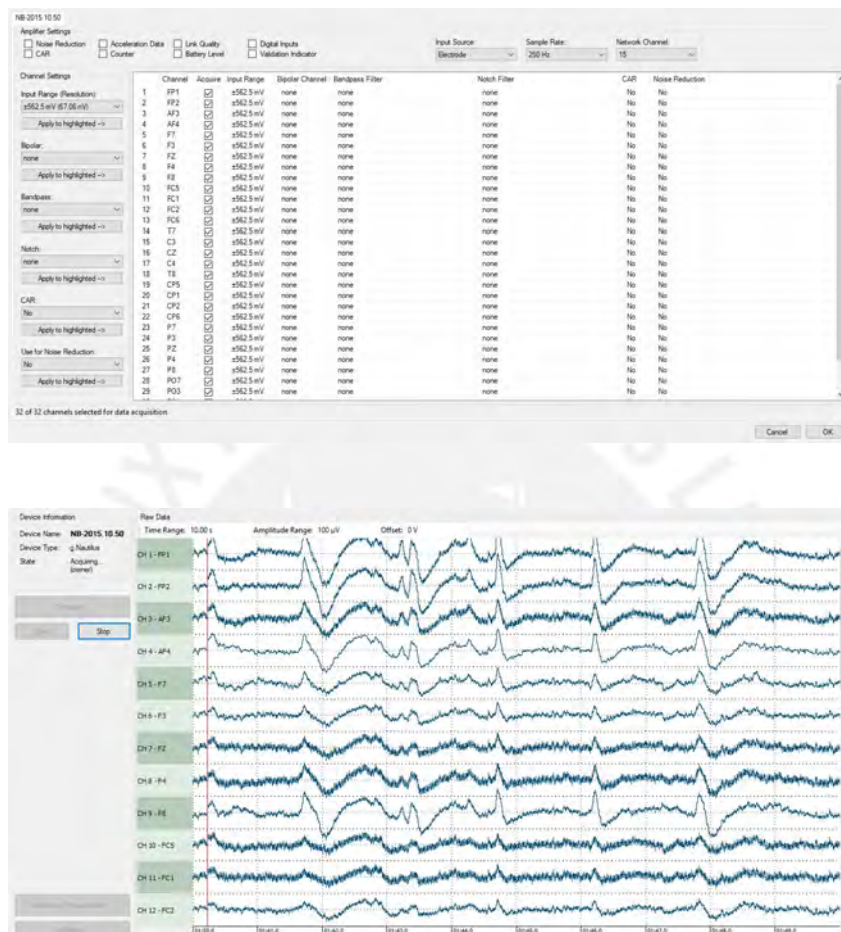


Figure A2: EEG settings and EEG scope. The Input Range has to be set to ± 562.5 mV, to get good results on the EEG scope it is also necessary to set a bandpass (or high pass) filter.

A.2 Commissioning of the Kinect system

To commissioning the Kinect[®] for Windows[®] v2 system via Matlab[®], it was necessary to have Windows 8 or 10 and the Matlab version 2016a or newer installed. Furthermore, the Kinect for Windows SDK 2.0 and the actual Kinect for Windows Sensor Support Package in Matlab had to be downloaded and installed [56].

The first test was using the Matlab Image Acquisition Toolbox[™] to take pictures with the integrated depth sensor and Color camera and track the 25 possible skeletal points. After this acquisition the tracked points were overlaid to the photos and in the color image the tracked points were connected via a connection map, see Figure A3.



Figure A3: Trackable skeletal points. The left picture shows two people taken by the Kinect Depth sensor and overlaid by tracked skeleton points. The picture on the right shows the same situation recorded by the Color Camera, overlaid by the skeletal points from the depth sensor and connected by a connection map.

A.3 Preliminary tests for the experiment

A.3.1 Memory requirements

Number of necessary computers

During a test run in the constellation of 8 MBs with 12 movement cycles per MB, recorded by the Kinect sensor, the RAM were observed by the Windows Task manager. The result of this test was that Matlab, in this constellation, needs up to 6.5 GB of the RAM. Since for the EEG system a minimum RAM of 4 GB is required and the available computers have just a 8 GB of RAM, it was decided to do the EEG and kinematic data acquisitions on two separate computers.

Optimal combination of Movement Blocks and Movement Cycles per Movement Block

Originally it was planned to make 6 MBs each with 15 Movement Cycles. However it turned out that, when running the script the system always crashed at the third MB. Also optimizations in the script (reducing of used variables and deleting of variables directly when they were not longer necessary) didn't have a significant effect on the problem.

The reason for the problem is that Matlab has memory leaks. When deleting variables and data, there are residues which can only be eliminated by a garbage collector. Matlab has such a Garbage Collector but this Garbage Collector becomes just active when the system "think" that it is necessary [57]. Hence, without the use of Matlab's Garbage Collector the "Memory used by MATLAB" becomes higher after every system run and at the same time the "Maximum

possible array” becomes less. Normally this is not a problem but when using the Kinect system, the Depth sensor first makes all the pictures and then the system evaluates it and copy it into a Matlab array. So, if for 1200 pictures (10 s Initializing + 30 s MB at a frame rate of 30 fps) with a solution of 512 x 424 pixels 25 joints are calculated, enormous amounts of data are generated, which all have to be saved in an array in a short time. Often the array with the metadata needs more space than the ”Maximum possible array” provides and this causes the crash of the system.

For the demonstration of the memory leaks, a test was implemented with a single MB of 15 Movement Cycles. Before and after every block the RAM was measured and all data from the RAM were deleted with the command ”clear all”. Figure A4 shows an illustration of the results.

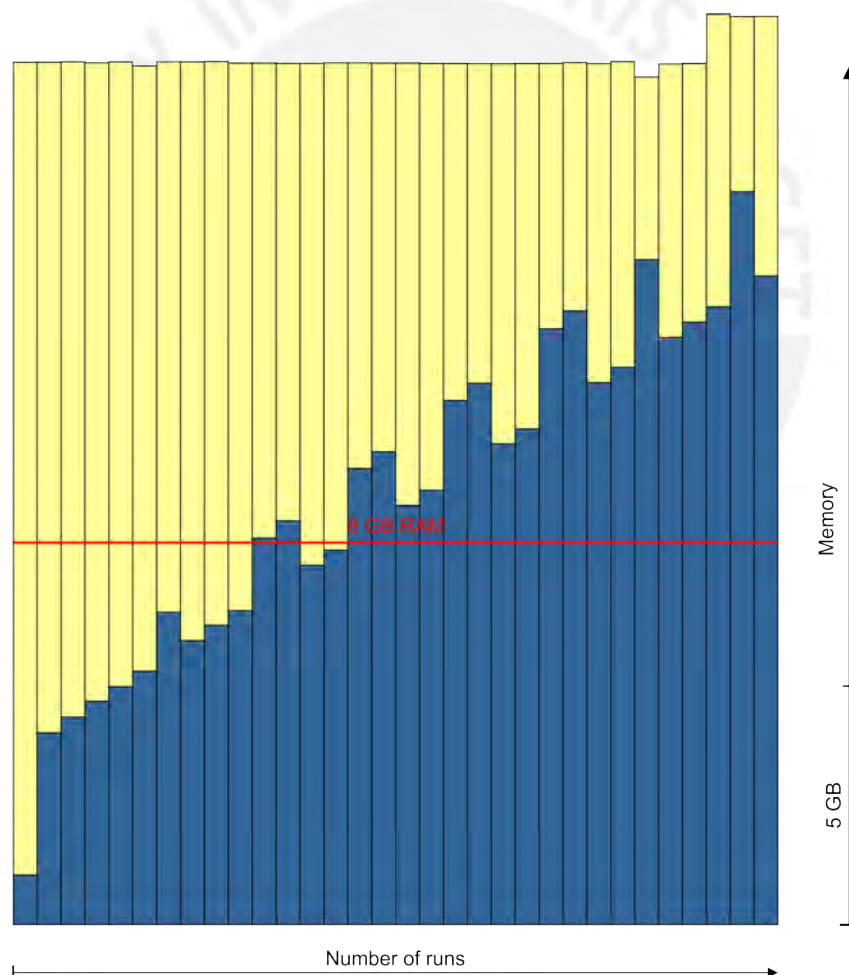


Figure A4: Demonstration of the Matlab memory leaks. The figure shows that the ”Memory used by Matlab” (shown as blue bars) increases while the ”Maximum possible array” (shown as yellow bars) decreases. The reason why the sum of the two parameter at the end change is probably because Matlab uses the memory of the hard disk drive (HDD), additional to the RAM.

To do the experiment with 6 MBs and 15 Movement Cycles like planned, there would be some alternatives to the described data registration:

- One possibility would be to use a normal camera instead of the Kinect Depth Sensor . With the camera, the movements could be filmed and a marker (attached to the hands of the participants or to the pen the participants use) can be tracked by a video analyzing system like "Kinovea" [58]. A drawback would be that the calibration of the system would be a bit more challenging and maybe not accurate enough for the little movements in the experiment. A bigger drawback would be an enormous expenditure of time to track every single picture manual. Using a camera with a frame rate of 30 fps means 900 pictures per block and 5400 pictures per participant which had to be track manual.
- another possibility would be to modify the script so that not first all pictures are made by the Kinect Depth sensor and then analyzed, but instead that the analysis of the picture is done immediately after every single picture, before taking a new picture, like it is done in the Kinect real-time tracking. The advance would be that the enormous amount of data would be saved over a longer period in the Matlab arrays, which would reduce the risk of crashes. However, the frame frequency would be lower than 30 fps and so kinematic information would be lost.
- A third possibility would be to start all the MBs separately. A test showed that for this case, the data acquisition still worked reliable after 20 repetitions. However, it is to be feared if there are many new starts of the program, the participants lose their concentration and the recorded EEG data degrade.

After weighing the alternatives, it was decided to do the data acquisition with the Kinect depth sensor like planned but the constellation of 6 MBs with 15 Movement Cycles each was changed. To find a constellation, which comes as close as possible to the planned constellation without crashing the system, some tests were done. In the tests it was tried to reach the planned 90 Movement Cycles or more in another constellation of MBs and Movement Cycles per MB. The experiment started with the constellation of 18 MBs with 5 Movement Cycles per MB. After every successful run, the number of Movement Cycles per MB was increased by one and the number of MBs has been adjusted to reach 90 Movement Cycles or more. To nearly have the same conditions after every test, Matlab was closed and restarted. Furthermore, no other application on the computer was active.

The following combinations of "Number of MBs x Movement Cycles/MB" were tested:

- 18 x 5 • 15 x 6 • 13 x 7 • 12 x 8 • 10 x 9 • 9 x 10
- 9 x 11 • 8 x 12 • 7 x 13 • 7 x 14

All the runs were successful until the combination of 7 MBs with 14 Movement Cycles per MB. For this reason, the next lower combination of 7 MBs with each 13 Movement Cycles was

tested for several times and it also failed sometimes. A combination of 8 MBs with 12 Movement Cycles was in the entire tests stable. For this reason, this combination was chosen as the optimal constellation of MBs and Movement Cycles per MB.

Later, the system also crashed sometimes in this constellation, but never because of the RAM. The crashes happened always because of disk performance issues. To avoid this reason for crashes, the Windows "superfetch service" was disabled [59]. With a disabled superfetch service all the runs worked reliable.

A.3.2 Best suited skeletal point

For the experiment, it seems possible to use the tracked data of the right hand, the right thumb or the right fingertip. To find out which tracked skeletal point is best suited for the usage in the experiment a test was done.

In this experiment, there were 12 Movement Cycles (3 to each target alternated and counter-clockwise beginning with the target on the right) according to Figure 3.3 done, recorded by the Kinect system and the measured points in a Cartesian coordinate system plotted. Furthermore, a calibration was done, in which the average value of the last 15 measured points of the initialization phase were subtracted from all measured points.

As you can see in Figure A5, the results of the hand coordinates were a bit closer to the ideal form. They showed a bit less measuring faults than the results of the fingertips. The results of the right thumb were worse than the others. The conclusion can be inferred that the tracked skeletal point of the right hand is the best-suited point for the experiment.

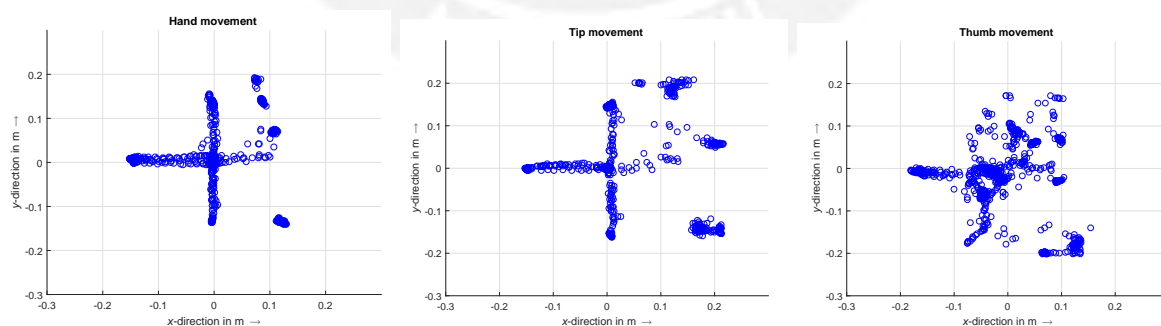


Figure A5: Comparison of the measuring points of different skeletal points. The three figures show measured points for the right hand (left), the right finger tip (middle) and the right thumb (right) during the execution of movements from a center point to four targets, which were in a 15 cm distance horizontal right and left and in a 15 cm distance upper and lower to the center point.

A.3.3 Optimization of the experimental setup

Target Plate position

After finding optimal software configurations and an optimal combination of MBs and Movement Cycles per MB, the experimental setup had to be optimized in optomechanical aspects.

The first experiment was to position the plate with the targets in a distance of around 1.5 m directly in front of the Kinect system and to observe the plate with the Kinect Depth sensor. It was conspicuous that a big black spot appeared directly in front of the Depth sensor on the plate (see Figure A6, left). That this spot originated by reflections of light could be excluded by darkening the space. The spot can be traced as the total reflection of the infrared light from the depth sensor. Since it can be assumed that this spot could falsify the results, the target plate was shifted horizontally and parallel to the Kinect, until the spot finally disappeared (see Figure A6). Since this position is still very central, this position was assumed to be as the ideal position (see Figure A6, right picture).

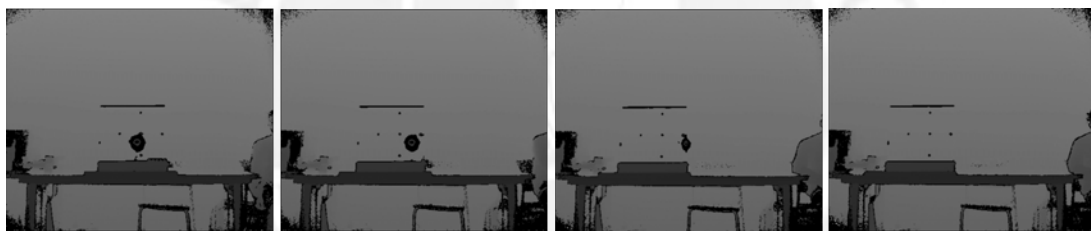


Figure A6: Spot on the target plate. On the left picture, there is a big spot in the center of the plate; resulting by total reflections of the infrared light of the Kinect depth sensor. While shifting the plate (figures from the left to the right) the spot disappears.

In the following preliminary tests, 12 Movement Cycles (3 to each target alternating and counterclockwise beginning with the target on the right) according to Figure 3.3 were done. They were recorded by the Kinect system and the measured points were in a Cartesian coordinate system plotted. Furthermore, a calibration was done, in which the average value of the last 15 measured points of the initialization phase were subtracted from all measured points.

Positioning of the targets

The measured hand position points (Figure A5, left) to the upper, left and lower targets looked quite good, however the points to the right target looked just good until around a 10 cm distance to the center point, then the points stay at a distance of 10 cm on the x-axis and make jumps on the y-axis. The reason why this happened could be that the right and left target points have just an 8 cm distance to the edges of the acrylic plate. Since the tests were done with the right

hand, the hand coordinates came really close at the movement to the right target point to the right edge of the plate, so the transition of the plate and the air caused this negative effect. To avoid these errors, all target points and the home position were shifted 6 cm to the left side.

Cleanliness of the plate

After repeating the experiment with the shifted target points, the problem with the missing 5 cm on the right seemed to be solved, however there was a new problem. The movements to the upper target point weren't measured (see Figure A7). The reason for this error was, that when moving the targets, which are adhesive strips, some glue staid on the acrylic plate and interfered the Kinect Depth sensor.

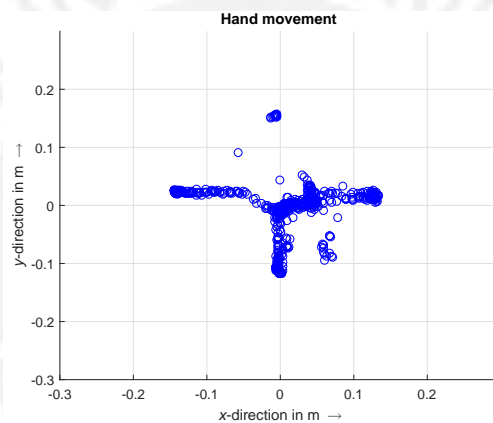


Figure A7: Measurement errors caused by a purified acrylic plate. The figure shows measured points of the right hand position, when doing movements (forward and backward) from a center point to 4 targets, which are in a 15 cm horizontal and vertical distance to the center point. The deviations to the ideal shape are due to the fact that the plate was dirty in the upper area.

Reflections on the plate

One new error appeared after cleaning the acrylic plate with isopropyl. There were suddenly many random measurement errors and the calibration was not working well (see Figure A8). It turned out that the cause of the failure was the TFT screen of the used computer, that was parallel to the acrylic plate, and provoked reflections on the acrylic glass, which disturbed the depth sensor when it becomes darker outside (around two hours before the sunset).

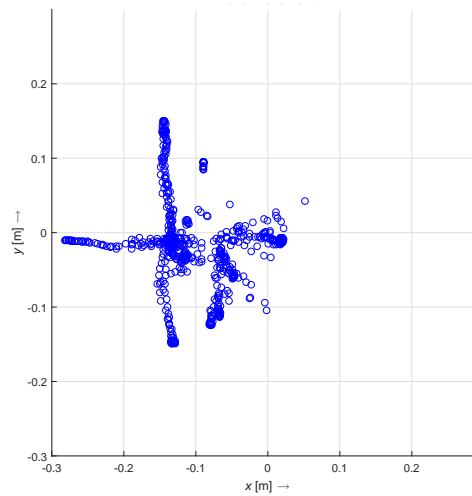


Figure A8: Measurement errors caused by reflections. The figure shows measured points of the right hand position when doing movements (forward and backward) from a center point to four targets. The targets are in a 15 cm horizontal and vertical distance to the center point. The deviations to the ideal shape and the not working calibration are due to reflections on the plate.

Furthermore, it was noted that when it's sunny outside there are also reflections on the acrylic plate that was parallel to the window. To solve this problem and the problem with the TFT screen, the experimental setup were turned by 90° and punctual light was shielded by a curtain.

Positioning of the targets 2

After all this optimizations, the result in Figure A9 was obtained. According to the Figures A5 to A9 the same errors were always found; an increased number of measuring points at the bottom right.

To specify the origin of the errors, a plot of the trajectories over the time separately in x and y direction were done (see Figure A10). The evaluation of this plots shows that when the movement to the lower target point is done, the x coordinates of the measured points make a jump. The reason for this is that the lower point is really close to the end of the plate and hence to the end the visible field of the depth sensor.

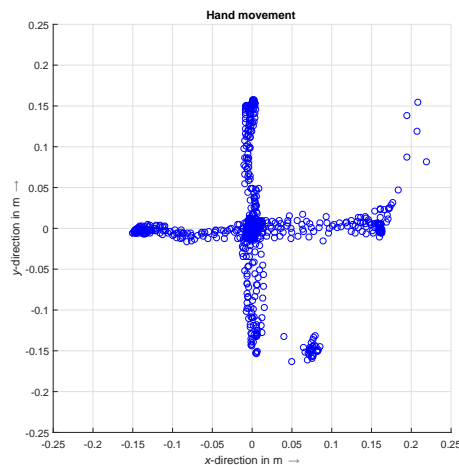


Figure A9: Measurement errors after optimizations. The figure shows measured points of the right hand position when doing movements (forward and backward) from a center point to 4 targets, which are in a 15 cm horizontal and vertical distance to the center point. The plotted measured points show that there are still some measurement errors after a process of optimization.

To eliminate these errors, a larger plate with more space from the targets to the borders could be used or the targets could be shifted closer to the center point. The decision was to reduce the distance from the target points to the center point from 15 to 10 cm. This change has the advantage that the resultant basic shape of 20 cm x 20 cm (see Figure 3.2) fit on a 21" screen, and so the experimental data could be better used for the development of a PC application.

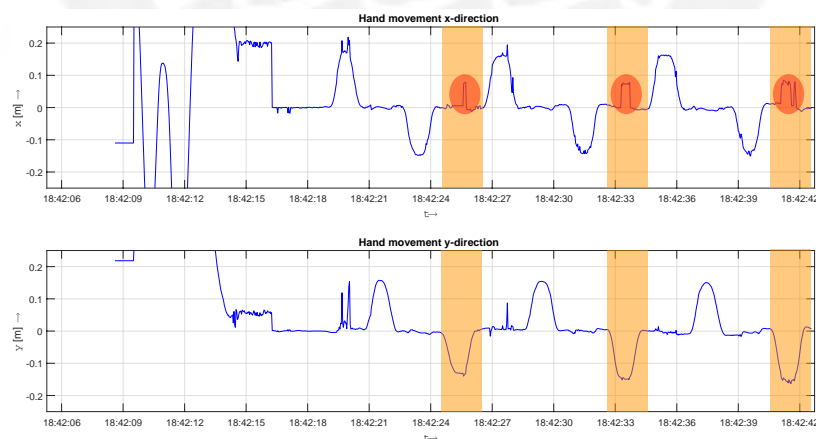


Figure A10: Specification of the origin of a recurring error. In this figure the movements in x and y direction were separately plotted over the absolute time. From around 18:42:09 to 18:42:19 was the initialization phase. After the initialization phase first a movement to a target 15 cm horizontally right of a center point and back were done, then to a target 15 cm vertical upper a center point and back, then to a target 15 cm horizontal left and back and finally to a target 15 cm vertical above to a center point and back. Before repeating the same procedure two more times. It is noticeable that for all movements to the lower target point (orange bar) the x coordinates make a jump (red ellipse), which means errors.

Results for the experimental setup improvement

The result of the tests with the new placement of the target and home position points as well as with new insights that an additional improvement could be achieved when the participants sat with their back close to a white wall, which reduces background noise and when the participants wear tight clothes is shown in Figure A11.

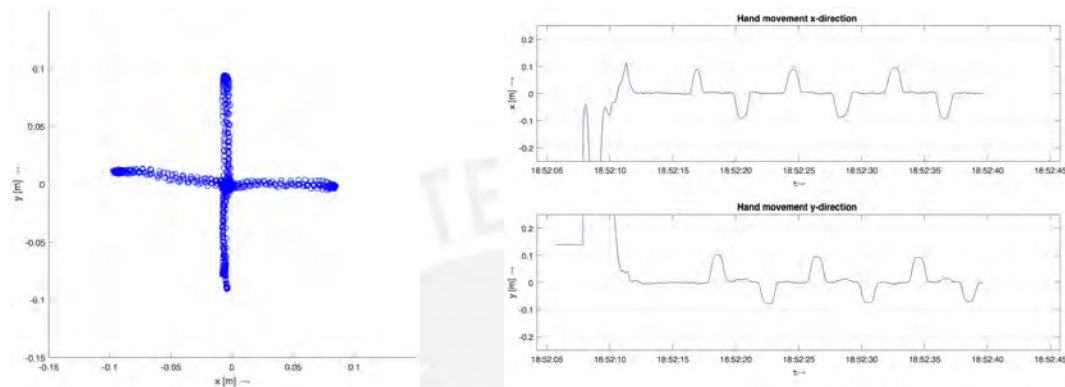


Figure A11: Results after optimization. The left figure shows nearly perfect measured points for the right hand when three movements from a center point to four targets on acrylic plate, which are in a 10 cm distance horizontal right and left and in a 10 cm distance upper and lower to the center point. In the right figure the movements in x and y direction were separately plotted over the absolute time. In this figure the movement order (in the phase of the MB, beginning at around 18:52:16) from the center point to a target point and back to the center point can be seen very good. It can also be assumed that there is no kinematic noise.

The results with the last constellation seem to be very good. Hence, in conclusion to get optimal results it is necessary that:

- the plate has a horizontal offset parallel to the Kinect
- the participants are close with their back to a bright wall
- the plate is not parallel to active screens
- the plate is in a right angle to the windows
- punctual light on the plate is shielded
- the distance between the target points and the edges of the plate is more than 10 cm
- the target plate has to be clean
- the hand is the tracked anatomical point
- the participants do not wear wide clothes

A.3.4 EEG findings

Transient phase

In a test, in which the EEG data were recorded it could be seen, that the g.nautilus system has a transient phase at the beginning of the recordings for approx. 15 s. For this reason it is recommendable not to use the data of the first 20 seconds for the evaluation of the experiment.

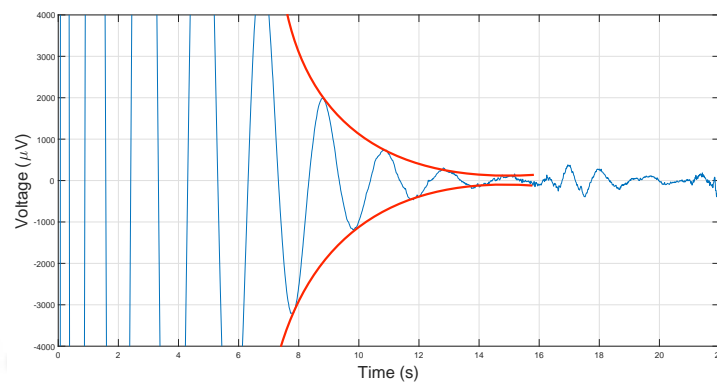


Figure A12: Transient phase at the beginning of the EEG data registration. The figure shows that the EEG system has an exponential decreasing transient phase at the beginning of the data recording.

A.4 Experimental Procedure

Preparation before all experiments

Computer "Kinect"	deactivating Win Superfetch Win Symbol + X -> Windows Power Shell -> net.exe stop superfetch starting Matlab choosing path opening script "test position" and check the position of the Kinect opening script "savedata" check if save data is activated opening script "test run"
Computer "EEG"	starting Matlab choosing path opening Matlab script check if save data is activated loading Simulink model and checking all the EEG settings

Preparation before each experiment

both Computer	check if no data can be replaced synchronization of the time on both computer
Preparation EEG	participant have to take his/her cellphone out of his/her pocket ground the participant (touching 3 seconds a metal) put on the ground and reference electrode on the participants head put on the EEG system on the participants head switching on the EEG system measuring the impedance and checking if the system is working with the gtec program g.Need access
Preparation general	explaining the experiment (movements, blinking, fixing the eyes etc.) doing exercise runs using the "test run" script

Performing of the experiment

before Experiment	starting EEG measurment runing Kinect script "savedata"
during Experiment	Write down blinks
after Experiment	terminating EEG measurment runing EEG Script "save data" rename EEG and Kinect data Moving the data in the folder "data"

A.5 Request and approval of the local ethics committee

A.5.1 Declaration of commitment to the ethical principles of research

Comité de Ética de la Investigación (CEI)

Oficina de Ética de la Investigación e Integridad Científica (OETIIC)

Vicerrectorado de Investigación

Declaración de Compromiso con los Principios Éticos de la Investigación

Datos del investigador o investigadora principal

Nombre completo: Matthias Petersamer

Afiliación PUCP: Estudiante de la PUCP

Profesión / Especialidad: Maestría en ingeniería mecatrónica

Datos de la propuesta de investigación

Título de la investigación: Predicción de trayectorias de movimiento basadas en Imaginación Motora para una Interfaz Cerebro-Computador

Declaro:

<input checked="" type="checkbox"/>	Que mi/nuestra investigación SÍ requiere de la participación de seres humanos, animales o ecosistemas, (pudiendo tratarse inclusive de embriones, fetos, células, fluidos, partes del cuerpo, cadáveres). Son parte de estas investigaciones los estudios que requieren la aplicación de encuestas, cuestionarios, pruebas (psicológicas, clínicas, médicas), entrevistas, grupos focales, observación natural y observación participante, uso de material fotográfico o grabaciones en audio y video, y validación de tecnologías (clínicas, ambientales, de construcción, etc.).
<input type="checkbox"/>	Que mi/nuestra investigación NO requiere de la participación de seres humanos, animales o ecosistemas (pudiendo tratarse inclusive de embriones, fetos, células, fluidos, partes del cuerpo, cadáveres); ni comprende ninguno de los instrumentos o técnicas de recolección de información ejemplificados en el párrafo anterior.

Al marcar la opción **SÍ**, me estoy comprometiendo a respetar los principios éticos que una investigación exige y que se encuentran en el Reglamento del Comité de Ética de la Investigación. Por esto me comprometo a explicar la manera en que los desarrollaré en mi investigación.

Los cinco principios éticos sobre los que he construido mi propuesta de investigación son:

- Respeto a las personas
- Beneficencia no maleficencia
- Justicia
- Integridad Científica
- Responsabilidad

Comité de Ética de la Investigación (CEI)

Oficina de Ética de la Investigación e Integridad Científica (OETIIC)

Vicerrectorado de Investigación

Por ello asumiré con responsabilidad lo señalado por el Reglamento del Comité de ética para la investigación con seres humanos y animales:

- Respetaré la autonomía de las personas que participen en mi investigación haciendo uso del consentimiento informado.
- Respetaré el derecho a la confidencialidad y privacidad, protegiendo la información brindada por los participantes de mi estudio.
- No causaré daño a las personas y/o animales involucrados en mi estudio.
- Tomaré las precauciones necesarias para disminuir los riesgos a los que podrían estar expuestos mis participantes durante mi investigación, y maximizaré los beneficios.
- Trataré de manera justa y equitativa a las personas que participen de los procesos, procedimientos y servicios asociados a la investigación.
- Declaro no tener participación efectiva o potencial en una relación financiera o de otro tipo, que afecte directa y significativamente, o que pudiera afectar mi juicio independiente e imparcial en mi deber para con la universidad.

Asimismo, desarrollaré las medidas consideradas indispensables para cumplir con estos principios en el protocolo de investigación (componente ético o consideraciones éticas).

Firmo el presente compromiso en San Miguel, el 11 de julio del 2017

Firma

A.5.2 Explanation of the project

Explicación del proyecto

**Predicción de trayectorias de movimiento basadas en Imaginación
Motora para una Interfaz Cerebro-Computador**

-

Proyecto de tesis de maestría

Autor: BSc. BEng. Matthias Petersamer

Asesor: MSc. David Ronald Achancarray Díaz

ÍNDICE

RESUMEN	3
CAPÍTULO I: INTRODUCCIÓN	4
1.1. PLANTEAMIENTO DEL PROBLEMA	4
1.2 JUSTIFICACIÓN	5
1.3 OBJETIVOS	5
1.3.1 Objetivo general	5
1.3.2 Objetivos específicos	5
1.4 HIPÓTESIS	5
CAPÍTULO II: MATERIAL Y MÉTODOS	5
2.1 DISEÑO	5
2.2 LUGAR DE ESTUDIO	5
2.3 POBLACIÓN Y MUESTRA	6
2.3.1. Criterios de inclusión	6
2.3.2. Criterios de exclusión	6
2.3.3. Tamaño de muestra	6
2.3.4. Muestreo	6
2.4 PROCEDIMIENTO	6
2.4.1. Ubicación y reclutamiento de participantes	6
2.4.2. Aplicación de consentimiento informado	6
2.4.3. Recolección de datos y evaluación	6
2.5. INSTRUMENTOS	8
2.6 ANÁLISIS DE DATOS	8
2.7. ASPECTOS ÉTICOS	8
2.7.1. Aprobación	8
2.7.2. Información a los participantes	8
2.7.3. Confidencialidad de la información	8
2.7.4 Análisis de riesgos y beneficios	9
CAPÍTULO III: Otros	9
3.1 Fin del proyecto	9
3.1 PRESUPUESTO	9
3.2 CONFLICTOS DE INTERÉS	9
BIBLIOGRAFÍA	10

RESUMEN

Una interfaz cerebro computador (BCI por sus siglas en inglés) es un sistema que mide las señales cerebrales y luego las procesa mediante un ordenador con la finalidad de obtener información relevante sobre el funcionamiento del cerebro. Estos dispositivos generalmente registran señales eléctricas (EEG), aunque también pueden registrar otro tipo de señales. Se ha probado que las técnicas basadas en el análisis de señales EEG pueden detectar una correlación entre la actividad cerebral medida y estímulos visuales, ángulo de la mirada, intenciones voluntarias y estados cognitivos, por lo cual se han dado lugar diversos tipos de sistemas basados en señales EEG dependiendo de las áreas corticales analizadas, las características extraídas y la forma en la cual se provee retroalimentación al sujeto.

El uso de sistemas BCI-EEG puede ser empleado en sujetos con diversos trastornos motores como esclerosis lateral amiotrófica, parálisis cerebral, accidente cerebrovascular, parálisis y amputación. Se propone el diseño y aplicación de un sistema basado en una interfaz cerebro-computador para el análisis de señales electroencefalográficas durante actividades de imaginación motora.

El presente estudio pretende aumentar el conocimiento en el área de Interfaces Cerebro-Computador, cuyas principales aplicaciones están destinadas a la mejora de la calidad de vida de personas con discapacidades como las que han sufrido accidentes cerebrovasculares, amputaciones, lesiones de médula espinal, entre otros.

El objetivo del presente estudio es analizar las señales cerebrales asociadas a la realización de movimientos, a través de un electroencefalograma y un sistema cinemático de medición.

Se recolectarán y analizarán datos de participantes en una sola sesión. El estudio se llevará a cabo en el Grupo de Investigación en Robótica Aplicada y Biomecánica (GIRAB-PUCP). Se usará un tamaño de muestra de 5 participantes, consistente en personas sanas de una edad mayor de 18 años, sin historial de enfermedades neurológicas y/o motoras. El equipo de electroencefalografía, así como el sistema cinemático de medición, son no invasivos y totalmente inocuo por lo que no implica ningún riesgo para el participante.

CAPÍTULO I: INTRODUCCIÓN

1.1. PLANTEAMIENTO DEL PROBLEMA

La imaginación de un movimiento implica un aumento o reducción de la amplitud en los ritmos μ y β en las regiones frontales y centrales del cerebro. Con práctica, la gente puede aprender a crear un patrón específico en los ritmos, conocidos como Ritmos Sensoriomotores (SMR), los cuales pueden ser extraídos y clasificados al compararlos con una referencia. Las características clasificadas permiten el control de una prótesis, el brazo de robot y otras aplicaciones. [1]

Normalmente los Interfaces Cerebro-Computador (BCI) basados en Ritmos Sensoriomotores permiten el control de dispositivos como prótesis, sillas de ruedas, movimiento del cursor, etc., en un entorno real o virtual, clasificando la imaginación de movimiento del brazo derecho, brazo izquierdo, los pies y la lengua.

Algunos SMR BCIs clasifican el movimiento imaginario de las extremidades en las aplicaciones que se deben mover en tiempo real. Aunque hay algunas SMR BCI que utilizan una clasificación Multi-Clase (MC) en un espacio de características multidimensionales, los paradigmas más exitosos se basan en sólo dos estados mentales. Esto significa que este tipo de BCI tiene que hacer frente a un número muy limitado de señales de control. [2]

MC SMR BCIs son adecuados para la decodificación de un cierto número de posiciones de destino final, aunque la decodificación de una trayectoria no es posible con esta técnica. Sin embargo, una reconstrucción imaginaria de una trayectoria de movimiento de las extremidades, así como la estimación de los vectores de velocidad durante un movimiento ejecutado o imaginario, se pueden activar por una nueva técnica que se llama Predicción de Trayectoria de Movimiento (MTP). Mientras que los usuarios de SMR BCIs se concentran en el movimiento de una extremidad (extensión, flexión, o rotación), los usuarios de MTP BCIs se concentran en el movimiento en general. Esto permite un control más natural de los dispositivos. El principio de la MTP BCIs es que se crea una correlación entre los datos cinemáticos (velocidad en dirección x , y , z) de movimiento real y los datos de cerebro que se registran en algunos experimentos. Esta correlación conduce a funciones de estimación que se pueden utilizar para reconstruir la trayectoria de los datos cerebrales. [3]

1.2 JUSTIFICACIÓN

El presente estudio pretende aumentar el conocimiento en el área de Interfaces Cerebro-Computador, cuyas principales aplicaciones están destinadas a la mejora de la calidad de vida de personas con discapacidades como las que han sufrido accidentes cerebrovasculares, amputaciones, lesiones de médula espinal, entre otros.

1.3 OBJETIVOS

1.3.1 Objetivo general

Predecir las trayectorias de movimiento a partir de señales de EEG.

1.3.2 Objetivos específicos

1. Encontrar una correlación entre los datos cinemáticos y los datos cerebrales, que pueden ser utilizados para predecir trayectorias cinemáticas.
2. Identificar si la baja resolución espacial del sistema EEG sugiere que algunos participantes son más adecuados para la predicción de trayectorias de movimiento que otros.

1.4 HIPÓTESIS

El cálculo de la correlación entre las señales EEG y la velocidad de la mano en las tres direcciones independientes x , y , z permitirá predecir las trayectorias de movimiento usando para el cálculo solo los datos EEG.

CAPÍTULO II: MATERIAL Y MÉTODOS

2.1 DISEÑO

Se recolectarán y analizarán los datos de los participantes en una sesión. No se requiere un seguimiento posterior.

2.2 LUGAR DE ESTUDIO

El estudio se llevará a cabo en el laboratorio del Grupo de Investigación en Robótica Aplicada y Biomecánica (GIRAB-PUCP). Los investigadores de este estudio tienen pleno

conocimiento del uso del equipo, el cual fue adquirido mediante la revisión de las guías y la realización de pruebas preliminares. El electroencefalógrafo es un dispositivo de baja potencia y no requiere sistemas de seguridad adicionales a los que ya vienen integrados con el equipo.

2.3 POBLACIÓN Y MUESTRA

2.3.1. Criterios de inclusión

Personas sanas y mayores de 18 años.

2.3.2. Criterios de exclusión

Personas con historial de enfermedades neurológicas y/o motoras, y personas zurdas.

2.3.3. Tamaño de muestra

El tamaño de la muestra tendrá de 5 personas.

2.3.4. Muestreo

Se escogerá aleatoriamente a un total de 5 participantes de entre todos los que hayan mostrado interés en participar.

2.4 PROCEDIMIENTO

2.4.1. Ubicación y reclutamiento de participantes

Se realizará una convocatoria abierta mediante redes sociales en Internet.

2.4.2. Aplicación de consentimiento informado

Se les entregará un documento de consentimiento informado a cada participante antes de la sesión. Se discutirá con él y se resolverán todas sus dudas respecto al experimento. Posteriormente se le pedirá que firme el consentimiento informado como muestra de estar de acuerdo con las condiciones. El participante se llevará una copia del documento.

2.4.3. Recolección de datos y evaluación

Al participante se le colocarán electrodos en la cabeza y se le registrarán sus señales cerebrales mientras ejecuta movimientos en dirección horizontal y vertical con su brazo derecho. Los movimientos tienen que ser hechos desde un punto central a cuatro puntos diferentes de destino. El punto central y los puntos de destino están marcados con cinta adhesiva sobre una placa de acrílico. El movimiento será sincronizado con tonos "bip". El

movimiento tiene que ser ejecutado 200 veces desde el punto central a los objetivos y de vuelta al punto central, en un tiempo de alrededor de diez minutos, en un orden al azar.

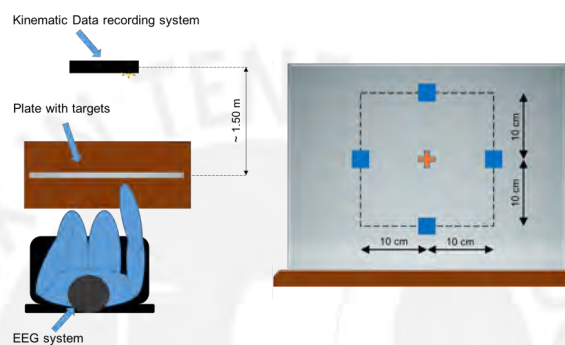


Figura 1: Configuración experimental (a la izquierda) y placa con los objetivos

En la segunda parte del experimento, los participantes serán instruidos para hacer movimientos desencadenados (cómo se observa en la figura 2). Los movimientos deben estar sincronizados con tonos "bip". Esta parte del experimento se utilizará para investigar si estos movimientos se pueden atribuir a la resolución espacial baja del EEG (en caso de obtener diferentes resultados en la primera parte experimental). Por lo tanto, con estos resultados será más precisa la elección de los participantes en el futuro.



Figura 2: Movimientos desencadenados

2.5. INSTRUMENTOS

Electroencefalógrafo: Es el dispositivo que capta, a través de electrodos, las pequeñas señales eléctricas en el cuero cabelludo provenientes del cerebro, las amplifica y las envía a un ordenador para su posterior procesamiento.

Sistema de medición cinemática: Los datos cinemáticos de la mano derecha se medirán con el sensor de profundidad del sistema Kinect de Microsoft.

Ordenador: Se encarga de procesar las señales EEG y de suministrar indicaciones al participante mediante una pantalla.

2.6 ANÁLISIS DE DATOS

Toda información será procesada en el computador. El procesamiento se llevará a cabo fuera de línea, es decir, no durante la prueba. Todo el procesamiento de información será realizado mediante un software llamado Matlab. La información recogida será estrictamente confidencial y se almacenará en un ordenador protegido con contraseña. La información se mantendrá guardada durante un período de 1 año, en caso de una auditoría.

2.7. ASPECTOS ÉTICOS

2.7.1. Aprobación

Este proyecto será revisado por el Comité de Ética de la PUCP, para su aprobación. Los procedimientos de este proyecto de investigación se llevarán a cabo únicamente después de la aprobación del Comité de Ética.

2.7.2. Información a los participantes

Se entregará una copia del consentimiento informado a cada participante. También podrán obtener algunos resultados del análisis realizado posteriormente.

2.7.3. Confidencialidad de la información

Todos los datos que se obtengan durante esta investigación solo estarán disponibles para los investigadores asignados a este proyecto. La información recolectada será almacenada en una base de datos virtual y protegida por contraseña.

2.7.4 Análisis de riesgos y beneficios

El equipo de electroencefalografía es un dispositivo sensor, es decir, solo registra las pequeñas señales eléctricas producidas por el cerebro sin emitir ningún tipo de señal o energía al participante. Además, es no invasivo, ya que se lo coloca encima del cuero cabelludo. Por esta razón, es totalmente inocuo y no implica ningún riesgo para el participante [4]. El sistema Kinect mide los movimientos de manera óptica y también es totalmente inofensivo para los participantes. Finalmente, es importante mencionar que el laboratorio del GIRAB cuenta con instalaciones eléctricas seguras y por las condiciones del proyecto no se requiere de la participación de personal médico.

CAPÍTULO III: Otros

3.1 Fin del proyecto

El proyecto se realizará hasta septiembre del presente año.

3.1 PRESUPUESTO

Los equipos y la mayoría de materiales ya han sido adquiridos y forman parte del laboratorio. Por ello, no se incluye ningún presupuesto adicional.

3.2 CONFLICTOS DE INTERÉS

Los autores de este proyecto declaran no tener ningún conflicto de interés.

BIBLIOGRAFÍA

- [1] Nicolas-Alonso, L. F.; Gomez-Gil, J.
Brain Computer Interfaces, a Review
Sensors 2012,12, p. 1225f
- [2] Allison, B. Z.; Dunne, S.; Leeb, R.; Millán, J. R.; Nijholt, A.
Towards Practical Brain-Computer Interfaces
Biological and Medical Physics, Biomedical Engineering
Springer-Verlag Berlin Heidelberg, p. 175
- [3] Korik, A.; Sosnik, R.; Siddique, N.; Coyle, D.
3D hand motion trajectory prediction from EEG mu and beta bandpower
Progress in Research, Brain-Computer Interfaces
Elsevier Verlag, pp. 71 - 101
- [4] Graimann, B., Allison, B. Z., & Pfurtscheller, G. (Eds.). (2010).
Brain-computer interfaces: Revolutionizing human-computer interaction.
Springer Science & Business Media.

A.5.3 Informed consent protocol for the participants

Comité de ética de la investigación – CEI
Vicerrectorado de Investigación – PUCP

PROTOCOLO DE CONSENTIMIENTO INFORMADO PARA PARTICIPANTES

El propósito principal de este protocolo es brindar a los participantes una explicación clara de la naturaleza de la misma, así como del rol que tienen en esta investigación.

La presente investigación es conducida por Matthias Petersamer, estudiante de la Pontificia Universidad Católica del Perú. El objetivo del estudio es encontrar una correlación entre señales cerebrales y datos cinemáticos durante la ejecución de movimientos. Los datos cerebrales serán registrados por un sistema electroencefalográfico y los datos cinemáticos serán medidos por un sensor infrarrojo.

Los sensores no implican ningún riesgo para el participante. El estudio nos va a permitir incrementar el conocimiento en el área de Interfaces Cerebro-Computacionales, cuyas principales aplicaciones están dirigidas a mejorar la calidad de vida de personas con discapacidad, como las que han sufrido accidentes cerebrovasculares, amputaciones, lesiones medulares, entre otras.

Si usted accede a participar en este estudio, se le colocarán electrodos sobre la cabeza y se registrarán sus señales cerebrales mientras observa una pantalla y sigue las indicaciones que se le darán. Esta toma de datos se realizará en una sesión que durará treinta minutos.

Su participación será voluntaria. La información que se recoja será estrictamente confidencial y no se podrá utilizar para ningún otro propósito después de culminada esta investigación.

La información recolectada será codificada mediante números de identificación. Además, la información será conservada por un periodo de tres meses, por si es necesaria alguna revisión posterior.

Si tuviera alguna duda con relación al desarrollo del proyecto, usted es libre de formular las preguntas que considere pertinentes. Además, puede finalizar su participación en cualquier momento del estudio sin que esto represente ningún perjuicio para usted. En caso de sentirse incómodo en algún momento durante las pruebas, puede ponerlo en conocimiento de la persona a cargo de la investigación y abstenerse de continuar.

Muchas gracias por su participación.

Al firmar este protocolo:

Doy mi consentimiento para participar en el estudio y soy consciente de que mi participación es enteramente voluntaria.

He recibido información en forma verbal y he leído la información escrita párrafos atrás sobre el estudio que se está realizando. He tenido la oportunidad de discutir sobre el estudio y hacer preguntas.

Entiendo que puedo finalizar mi participación en el estudio en cualquier momento, sin que esto represente ningún perjuicio para mí.

Entiendo que recibiré una copia de este consentimiento, así como información del estudio y que puedo pedir información sobre los resultados de este estudio cuando éste haya concluido. Para esto, puedo comunicarme con Matthias Petersamer al correo matthias.petersamer@pucp.edu.pe o al teléfono 944561482.

Nombre completo del (de la) participante

Firma

Fecha

Nombre del Investigador responsable

Firma

Fecha

A.5.4 Approved opinion

VICERRECTORADO DE
INVESTIGACIÓN
COMITÉ DE ÉTICA DE LA INVESTIGACIÓN



DICTAMEN

El Comité de Ética de la Investigación (CEI) informa que, en la sesión del 20 de julio de 2017, ha revisado la documentación presentada sobre la investigación titulada "Predicción de trayectorias de movimiento basadas en imaginación motora para una interfaz cerebro-computador" y ha emitido el dictamen **N°0016-2017/CEI-PUCP** (antecedente: Solicitud N°0020-2017/VRI-OETIIC).

Los documentos revisados pertenecientes a esta investigación fueron los siguientes:

- Comunicación dirigida al CEI solicitando la revisión ética del protocolo de investigación
- Declaración de compromiso con los principios éticos de la investigación
- Protocolo de investigación (proyecto de tesis)
- Protocolo de consentimiento informado para participantes.

Luego de la revisión, el Comité por unanimidad emitió el dictamen de APROBADO con recomendaciones. Ello, al amparo de su mandato que señala tienen el deber de: "asegurar el compromiso ético de los investigadores, así como certificar y supervisar que las investigaciones que sean sometidas a su consideración, tanto que sean llevadas a cabo o promovidas por la universidad como por terceros, cumplan con los principios éticos de la investigación"¹.

El Comité recomienda al investigador establecer el mismo período de conservación de la información recabada, tanto en el protocolo de Consentimiento Informado (CI) como en el protocolo de investigación. En ese sentido, se debe establecer si la información será conservada por un período de tres meses o un año. Asimismo, se indica que a nivel internacional se recomienda conservar la información recabados por un periodo no menor de 5 años por temas de posibles auditorías éticas posteriores.

Agradeceremos que para las comunicaciones futuras aluda al número de dictamen aquí asignado.

Atentamente,

María Isabel la Rosa Cormack
Presidente
Comité de Ética de la Investigación

¹ Artículo 1° del Reglamento del Comité de Ética de la Investigación de la PUCP. Puede ver la versión completa en: <http://cdn02.pucp.edu.pe/investigacion/2016/10/14160435/Reglamento-2.pdf>

Bibliography

- [1] Alvaro Rodrigo Fuentes Cabrera. *Feature extraction and classification for Brain-Computer Interfaces*. PhD thesis, Aalborg Universitet Aalborg Universitet, 2009.
- [2] Luis Fernando Nicolas-Alonso and Jaime Gomez-Gil. Brain computer interfaces, a review. *Sensors*, 12(2):1211–1279, 2012.
- [3] Muhammad Bilal Khalid, Naveed Iqbal Rao, Intisar Rizwan-i Haque, Sarmad Munir, and Farhan Tahir. Towards a brain computer interface using wavelet transform with averaged and time segmented adapted wavelets. In *Computer, Control and Communication, 2009. IC4 2009. 2nd International Conference on*, pages 1–4. IEEE, 2009.
- [4] Gert Pfurtscheller and Christa Neuper. Motor imagery and direct brain-computer communication. *Proceedings of the IEEE*, 89(7):1123–1134, 2001.
- [5] Patrick Ofner and Gernot R Müller-Putz. Using a noninvasive decoding method to classify rhythmic movement imaginations of the arm in two planes. *IEEE Transactions on Biomedical Engineering*, 62(3):972–981, 2015.
- [6] Brendan Z Allison, Stephen Dunne, Robert Leeb, José Del R Millán, and Anton Nijholt. *Towards practical brain-computer interfaces: bridging the gap from research to real-world applications*. Springer Science & Business Media, 2012.
- [7] Patrick Ofner and Gernot R Müller-Putz. Decoding of velocities and positions of 3d arm movement from eeg. In *Engineering in Medicine and Biology Society (EMBC), 2012 Annual International Conference of the IEEE*, pages 6406–6409. IEEE, 2012.
- [8] J. R. Wolpaw. Brain-computer interfaces: signals, methods, and goals. In *First International IEEE EMBS Conference on Neural Engineering, 2003. Conference Proceedings.*, pages 584–585, March 2003.
- [9] Itsu Sync. Different types of brain waves: Delta, theta, alpha, beta, gamma [online]. Available at: <http://itsusync.com/different-types-of-brain-waves-delta-theta-alpha-beta-gamma>, 2017 [access: 07/05/17].
- [10] Aboul Ella Hassanien and Ahm Ad T Aher Az Ar. *Brain-Computer Interfaces*. Springer, 2015.
- [11] Hannah M Hobson and Dorothy VM Bishop. Mu suppression—a good measure of the human mirror neuron system? *Cortex*, 82:290–310, 2016.

- [12] A Korik, R Sosnik, N Siddique, and D Coyle. 3d hand motion trajectory prediction from eeg mu and beta bandpower. *Progress in brain research*, 228:71–105, 2016.
- [13] Han Yuan and Bin He. Brain–computer interfaces using sensorimotor rhythms: current state and future perspectives. *IEEE Transactions on Biomedical Engineering*, 61(5):1425–1435, 2014.
- [14] Jörg Mayer. Lokalisation der sprache im gehirn - bildgebende verfahren [online]. Available at: www2.ims.uni-stuttgart.de/sgtutorial/neurorad, 2014 [access: 07/05/17].
- [15] Grega Repovš. Dealing with noise in eeg recording and data analysis. In *Informatica Medica Slovenica*, volume 15, pages 18–25, 2010.
- [16] M Stöhr and Regina Kraus. Einführung in die klinische neurophysiologie. *EMG–EEG–Evozierte Potentiale*. Darmstadt: Steinkopff Verlag, 2002.
- [17] Michal Teplan et al. Fundamentals of eeg measurement. *Measurement science review*, 2(2):1–11, 2002.
- [18] Peter Husar. *Biosignalverarbeitung*. Springer-Verlag, 2010.
- [19] Frederico AC Azevedo, Ludmila RB Carvalho, Lea T Grinberg, José Marcelo Farfel, Renata EL Ferretti, Renata EP Leite, Roberto Lent, Suzana Herculano-Houzel, et al. Equal numbers of neuronal and nonneuronal cells make the human brain an isometrically scaled-up primate brain. *Journal of Comparative Neurology*, 513(5):532–541, 2009.
- [20] Rice University. Discrete time signals and systems, part 2: Frequency domain, week 4: Discrete-time filters, 2015.
- [21] Ali Bashashati, Mehrdad Fatourehchi, Rabab K Ward, and Gary E Birch. A survey of signal processing algorithms in brain–computer interfaces based on electrical brain signals. *Journal of Neural engineering*, 4(2):R32, 2007.
- [22] Herbert Ramoser, Johannes Muller-Gerking, and Gert Pfurtscheller. Optimal spatial filtering of single trial eeg during imagined hand movement. *IEEE transactions on rehabilitation engineering*, 8(4):441–446, 2000.
- [23] Attila Korik, Nazmul Siddique, and Damien Coyle. Brief review of non-invasive motion trajectory prediction based brain-computer interfaces. In *PGBiomed International Student Conference, Warwick*, 2014.
- [24] Kyuwan Choi. Reconstructing for joint angles on the shoulder and elbow from non-invasive electroencephalographic signals through electromyography. 2013.
- [25] Trent J Bradberry, Rodolphe J Gentili, and José L Contreras-Vidal. Reconstructing three-dimensional hand movements from noninvasive electroencephalographic signals. *Journal of Neuroscience*, 30(9):3432–3437, 2010.

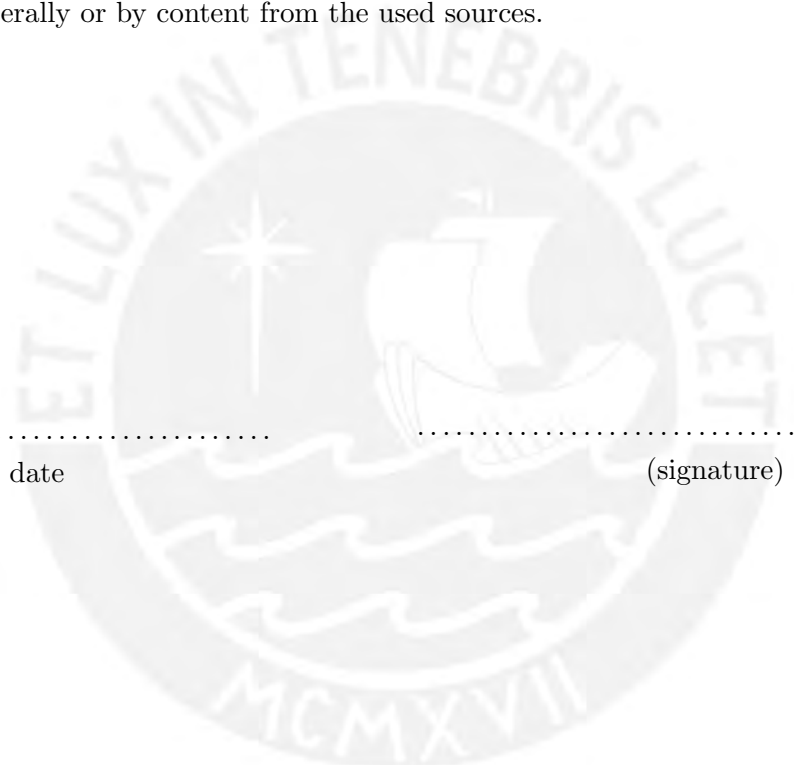
- [26] Javier M Antelis, Luis Montesano, Ander Ramos-Murguialday, Niels Birbaumer, and Javier Minguez. On the usage of linear regression models to reconstruct limb kinematics from low frequency eeg signals. *PLoS One*, 8(4):e61976, 2013.
- [27] Andrew Young Paek, Harshavardhan Agashe, and Jose Luis Contreras-Vidal. Decoding repetitive finger movements with brain activity acquired via non-invasive electroencephalography. *Frontiers in neuroengineering*, 7:3, 2014.
- [28] Alessandro Presacco, Ronald Goodman, Larry Forrester, and Jose Luis Contreras-Vidal. Neural decoding of treadmill walking from noninvasive electroencephalographic signals. *Journal of neurophysiology*, 106(4):1875–1887, 2011.
- [29] Rodolphe J Gentili, Trent J Bradberry, Bradley D Hatfield, and José L Contreras-Vidal. A new generation of non-invasive biomarkers of cognitive-motor states with application to smart brain-computer interfaces. In *Signal Processing Conference, 2008 16th European*, pages 1–5. IEEE, 2008.
- [30] Soumyadipta Acharya, Matthew S Fifer, Heather L Benz, Nathan E Crone, and Nitish V Thakor. Electrocorticographic amplitude predicts finger positions during slow grasping motions of the hand. *Journal of neural engineering*, 7(4):046002, 2010.
- [31] Minfen Shen, Xinjun Zhang, and Xianhui Li. Independent component analysis of electroencephalographic signals. In *Signal Processing, 2002 6th International Conference on*, volume 2, pages 1548–1551. IEEE, 2002.
- [32] Lia Petracovici and Department of Mathematics Joseph M. Rosenblatt, University of Illinois at Urbana-Champaign. Introduction to sampling. Available at: <http://www.math.uiuc.edu/SPHAA/98FA/sampling.pdf>, 9 1998.
- [33] Analog Devices Inc. Moving average filters. Available at: http://www.analog.com/media/en/technical-documentation/dsp-book/dsp_book_Ch15.pdf, access: 20/06/17.
- [34] Jeong-Hun Kim, Felix Biessmann, and Seong-Whan Lee. Reconstruction of hand movements from eeg signals based on non-linear regression. In *Brain-Computer Interface (BCI), 2014 International Winter Workshop on*, pages 1–3. IEEE, 2014.
- [35] Attila Korik, N Siddique, Ronen Sosnik, and Damien Coyle. 3d hand movement velocity reconstruction using power spectral density of eeg signals and neural network. In *Engineering in Medicine and Biology Society (EMBC), 2015 37th Annual International Conference of the IEEE*, pages 8103–8106. IEEE, 2015.
- [36] Jeff Schneider and Andrew W. Moore. A locally weighted learning tutorial using vizier 1.0, cross validation. Available at: <https://www.cs.cmu.edu/~schneide/tut5/node42.html#SECTION00092000000000000000>, 2 1997.

- [37] Hong Gi Yeom, June Sic Kim, and Chun Kee Chung. Estimation of the velocity and trajectory of three-dimensional reaching movements from non-invasive magnetoencephalography signals. *Journal of neural engineering*, 10(2):026006, 2013.
- [38] Yasuhiko Nakanishi, Takufumi Yanagisawa, Duk Shin, Ryohei Fukuma, Chao Chen, Hiroyuki Kambara, Natsue Yoshimura, Masayuki Hirata, Toshiki Yoshimine, and Yasuharu Koike. Prediction of three-dimensional arm trajectories based on ecog signals recorded from human sensorimotor cortex. *PloS one*, 8(8):e72085, 2013.
- [39] g.tec medical engineering GmbH. g.tec product catalogue, 2016.
- [40] g.tec medical engineering GmbH. g.nautilus wireless biosignal acquisition - g.nautilus research - instructions for use v1.14.02, April 2016.
- [41] Microsoft. Set up kinect for windows v2 or an xbox kinect sensor with kinect adapter for windows [online]. Available at: <http://support.xbox.com/en-US/xbox-on-windows/accessories/kinect-for-windows-v2-setup#b4b6153b4fd4408c973ccb76812ba44a>, 2017 [access: 12/05/17].
- [42] Microsoft. Kinect hardware [online]. Available at: <https://developer.microsoft.com/en-us/windows/kinect/hardware>, access: 11/05/17.
- [43] Microsoft. Kinect for xbox one [online]. Available at: <http://www.xbox.com/en-GB/xbox-one/accessories/kinect>, 2017 [access: 11/05/17].
- [44] Microsoft. Jointtype enumeration. Available at: <https://msdn.microsoft.com/en-us/library/microsoft.kinect.jointtype.aspx>, access: 14/05/17.
- [45] Physikalisch-Technische Bundesanstalt. Zeitsynchronisation von rechnern mit hilfe des "network time protocol" (ntp). Available at: <https://www.ptb.de/cms/ptb/fachabteilungen/abtq/fb-q4/ag-q42/zeitsynchronisation-von-rechnern-mit-hilfe-des-network-time-protocol-ntp.html>, access: 07/06/17.
- [46] g.tec medical engineering GmbH. g.nautilus wireless biosignal acquisition - simulink high-speed on-line processing - user manual v3.16.00, 2016.
- [47] Ivan Selesnick. Linerar-phase fir filters. Lecture Notes, EL 713: Digital Signal Processing II, 2017.
- [48] Inc. The MathWorks. filtfilt. Available at: <https://de.mathworks.com/help/signal/ref/filtfilt.html>, access: 09/07/17.
- [49] Swartz Center for Computational Neuroscience. What is eeglab? Available at: <https://sccn.ucsd.edu/eeglab/index.php>, access: 02/07/17.
- [50] Swartz Center for Computational Neuroscience. Eeglab tutorial, i. single subject data processing, chapter 09: Decomposing data using ica. Available at: https://sccn.ucsd.edu/wiki/Chapter_09:_Decomposing_Data_Using_ICA, access: 02/07/17.

- [51] Julián Messina, Claudio Michelacci, Jarkko Turunen, and Gylfi Zoega. *Labour market adjustments in Europe*. Edward Elgar Publishing, 2006.
- [52] Laerd statistics. Pearson product-moment correlation. Available at: <https://statistics.laerd.com/statistical-guides/pearson-correlation-coefficient-statistical-guide.php>, 2013 [access: 21/09/17].
- [53] A. Landi, P. Piaggi, M. Laurino, and D. Menicucci. Artificial neural networks for nonlinear regression and classification. In *2010 10th International Conference on Intelligent Systems Design and Applications*, pages 115–120, Nov 2010.
- [54] Trent J Bradberry, Feng Rong, and José L Contreras-Vidal. Decoding center-out hand velocity from meg signals during visuomotor adaptation. *Neuroimage*, 47(4):1691–1700, 2009.
- [55] Government of Alberta. Finger: Exercises [online]. Available at: <https://myhealth.alberta.ca/Health/aftercareinformation/pages/conditions.aspx?hwid=bo1571>, 2017 [access: 08/05/17].
- [56] Inc. The MathWorks. Microsoft kinect for windows support from image acquisition toolbox. Available at: <https://de.mathworks.com/hardware-support/kinect-windows.html>, access: 05/03/17.
- [57] Inc. The MathWorks. forcegarbagecollection. Available at: https://de.mathworks.com/help/symbolic/mupad_ref/forcegarbagecollection.html, access: 21/05/17.
- [58] Creative Commons Attribution 3.0. Kinovea, a microscope for your videos. Available at: <http://www.kinovea.org>, access: 21/05/17.
- [59] Easeware Technology Limited. Windows 10 100. Available at: <https://www.drivereasy.com/knowledge/fix-100-disk-usage-in-task-manager-improve-pc-performance-on-windows-10>, access: 04/06/17.

Statutory Declaration

I declare that I have authored this thesis independently, that I have not used other than the declared sources / resources, and that I have explicitly marked all material which has been quoted either literally or by content from the used sources.



.....

date

(signature)